

POLYIMIDE AND PEBAX FLAT AND HOLLOW FIBER MEMBRANES FOR  
GAS SEPARATION

A THESIS SUBMITTED TO  
THE GRADUATE SCHOOL OF NATURAL AND APPLIED SCIENCES  
OF  
MIDDLE EAST TECHNICAL UNIVERSITY

BY

NUR KONÇÜY ÖZDEMİR

IN PARTIAL FULLFILMENT OF THE REQUIREMENTS  
FOR  
THE DEGREE OF MASTER OF SCIENCE  
IN  
CHEMICAL ENGINEERING

JULY 2017



Approval of the thesis:

**POLYIMIDE AND PEBAX FLAT AND HOLLOW FIBER MEMBRANES  
FOR GAS SEPARATION**

submitted by **NUR KONÇÜY ÖZDEMİR** in partial fulfillment of the requirements  
for the degree of **Master of Science in Chemical Engineering Department,**  
**Middle East Technical University** by,

Prof. Dr. Gülbin Dural Ünver  
Dean, Graduate School of **Natural and Applied Sciences** \_\_\_\_\_

Prof. Dr. Halil Kalıpçılar  
Head of Department, **Chemical Engineering** \_\_\_\_\_

Prof. Dr. Halil Kalıpçılar  
Supervisor, **Chemical Engineering Dept., METU** \_\_\_\_\_

**Examining Committee Members:**

Prof. Dr. Levent Yılmaz  
Chemical Engineering Dept., METU \_\_\_\_\_

Prof. Dr. Halil Kalıpçılar  
Chemical Engineering Dept., METU \_\_\_\_\_

Asst. Prof. Dr. Berna Topuz,  
Chemical Engineering Dept., Ankara University \_\_\_\_\_

Asst. Prof. Dr. Emre Büküşoğlu  
Chemical Engineering Dept., METU \_\_\_\_\_

Asst. Prof. Dr. Erhan Bat  
Chemical Engineering Dept., METU \_\_\_\_\_

**Date:** 07.14.2017

**I hereby declare that all information in this document has been obtained and presented in accordance with academic rules and ethical conduct. I also declare that, as required by these rules and conduct, I have fully cited and referenced all material and results that are not original to this work.**

Name, Last name: Nur Konçüy Özdemir

Signature:

## ABSTRACT

### **POLYIMIDE AND PEBAX FLAT AND HOLLOW FIBER MEMBRANES FOR GAS SEPARATION**

Özdemir, Nur Konçüy  
M.S., Department of Chemical Engineering  
Supervisor: Prof. Dr. Halil Kalıpçılar

July 2017, 137 pages

This thesis analyzes the effect of polyimide (PI) hollow fiber membrane spinning conditions including dope solution flow rate, bore liquid flow rate, addition of more volatile solvent to dope solution, air gap height and heating zone temperature on the ideal gas separation performance and membrane morphology. The effect of PEBAX1657 coating of PI hollow fiber membrane was also investigated. The effect of incorporation of ZIF-8 crystals to PEBAX1657 flat sheet membrane, the effect of coagulant type for the preparation of porous polyethersulfone (PES) flat sheet membrane, the effect of PEBAX1657 and PEBAX1657/ZIF-8 coating of PES flat sheet membrane on the membrane gas separation performance and morphology were investigated.

In this study, asymmetric PI hollow fiber membranes were produced by dry-wet spinning method via twin orifice spinneret at room conditions from dope liquid containing dimethylformamide (DMF) and tetrahydrofuran (THF) and bore liquid solution containing 90 wt. % of DMF and 10 wt. % of distilled water. Tap water was used as non-solvent in the coagulation bath. Gas separation membrane performance of virgin hollow fiber membranes were not sufficiently high for biogas refining. PEBAX1657 coating enhanced gas separation performance of the virgin hollow fiber membranes. PEBAX1657 and PEBAX1657/ZIF-8 coating of porous PES flat sheet membranes increased ideal CO<sub>2</sub>/N<sub>2</sub> and CO<sub>2</sub>/CH<sub>4</sub> selectivity. Hollow fiber membranes were characterized by scanning electron microscopy (SEM). Flat sheet

membranes were characterized by SEM, Fourier transform infrared spectroscopy (FTIR), thermal gravimetric analysis (TGA). ZIF-8 crystals were characterized by N<sub>2</sub> adsorption desorption isotherms, SEM, X-ray diffraction (XRD). ZIF-8 particles having high crystallinity was synthesized with average size of  $69 \pm 14$  nm

Keywords: Gas Separation, Hollow Fiber Membrane Coating, Polyimide (PI), PEBAX 1657, ZIF-8

## ÖZ

### GAZ AYRIMI İÇİN POLİİMİD VE PEBAX İNCE FİLM VE KOVUKLU ELYAF MEMBRANLAR

Özdemir, Nur Konçüy  
Yüksek Lisans, Kimya Mühendisliği Bölümü  
Tez Yöneticisi: Prof. Dr. Halil Kalıpçılar

Temmuz 2017, 137 sayfa

Bu çalışmada, hazırlanan poliimid (PI) kovuklu elyaf membranların eğirme koşullarından olan polimer solüsyonu akış hızının, oluk sıvısı akış hızının, polimer solüsyonuna uçuculuğu daha yüksek çözücü eklenmesinin, hava boşluğu yüksekliğinin ve ısıtma bölgesinin sıcaklığının membranın ideal gaz ayırım performansına ve morfolojisine etkileri incelenmiştir. PI kovuklu elyaf membranların PEBAX 1657 ile kaplanmasının da etkileri incelenmiştir. PEBAX 1657 film membranlara ZIF-8 eklenmesinin, poliethersülfon (PES) film membranların hazırlanmasında koagülant tipinin, gözenekli PES film membranların PEBAX 1657 ve PEBAX 1657/ZIF-8 ile kaplanmasının membranların gaz ayırım performansına ve morfolojisine etkileri incelenmiştir.

Bu çalışmada, iki ağızlı iplik borusu yardımıyla asimetric PI kovuklu elyaf membranlar kuru-ıslak faz değişim metodu ile dimetilformamit (DMF) ve tetrahidrofuran (THF) içeren polimer solüsyonu ile % 90 (m) DMF ve %10 (m) damıtık su içeren oluk sıvısı kullanılarak oda koşullarında üretilmiştir. Koagülasyon banyosunda çözücü olmayan sıvı olarak çeşme suyu kullanılmıştır. Üretilen kovuklu elyaf membranların gaz ayırım performansı biyogaz ayırımı için yeterli yükseklikte değildir. Kovuklu elyaf membranların PEBAX 1657 ile kaplanması gaz ayırım performansını iyileştirmiştir. Gözenekli PES film membranların PEBAX 1657 ve PEBAX 1657/ZIF-8 ile kaplanması CO<sub>2</sub>/N<sub>2</sub> and CO<sub>2</sub>/CH<sub>4</sub> ideal seçiliğini artmıştır. Kovuklu elyaf membranlar taramalı elektron mikroskobu (SEM) ile karakterize

edilmiştir. İnce film membranlar (SEM), FTIR spektrometrisi (FTIR) ve termogravimetrik (TGA) analizi kullanılarak karakterize edilmiştir. ZIF-8 kristalleri azot adsorpsiyon-desorpsiyon izotermi, SEM ve X-ışını difraksiyonu (XRD) metodu kullanılarak karakterize edilmiştir. Yüksek kristaliteye sahip ZIF-8 parçacıkları ortalama  $69 \pm 14$  nm boyutunda üretilmiştir.

Anahtar Kelimeler: Gaz Ayırımı, Kovuklu Elyaf Membranların Kaplanması, Polimid (PI), PEBAX 1657, ZIF-8

To My Dearest Family

## ACKNOWLEDGEMENTS

I wish to express my sincere gratitude to my supervisor Prof. Dr. Halil Kalıpçılar for his guidance, patience, suggestions, support and interest throughout this study. I would like to thank Prof. Dr. Levent Yılmaz and Assoc. Prof. Dr. Zeynep Çulfaz Emecen for their suggestions and sharing their precious experiences about membrane separation processes.

I would like to thank The Scientific and Technological Council of Turkey (TUBITAK) through the grant number 213M546 and Middle East Technical University coordinatorship of scientific research projects (BAP) for financial support.

I would like to thank technical staff of Chemical Engineering Department Machinery Shop of Middle East Technical University for sharing their experiences about production of parts of my experimental setup. I could not improve my experimental setup without their help.

I would like to thank my colleagues Seren Kibar, Kübra Konca and Hande Kulaç for their friendship, endless support, encouragements, understanding, helps, suggestions during my university life and graduate study. I would also like to thank their families for accepting me like one of the family member.

I would like to thank my family for their encouragements, understanding, patience and endless support. I am indebted to my mother Filiz Okumuş to listen me patiently during my master study.

I would like to thank my spouse Burak Özdemir for his sacrifices, encouragements, understanding, patience, helps, suggestions, endless support and loyalty through good and bad times since preparatory year. I feel very lucky to deserve his love and affection.

## TABLE OF CONTENTS

ABSTRACT .....	v
ÖZ .....	vii
ACKNOWLEDGEMENTS .....	x
TABLE OF CONTENTS .....	xi
LIST OF TABLES .....	xiv
LIST OF FIGURES.....	xviii
CHAPTERS .....	1
1 INTRODUCTION .....	1
2 LITERATURE RESEARCH.....	7
2.1 Polymeric Gas Separation Membranes.....	7
2.1.1 Flat Sheet Membranes .....	9
2.1.2 Hollow Fiber Membranes .....	12
3 EXPERIMENTAL METHODOLOGY .....	27
3.1 Preparation of Pure PI Hollow Fiber Membranes .....	27
3.1.1 Materials of PI Hollow Fiber Membranes .....	27
3.1.2 Preparation of Hollow Fiber Membranes.....	27
3.1.3 Hollow Fiber Membrane Coating Methodology.....	31
3.2 Preparation of PEBAX 1657 Membranes, Flat Sheet PES Support Membranes, and PEBAX 1657 and PEBAX 1657/ZIF-8 coated PES Support Membranes .....	31
3.2.1 Materials for Flat Sheet Membrane Preparation .....	31

3.2.2	Synthesis Method of ZIF-8 crystals .....	32
3.2.3	Preparation of Flat Sheet Membranes .....	32
3.2.4	Coating of Flat Sheet PES membranes by PEBAX 1657 and PEBAX 1657/ZIF-8 solution .....	34
3.3	Characterization of Pure and Mixed Matrix Membranes and ZIF-8 Crystals 34	
3.3.1	Fourier Transform Infrared Spectroscopy (FTIR).....	34
3.3.2	N <sub>2</sub> Adsorption Desorption Isotherms .....	34
3.3.3	Thermal Gravimetric Analysis (TGA) .....	35
3.3.4	Scanning Electron Microscopy (SEM).....	35
3.3.5	X-ray Diffraction (XRD).....	35
3.4	Gas Permeation Measurements.....	35
4	RESULTS AND DISCUSSION .....	39
4.1	Characterization of ZIF-8 crystals .....	39
4.1.1	X-ray Diffraction (XRD).....	39
4.1.2	Scanning Electron Microscopy (SEM).....	41
4.1.3	N <sub>2</sub> Adsorption Desorption Isotherms .....	42
4.2	Selection of the Type of Polymer for the Preparation of Membranes.....	43
4.3	Characterization and Gas Separation Performance of Polyimide Hollow Fiber Membranes .....	44
4.3.1	Change of Membrane Dimensions with Spinning Conditions.....	46
4.3.2	Change of skin layer thickness with spinning conditions .....	51
4.3.3	The Effect of Spinning Conditions on the Macrovoid Structure of Membranes.....	55
4.3.4	Gas Permeation through Hollow Fiber Membranes.....	57
4.3.5	The Effects of PEBAX 1657 Coating on the Membrane Morphology and Gas Separation Performance .....	61

4.4	Characterization and Gas Separation Performance of Flat Sheet Membranes .....	65
4.4.1	Fourier Transform Infrared Spectroscopy (FTIR) .....	79
4.4.2	Thermal Gravimetric Analysis (TGA).....	81
5	CONCLUSIONS .....	85
	REFERENCES.....	87
	APPENDICES.....	95
A.	CALCULATION OF SINGLE GAS PERMEANCE AND PERMEABILITY .....	95
B.	AVERAGE PARTICLE SIZE OF THE ZIF-8 CRYSTALS .....	97
C.	TGA THERMOGRAMS OF THE PREPARED MEMBRANES.....	99
D.	REPRODUCIBILITY OF THE FLAT SHEET MEMBRANE PREPARATION .....	103
E.	UNIFORMITY OF HOLLOW FIBER MEMBRANES THROUGHOUT THE SPINNING PROCESS.....	109
F.	EFFECTS OF THE DOPE SOLUTION FLOW RATE ON THE HOLLOW FIBER MEMBRANE MORPHOLOGY .....	113
G.	EFFECTS OF THE BORE SOLUTION FLOW RATE ON THE HOLLOW FIBER MEMBRANE MORPHOLOGY .....	117
H.	EFFECTS OF THE THF ADDITION ON THE HOLLOW FIBER MEMBRANE MORPHOLOGY .....	125
I.	EFFECTS OF THE AIR GAP HEIGHT ON THE HOLLOW FIBER MEMBRANE MORPHOLOGY .....	129
J.	EFFECTS OF THE TEMPERATURE ON THE HOLLOW FIBER MEMBRANE MORPHOLOGY .....	135

## LIST OF TABLES

### TABLES

Table 1.1. Membrane terminology used for calculation of permeability and selectivity.....	2
Table 1.2: CO <sub>2</sub> /CH <sub>4</sub> selectivity based on types of material used for membrane production under the same working conditions .....	4
Table 2.1. Gas separation performance of mixed matrix PEBAX 1657 membranes .....	11
Table 2.2. Type of polymer used for production of hollow fiber membrane [6,34] .....	13
Table 2.3: The effect of composition and types of bore liquid on the gas permeance and selectivities .....	16
Table 2.4: The effect of non-solvent addition to spinning dope liquid on the PES hollow fiber membrane gas separation performance .....	17
Table 2.5: Effect of the dope liquid polymer composition on the membrane gas separation performance .....	17
Table 2.6: The effect of different flow angles on PES hollow fiber membrane gas separation performance .....	18
Table 2.7: The effect of take up wheel on the dual layer hollow fiber membrane gas separation performance containing poly[2,2'-(1,3-phenylene)-5,5'-bibenzimidazole(PBI)/Matrimid and polysulfone (PS) layers .....	19
Table 2.8: The effect of air gap height on the membrane gas separation performance .....	20
Table 2.9 : The effect of coating of hollow fiber membranes to the gas separation performance of the membrane.....	21
Table 2.10: The effect of filler type to the gas separation performance of different types of polymeric membranes.....	24
Table 3.1 Real flow rates corresponding the pump settings used for defining membrane codes .....	30

Table 3.2. The recipe for flat membrane preparation.....	33
Table 3.3. Membrane codes based on coagulation bath compositions .....	34
Table 4.1. Total peak area under the characteristic peaks of synthesized ZIF-8 crystals.....	41
Table 4.2. The effect of dope solution flow rate on the number of finger-like macrovoids compared to circular-shaped macrovoids and the covered area of those structures on the supporting layer [35°C, AG 12, 30 Polymer:0 THF:70 DMF ]..	55
Table 4.3. The effect of bore solution flow rate on the number of finger-like macrovoids compared to circular-shaped macrovoids and the covered area of those structures on the supporting layer [35°C, AG 12, 30 Polymer:0 THF:70 DMF ]..	56
Table 4.4. The effect of THF addition on the number of finger-like macrovoids compared to circular-shaped macrovoids and the covered area of those structures on the supporting layer [15°C, AG 12, D 1.0 g/min] .....	56
Table 4.5. The effect of air gap height on the number of finger-like macrovoids compared to circular-shaped macrovoids and the covered area of those structures on the supporting layer [35°C, D 1.0 g/min, 30 Polymer:0 THF:70 DMF] .....	57
Table 4.6. The effect of temperature on the number of finger-like macrovoids compared to circular-shaped macrovoids and the covered area of those structures on the supporting layer (Dope liquid composition 30 PI:0 THF: 70 DMF) .....	57
Table 4.7. The effect of dope solution flow rate on the hollow fiber membrane gas separation performance (convective heating zone temperature 35°C and Dope liquid composition 30 PI:0 THF: 70 DMF, B20: 0.50 g/min, B40:1.00 g/min, D30: 1.0 g/min, D100: 2.6 g/min).....	58
Table 4.8. The effect of bore solution flow rate on the hollow fiber membrane gas separation performance (convective heating zone temperature 15°C and Dope liquid composition 30 PI:0 THF: 70 DMF, B20: 0.50 g/min, B30:0.75 g/min, B40: 1.00 g/min, D30:1.0 g/min).....	59
Table 4.9. The effect of more volatile solvent addition to dope solution on the hollow fiber membrane gas separation performance (convective heating zone temperature 15°C, B20: 0.50 g/min, D30: 1.0 g/min) .....	59
Table 4.10. The effect of air gap height between spinneret and coagulation bath on the hollow fiber membrane gas separation performance (convective heating zone	

temperature 15°C and Dope liquid composition 30 PI:0 THF: 70 DMF, B20: 0.50 g/min, B30:0.75 g/min, D30: 1.0 g/min).....	60
Table 4.11. The effect of temperature on the hollow fiber membrane gas separation performance (Dope liquid composition 30 PI:0 THF: 70 DMF, B20: 0.50 g/min, B40: 1.00 g/min, D30:1.0 g/min) .....	60
Table 4.12. The effect of PEBAX 1657 coating on the hollow fiber membrane gas separation performance (convective heating zone temperature 35°C and Dope liquid composition 30 PI:0 THF: 70 DMF, B20:0.50 g/min, B40:1.00 g/min, D30:1.0 g/min, D100:2.6 g/min) .....	62
Table 4.13. The gas separation performance of pure PEBAX 1657 and PEBAX 1657/ZIF-8 flat sheet membranes.....	68
Table 4.14. The gas separation performance of PES flat sheet membranes [Knudsen selectivity for CO <sub>2</sub> /N <sub>2</sub> and CO <sub>2</sub> /CH <sub>4</sub> is 0.80 and 0.60, respectively].....	71
Table 4.15. The gas separation performance of prepared virgin PES/Water and PES/IPA/Water flat sheet membranes and PEBAX 1657 coated PES/Water and PES/IPA/Water flat sheet membranes.....	75
Table 4.16. The gas separation performance of prepared virgin PES/Water and PES/IPA/Water flat sheet membranes and PEBAX 1657/ZIF-8 coated PES/Water and PES/IPA/Water flat sheet membranes .....	78
Table B.1. Particle size measurement of different ZIF-8 crystals measured from SEM images .....	97
Table D.1. Reproducibility of the dense PEBAX 1657 membrane preparation ..	103
Table D.2. Reproducibility of the dense PEBAX 1657/ZIF-8 membrane preparation .....	104
Table D.3. Reproducibility of the PES/Water membrane preparation.....	104
Table D.4. Reproducibility of the PES/IPA/Water membrane preparation .....	105
Table D.5. Reproducibility of the PES/IPA membrane preparation .....	105
Table D.6. Reproducibility of the PEBAX 1657 coated PES/Water membrane preparation.....	106
Table D.7. Reproducibility of the PEBAX 1657 coated PES/IPA/Water membrane preparation.....	106

Table D.8. Reproducibility of the PEBAX 1657/ZIF-8 coated PES/Water membrane preparation.....	107
Table D.9. Reproducibility of the PEBAX 1657/ZIF-8 coated PES/IPA/Water membrane preparation.....	107
Table E.1. Uniformity of the prepared hollow fiber membranes with a 30 PI:7 THF: 63DMF dope liquid composition and 15°C heating zone temperature .....	109
Table E.2. Uniformity of the prepared hollow fiber membranes with a 30 PI:0 THF: 70 DMF dope liquid composition and 15°C heating zone temperature .....	110
Table E.3. Uniformity of the prepared hollow fiber membranes with a 30 PI:0 THF: 70 DMF dope liquid composition and 35°C heating zone temperature .....	111

## LIST OF FIGURES

### FIGURES

Figure 1.1. Upper bound correlation for selectivity and permeability [8] .....	3
Figure 2.1. Schematic of the ternary phase diagram [6] .....	8
Figure 2.2. Schematic view of flat sheet membrane [23].....	9
Figure 2.3: Production steps of dry-wet spinning of hollow fiber membranes [6]	14
Figure 2.4. Schematic diagram of spinneret indicating flow angle.....	18
Figure 3.1. Schematic view of twin orifice spinneret.....	28
Figure 3.2. The schematic view of hollow fiber spinning system based on the free fall method.....	29
Figure 3.3. Structural formula of PES [61] .....	31
Figure 3.4. Structural formula of PEBAX 1657 [28].....	32
Figure 3.5. The schematic diagram of the gas permeation test setup.....	36
Figure 3.6. Schematic view of membrane cell for the flat sheet membrane gas permeation test .....	36
Figure 3.7: Schematic view of membrane cell for the hollow fiber membrane gas permeation test .....	37
Figure 4.1. X-ray pattern of ZIF-8 crystals .....	40
Figure 4.2. SEM micrographs of ZIF-8 crystals .....	42
Figure 4.3. N <sub>2</sub> adsorption-desorption isotherms of synthesized ZIF-8 crystals .....	42
Figure 4.4. Comparison of CO <sub>2</sub> /CH <sub>4</sub> ideal selectivity and CO <sub>2</sub> permability for different types polymeric membranes compared to Robeson upper bound [16,63,64] .....	43
Figure 4.5. The SEM images of hollow fiber membrane produced by using 35°C convective heating zone with the mass ratio of 30 PI: 7 THF: 63 DMF PI.B20.D30.AG 6.....	45
Figure 4.6. The effect of dope and bore flow rate, and THF content of the dope solution on the bore and membrane diameter .....	49

Figure 4.7. The effect of air gap height and temperature on the bore and membrane diameter.....	50
Figure 4.8. The effect of dope and bore flow rate, and THF content of the dope solution on the selective layer thickness .....	53
Figure 4.9. The effect of air gap height and temperature on the selective layer thickness.....	54
Figure 4.10. The SEM images of PEBAX 1657 coated hollow fiber membranes produced by using 35°C convective heating zone with the mass ratio of 30 PI: 0 THF: 70 DMF a) PI.B20.D100.AG12 b) PI.B40.D100.AG12 c) PI.B20.D30.AG12 d) PI.B40.D30. AG12.....	64
Figure 4.11. The SEM images of a) pure PEBAX 1657 b) PEBAX 1657/ZIF-8 c) PEBAX 1657/PNA d) PEBAX 1657/ZIF-8/PNA flat sheet membranes.....	66
Figure 4.12. The SEM image of ZIF-8 crystals distributed in polymer matrix a) PEBAX 1657/ZIF-8 b) PEBAX 1657/ZIF-8/PNA flat sheet membranes c) PES/PI/ZIF-8 20/80/10 membrane (not compatible ZIF-8 crystals with PES/PI polymer matrix) [64].....	67
Figure 4.13. The SEM images of PES flat sheet membranes coagulated by using different types of non-solvent a) Pure water b) 50 wt. % water / 50 wt. % IPA c) pure IPA .....	70
Figure 4.14. The SEM images of PES/Water flat sheet membranes a) virgin PES/Water flat sheet membranes b) PEBAX 1657 coated PES/Water flat sheet membranes .....	73
Figure 4.15. The SEM images of PES/IPA/Water flat sheet membranes a) virgin PES/IPA/Water flat sheet membranes b) PEBAX 1657 coated PES/IPA/Water flat sheet membranes .....	74
Figure 4.16. The SEM images of PES/Water flat sheet membranes a) virgin PES/Water flat sheet membranes b) PEBAX 1657/ZIF-8 coated PES/Water flat sheet membranes .....	76
Figure 4.17. The SEM images of PES/IPA/Water flat sheet membranes a) virgin PES/IPA/Water flat sheet membranes b) PEBAX 1657/ZIF-8 coated PES/IPA/Water flat sheet membranes .....	77
Figure 4.18. The SEM image of ZIF-8 crystals distributed in polymer matrix .....	79

Figure 4.19. FTIR spectra of pure PEBAX 1657, PEBAX 1657/PNA, PEBAX/ZIF-8, PEBAX/PNA/ZIF-8 membranes and PNA and ZIF 8 solids .....	80
Figure 4.20. TGA results of PEBAX 1657 based membranes .....	82
Figure A.1. The time (s) vs. permeate pressure (bar g) graph for CH <sub>4</sub> permeation test of PES/IPA membrane .....	95
Figure C.1. The TGA thermogram of PES flat sheet membrane .....	99
Figure C.2. The TGA thermogram of PEBAX 1657 flat sheet membrane .....	100
Figure C.3. The TGA thermogram of PEBAX 1657/PNAZIF-8 flat sheet membrane .....	100
Figure C.4. The TGA thermogram of PEBAX 1657/ZIF-8 flat sheet membrane (part 1).....	101
Figure C.5. The TGA thermogram of PEBAX 1657/ZIF-8 flat sheet membrane (part 2).....	102
Figure C.6. The TGA thermogram of PEBAX 1657/ZIF-8 flat sheet membrane (part 3).....	102
Figure F.1. The SEM images of hollow fiber membranes produced by using 35°C convective heating zone with the mass ratio of 30 PI: 0 THF: 70 DMF a) PI.B20.D30.AG 12 b) PI.B20.D100.AG 12 .....	114
Figure F.2. The SEM images of hollow fiber membranes produced by using 35°C convective heating zone with the mass ratio of 30 PI: 0 THF: 70 DMF a) PI.B40.D30.AG 12 b) PI.B40.D100.AG 12 .....	115
Figure G.1. The SEM images of hollow fiber membranes produced by using 15°C convective heating zone with the mass ratio of 30 PI: 0 THF: 70 DMF a) PI.B20.D30.AG 6 b) PI.B30.D30.AG 6 .....	118
Figure G.2. The SEM images of hollow fiber membranes produced by using 15°C convective heating zone with the mass ratio of 30 PI: 0 THF: 70 DMF a) PI.B20.D30.AG 12 b) PI.B40.D30.AG 12 .....	119
Figure G.3. The SEM images of hollow fiber membranes produced by using 35°C convective heating zone with the mass ratio of 30 PI: 7 THF: 63 DMF a) PI.B20.D30.AG 6 b) PI.B40.D30.AG 6 .....	120

Figure G.4. The SEM images of hollow fiber membranes produced by using 35°C convective heating zone with the mass ratio of 30 PI: 7 THF: 63 DMF a) PI.B20.D100.AG 10 b) PI.B40.D100.AG 10.....	121
Figure G.5. The SEM images of hollow fiber membranes produced by using 35°C convective heating zone with the mass ratio of 30 PI: 0 THF: 70 DMF a) PI.B30.D30.AG 20 b) PI.B40.D30.AG 20.....	122
Figure G.6. The SEM images of hollow fiber membranes produced by using 35°C convective heating zone with the mass ratio of 30 PI: 0 THF: 70 DMF a) PI.B20.D30.AG 12 b) PI.B40.D30.AG 12.....	123
Figure G.7. The SEM images of hollow fiber membranes produced by using 35°C convective heating zone with the mass ratio of 30 PI: 0 THF: 70 DMF a) PI.B30.D100.AG 12 b) PI.B40.D100.AG 12.....	124
Figure H.1. The SEM images of hollow fiber membranes with a membrane code PI.B20.D30.AG 12 produced by using 15°C convective heating zone a) (PI: THF: DMF) (w/w) 30:0:70 b) (PI: THF: DMF) (w/w) 30:7:63 .....	126
Figure H.2. The SEM images of hollow fiber membranes with a membrane code PI.B30.D30.AG 12 produced by using 15°C convective heating zone a) (PI: THF: DMF) (w/w) 30:0:70 b) (PI: THF: DMF) (w/w) 30:7:63 .....	127
Figure I.1. The SEM images of hollow fiber membranes produced by using 15°C convective heating zone with the mass ratio of 30 PI: 0 THF: 70 DMF a) PI.B20.D30.AG 6 b) PI.B20.D30.AG 12.....	130
Figure I.2. The SEM images of hollow fiber membranes produced by using 15°C convective heating zone with the mass ratio of 30 PI: 0 THF: 70 DMF a) PI.B30.D30.AG 6 b) PI.B30.D30.AG 12.....	131
Figure I.3. The SEM images of hollow fiber membranes produced by using 15°C convective heating zone with the mass ratio of 30 PI: 0 THF: 70 DMF a) PI.B40.D30.AG 6 b) PI.B40.D30.AG 12.....	132
Figure I.4. The SEM images of hollow fiber membranes produced by using 35°C convective heating zone with the mass ratio of 30 PI: 0 THF: 70 DMF a) PI.B20.D30.AG 12 b) PI.B20.D30.AG 20.....	133

Figure I.5. The SEM images of hollow fiber membranes produced by using 35°C convective heating zone with the mass ratio of 30 PI: 0 THF: 70 DMF a) PI.B40.D30.AG 12 b) PI.B40.D30.AG 20 ..... 134

Figure J.1. The SEM images of PI.B20.D30.AG12 hollow fiber membranes produced with the mass ratio of 30 PI: 0 THF: 70 DMF a) 35°C b) 15°C ..... 136

Figure J.2. The SEM images of PI.B40.D30.AG12 hollow fiber membranes produced with the mass ratio of 30 PI: 0 THF: 70 DMF a) 35°C b) 15°C ..... 137

## CHAPTER 1

### INTRODUCTION

Energy is crucial for the life of human being. Fossil fuels, nuclear fuels and renewable energy sources (i.e. solar, wind, biomass, geothermal, hydropower) are several types of energy resources. Energy obtained from fossil fuels have impacts on the environment such as climate change, acid deposition and air pollution. Therefore, sustainable and renewable energy sources and effective usage of them are the main concerns of the current century [1].

Biogas is renewable energy source that is alternative to fossil fuels [2]. Biogas consists of 50% -70 % methane ( $\text{CH}_4$ ), 30 % - 40 % carbon dioxide ( $\text{CO}_2$ ), 5 % - 10 % hydrogen ( $\text{H}_2$ ), 1 % - 2 % nitrogen ( $\text{N}_2$ ), 0.3 % water vapor ( $\text{H}_2\text{O}$ ), 20 ppm – 20,000 ppm hydrogen sulphide ( $\text{H}_2\text{S}$ ) [3]. Due to its high methane content, it can be used as a fuel in domestic and industrial applications. However, biogas should be refined to remove  $\text{CO}_2$  because it decreases the calorific value of biogas and increases the transportation cost [4].

Solvent absorption, pressure-and temperature-swing adsorption and cryogenic distillation are conventional methods for biogas refining. Membrane based separation processes have recently been proposed over conventional methods since they have lower environmental impact and energy consumption, and could be scaled-up easily [5].

Membrane is defined as a semi permeable barrier that preferentially permeate some components over others. The gas separation performance of a membrane is determined by permeability and selectivity of the membrane. Permeability depends on the permeant and membrane material. Terminology used to show the membrane performance is shown in Table 1.1 [6].

Table 1.1. Membrane terminology used for calculation of permeability and selectivity

Terminology	Abbreviation	Unit
Flux	$J$	$\frac{cm^3(STP)}{cm^2 \times s}$
Permeance	$\mathcal{P} = \frac{P}{l}$	$\frac{cm^3(STP)}{cm^2 \times s \times cmHg}$
Permeability	$P_i = \frac{J \times l}{\Delta P}$	$\frac{cm^3(STP) \times cm}{cm^2 \times s \times cmHg}$
Ideal Selectivity	$\alpha_{ij} = \frac{P_i}{P_j}$	-

\* l: membrane thickness (cm) ,  $\Delta P$ : transmembrane pressure difference (cmHg)

In order to express permeability through a membrane, “Barrer” is commonly used as the permeability unit and GPU (gas permeation unit) is used as the unit of permeance which are defined in Equation 1.1 and Equation 1.2, respectively [6].

$$1 \text{ Barrer} = 10^{-10} \frac{cm^3(STP) \times cm}{cm^2 \times s \times cmHg} \quad \text{Equation 1.1}$$

$$1 \text{ GPU} = 10^{-6} \frac{cm^3(STP)}{cm^2 \times s \times cmHg} \quad \text{Equation 1.2}$$

Polymers like polyethersulfone (PES), cellulose acetate (CA), polyimide (PI), polydimethylsiloxane (PDMS) and microporous inorganic materials like molecular carbon sieve, zeolite, ceramic are used to prepare membranes for gas separation. Among these, polymeric membranes are generally used for biogas refining processes owing to their good mechanical stability, easy processability with economical selectivity and fluxes. Nearly, 80 % of the membranes used for this

purpose are made of polyimide and cellulose acetate owing to their favorable permeability and selectivity values [5,7].

Polymeric membranes has a trade-off between their permeability and selectivity known as “Robeson upper bound” which shows an inverse relationship between selectivity and permeability as shown in Figure 1.1 [5,7].

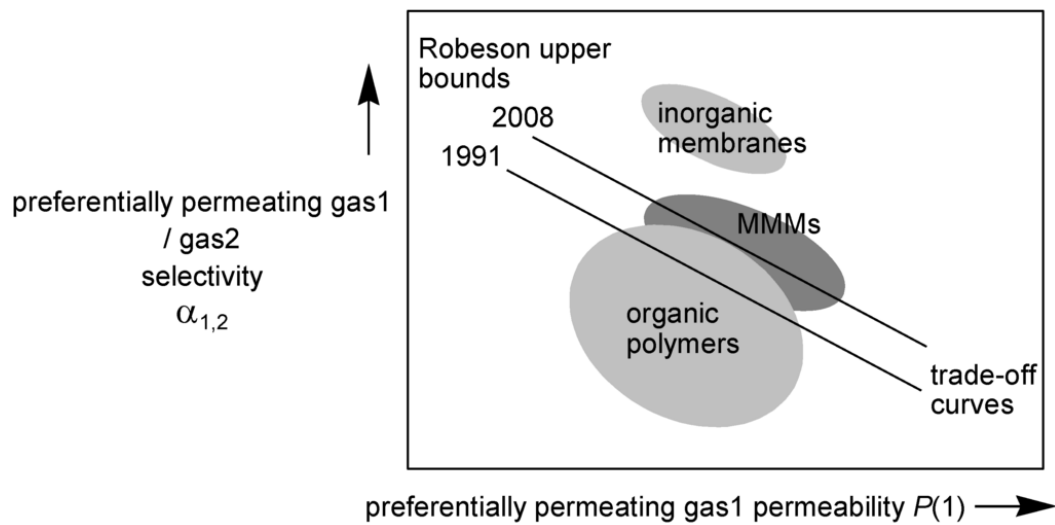


Figure 1.1. Upper bound correlation for selectivity and permeability [8]

Microporous inorganic membranes have higher permeabilities and selectivities than polymeric membranes as shown in Table 1.2. They could be operated at high temperature due to their high thermal and chemical resistances however they are expensive materials and have low mechanical strength, which decreases the commercial potential of this kind of membranes [6,7].

Table 1.2: CO<sub>2</sub>/CH<sub>4</sub> selectivity based on types of material used for membrane production under the same working conditions

<b>Types of Membrane Material</b>	<b>CO<sub>2</sub>/CH<sub>4</sub> Selectivity</b>	<b>Reference</b>
Cellulose acetate	35	[4]
Polyimide	49	[4]
Polyphenylene oxide	42	[4]
DD3R zeolite membrane on $\alpha$ -alumina disc support	600	[9]

Mixed matrix polymeric membranes have been developed to combine high gas separation performance of inorganic membranes and ease of fabrication and flexibility of polymeric membranes. Suitable configuration of polymer matrix and inorganic filler helps to enhance gas separation performance of the membranes compared to neat ones. Li et al. increased O<sub>2</sub> permeability and O<sub>2</sub>/N<sub>2</sub> selectivity with the incorporation of zeolite from 0.47 Barrer and 5.8 to 0.70 Barrer and 7.4, respectively [5,10,11,12].

The principle types of membranes are classified as symmetrical membranes and anisotropic membranes. The former is divided into three groups named as isotropic microporous membrane, non-porous dense membrane and electrically charged membrane. Non-porous dense membrane consists of a dense layer where permeants are transported by solution-diffusion under a driving force of concentration gradient. They are prepared by solution casting or thermal melt-pressing. On the other hand, anisotropic membranes are divided into three groups namely Loeb-Sourirajan anisotropic membrane, thin film composite anisotropic membrane and supported liquid membrane. Anisotropic membranes consist of thin and dense selective layer supported by thicker porous substructure. The dense layer is responsible from separation by solution-diffusion mechanism and porous support provides mechanical strength. This makes them economically desirable due to their high

fluxes and improved mechanical strength. Anisotropic membranes are generally prepared by phase separation, and solution coating methods [6].

For economical gas separation, membranes with large effective area are required, and to reduce the module cost, the membranes should fit into small volumes. Therefore, membranes in the form of hollow fibers which have large area per unit volume are desirable in membrane based gas separation processes. Hollow fiber membranes are often produced by dry-wet phase inversion, which yields asymmetric membranes.

In order to enhance the gas separation performance of the membranes, thickness of the selective layer should be as thin as possible. Gas bubbles, dust particles, and imperfections of the support membrane may cause defects on the selective layer, which decreases the membrane's gas separation performance. In order to seal the membrane defects, the selective layer is usually coated by a highly permeable rubbery polymer such as PDMS [6]. For instance, Ismail research group increased CO<sub>2</sub>/CH<sub>4</sub> ideal selectivity of PSF hollow fiber membranes from 4.15 to 41.5 by coating hollow fiber membranes with PDMS [13].

PEBAX 1657 has often been studied for CO<sub>2</sub> removal in recent years because of its high affinity for CO<sub>2</sub>. PEBAX 1657 is a block copolymer containing 40 wt. % aliphatic polyamide (PA 6) and 60 wt. % soft polyether (PEO) segments which has affinity for CO<sub>2</sub> [14]. Therefore, it is used as polymer matrix and coating layer for the preparation of mixed matrix and composite membranes, respectively. Rahman et al. prepared PVDF membranes showing CO<sub>2</sub>/CH<sub>4</sub> ideal selectivity of 1.11, which was increased to 29.16 after coating by PEBAX 1657 [15]. Ismail et al. prepared PEBAX and PEBAX/Zeolite 4A mixed matrix membranes. The CO<sub>2</sub> permeability and CO<sub>2</sub>/CH<sub>4</sub> ideal selectivity of Pure PEBAX 1657 membranes were 55.8 Barrer and 18, respectively. They increased to 97 Barrer and 26.5, respectively by the incorporation of 4A Zeolite [16].

In this study, asymmetric pure polyimide (PI) hollow fiber membranes were produced by dry-wet spinning method via twin orifice spinneret in order to investigate effect of spinning process conditions including dope solution flow rate,

bore liquid flow rate, addition of a more volatile solvent to dope solution, air gap height, and heating zone temperature on the gas separation performance and membrane morphology. Gas separation performance of virgin hollow fiber membranes, tested by pure H<sub>2</sub>, CO<sub>2</sub> and CH<sub>4</sub> gases at 35°C and 3 bar TMP, were not sufficiently high for biogas refining. Hollow fiber membranes were coated with PEBAX 1657 in order to enhance gas separation performance. For further investigation of the gas separation performance of PEBAX 1657 polymer, flat sheet PEBAX 1657 membranes were prepared. In order to investigate compatibility between PEBAX 1657 polymer matrix and ZIF-8 crystals, flat sheet PEBAX 1657/ZIF-8 and PEBAX 1657/ZIF-8/PNA membranes were prepared. The effect of addition of p-nitroaniline (PNA) and ZIF-8 to PEBAX 1657 membrane solution on the membrane morphology were investigated. In order to imitate hollow fiber membranes having surface defects, ultrafiltration PES flat sheet membranes were prepared by coagulating them in different non-solvent bath containing distilled water and isopropyl alcohol (IPA) at various compositions and coated with PEBAX 1657 and PEBAX 1657/ZIF-8 solution. Prepared flat sheet mixed matrix and composite membranes were characterized based on pure N<sub>2</sub>, CO<sub>2</sub> and CH<sub>4</sub> gas permeances at 35°C and 3 bar TMP.

## CHAPTER 2

### LITERATURE RESEARCH

The transport mechanism of gases through the dense gas separation membranes is explained by solution diffusion model which is basically dissolution of gases in the membrane material and then diffusion through the membrane due to a concentration gradient. For gas separation processes, diffusion rate and solubility of the gases through membrane material are the key factors affecting membrane gas separation performance [6].

#### 2.1 Polymeric Gas Separation Membranes

Polymeric gas separation membranes are divided into two categories namely symmetric and asymmetric membranes. Most of the polymeric gas separation membranes have been prepared by phase inversion process which is a process controlling the polymer transformation from a liquid to solid phase. Phase inversion membranes are prepared by immersion precipitation, precipitation by controlled evaporation, precipitation from the vapor phase, solvent evaporation and thermally induced phase separation. Solvent evaporation is often used to produce symmetric membranes. In this method, polymer solution is cast onto a plate and the solvent is allowed to evaporate in an inert atmosphere to produce dense homogeneous membrane. Symmetric membranes are not preferable for membrane separation processes due to low transmembrane flux for a wide range of applications [17,18,19]. Immersion precipitation method is the most widely used method to obtain asymmetric membranes. In this phase inversion method, polymer solution composed of a polymer and solvent is cast and coagulated in a coagulation bath containing non-solvent. Polymer precipitates in the coagulation bath due to solvent and non-solvent exchange [6]. The theoretical approach for membrane formation was explained by ternary phase diagram as shown in Figure 2.1.

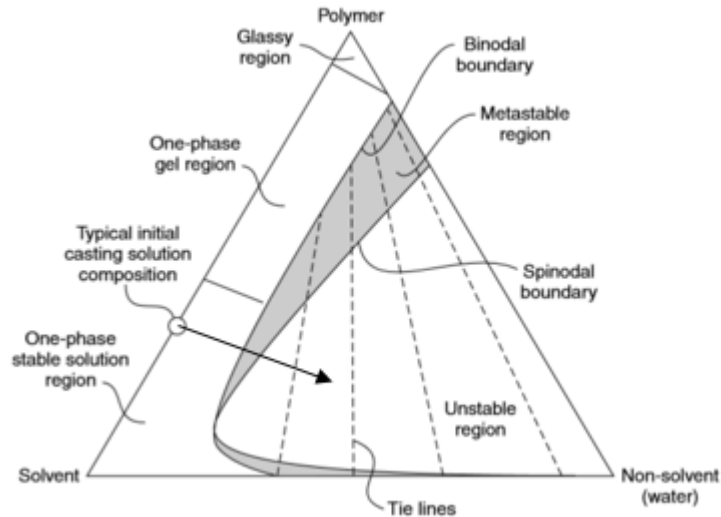


Figure 2.1. Schematic of the ternary phase diagram [6]

One phase region and two phase region are the main regions in the phase diagram. In the former one, all components are miscible, but solid and liquid phases are distinguishable in two phase region. Selection of the composition of casting solution is critical to prepare stable casting solutions since high polymer concentrations result in a solid polymer gel and a solid glass which are not suitable for casting process due to restrictions in the rotation of polymer chains [6]. Solvent exchange in the casting solution with the addition of non-solvent results in a change in the composition of membrane casting solution from one phase region to two phase region by crossing the binodal boundary. Polymer precipitation does not occur in metastable region without well nucleation. In unstable region, two phases of the polymer solution are distinguishable. Thermodynamic and kinetic factors of a ternary system influences membrane formation process. The rate of precipitation and the precipitation path influences membrane structure. The location of binodal boundary, spinodal boundary, area of metastable region, and slope of the tie lines are specific for different sets of solvent-polymer-non solvent based on molecular weight of the polymer, miscibility of the polymer, solvent-non solvent affinity. In other words, types of polymer, solvent and non-solvent used for preparation of

membrane casting solution influences membrane separation performance and morphology [6,20,21].

The type of polymers influences which gas molecules permeate through membrane material first. According to the glass transition temperature of polymers whether it is below or above the room temperature, they are named as glassy or rubbery polymer. The glass transition temperature of the former is above the room temperature. Small gas molecules are preferential for glassy polymers compared the rubbery ones based on the dominant mobility term compared to sorption selectivity term. Gas separation membranes made of glassy polymers have high selectivity and low permeability values compared to rubbery ones based on Robeson plot [8].

For feasible industrial applications, the choice of membrane configuration including flat sheet membrane, hollow fiber membrane is important in terms of changing membrane area per unit volume to increase membrane flux with a cost effective way. For equivalent size of membrane modules, the membrane area for spiral wound module changes between 20 m<sup>2</sup> and 40 m<sup>2</sup> but the hollow fiber module contains 300 m<sup>2</sup> of membrane area [6].

### 2.1.1 Flat Sheet Membranes

Flat sheet membranes are easily manufactured by using wide range of polymers compared to hollow fiber membranes since spinnability of the polymer is not taken into consideration for the production of flat sheet membranes shown in Figure 2.2 [22].

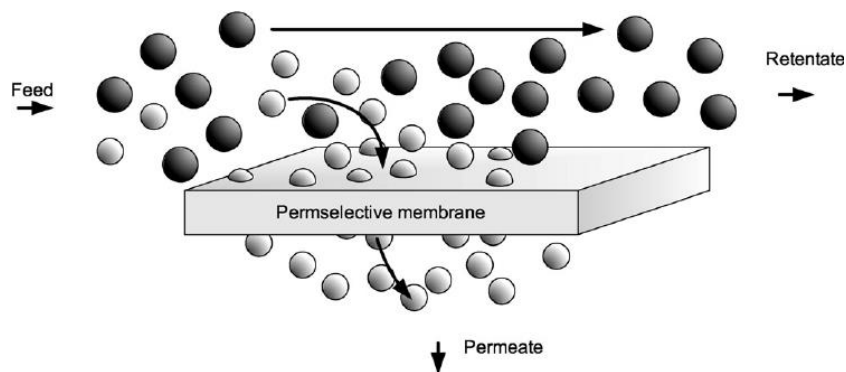


Figure 2.2. Schematic view of flat sheet membrane [23]

Solution casting is widely used for small scale flat sheet membrane production. Composition of the membrane casting solution, polymer type, solvent and non-solvent used for preparation of casting solution, phase inversion method influences membrane gas separation performance and morphology [6].

Polyether sulfone (PES) shows a reasonable relation between selectivity coefficients and permeability values for gas separation applications besides its good chemical and thermal stabilities [24]. PES is also widely used as membrane support since it can be easily manufactured in various configurations with a wide range of pore sizes and structures [25].

PEBAX 1657 is a special type of thermoplastic elastomer polymer containing 40 wt. % aliphatic polyamide (PA 6) and 60 wt. % soft polyether (PEO). The polyamide segment and flexible polyether segment provides mechanical strength and gas separation ability, respectively [26]. PEBAX 1657 has high chain mobility and good interaction with a filler besides its economical feasibility, easy film formation, high mechanical strength, and good temperature resistance [5]. Gas separation performance of PEBAX 1657 membranes were shown in Table 2.1.

Mixed matrix PEBAX 1657 flat sheet membranes are produced to enhance gas separation performance of the membrane in order to change polymer chain mobility, and fractional free volume by changing crystallinity of the membrane [5]. The effects of filler addition on the membrane gas separation performance were shown in Table 2.1.

Table 2.1. Gas separation performance of mixed matrix PEBAx 1657 membranes

Filler Type	Permeability (Barrer)			Ideal Selectivity		Reference
	CO <sub>2</sub>	CH <sub>4</sub>	N <sub>2</sub>	CO <sub>2</sub> /CH <sub>4</sub>	CO <sub>2</sub> /N <sub>2</sub>	
-	55.8	3.1	1.4	18	40.2	[16]
10 wt % 4A Zeolite	97.0 ± 4.9	3.7 ± 0.2	1.8 ± 0.1	26.5 ± 1.9	54.0 ± 2.5	
-	122	-	1.71	-	71.3	[27]
10 wt % Silica	154	-	2.13	-	72.3	
-	55.85	-	1.39	-	40.2	[28]
5 wt % MWC NT	262.15	-	4.48	-	58.5	
-	72	-	-	14	34	[29]
34 wt % ZIF-7	41	-	-	44	105	
1 wt % ZIF-8	464 ± 21	33.5 ± 12	-	13.8 ± 0.4	-	[30]
4 wt % ZIF-8	449 ± 23	30.5 ± 9	-	14.7 ± 0.2	-	
-	110	6	2	19.4 ± 0.1	47.0 ± 0.5	[31]
20 wt % ZIF-8	200	15	4	15.1 ± 0.2	41.1 ± 1.6	

According to the solution diffusion model, transport of gases is affected by solubility of the gases through the membrane material and diffusion rate. Solubility of the gases is related to their critical temperature. The critical temperatures of CO<sub>2</sub> and N<sub>2</sub> are 304.1 K and 126.2 K, respectively. This shows that those gases could be separated by their solubility difference [6]. Diffusion rate of the gases is related to

the kinetic diameter of the gases. The kinetic diameters of CO<sub>2</sub>, CH<sub>4</sub>, and N<sub>2</sub> are 0.33 nm, 0.38 nm, 0.36 nm, respectively. This shows that diffusivity term could be used as a determining factor for CO<sub>2</sub>/CH<sub>4</sub> separation [5]. Addition of fillers to PEBAX 1657 based membranes affects chain mobility, gas diffusivity and CO<sub>2</sub> solubility by affecting crystallinity of both PA6 and PEO phases. Zeolite addition increases both permeability of gases and selectivity. Zeolitic composition, pore size and pore structure of the zeolites influences the gas transport through zeolites due to the effect of solution diffusion and molecular sieving mechanism [16]. Silica addition decreases the crystallinity of PA 6 phase. This increases gas permeability due to increase in the total volume of amorphous region available for gas flow [27]. Multi-walled carbon nanotube (MWCNT) addition decreases crystallinity and increases chain mobility, gas diffusivity and CO<sub>2</sub> solubility. This explains the increase in CO<sub>2</sub> and N<sub>2</sub> permeability and CO<sub>2</sub>/N<sub>2</sub> selectivity with the addition of MWCNT [32]. ZIF-7 and ZIF-8 addition decreases gas permeability but increases selectivity due to the more rigidified polymer chains [29].

### **2.1.2 Hollow Fiber Membranes**

Hollow fiber membranes were discovered in 1966 by Mahon research group [6]. They have higher surface area per unit volume compared to flat sheet membranes. Hollow fiber membranes could have asymmetric or symmetric structure based on the selection of production method. Asymmetric membranes are economically desirable due to their high fluxes and improved mechanical strength. Selective layer of the hollow fiber membrane could be formed on the internal or external surface of the asymmetric hollow fiber membrane during the spinning process based on the chosen bore liquid and coagulant. Selective layer could also be formed by coating the porous hollow fiber membrane with a dense layer of the same or another type of polymer after spinning process. Diameter of the hollow fiber membranes are ranged between 50 μm and 3000 μm. Membranes with a diameter of less than 200 μm and a diameter of less than 400 μm are typically used in high pressure gas and medium pressure gas separation applications, respectively. Hollow fiber membranes as large as 3000 μm are often employed in ultrafiltration [6].

Hollow fiber membranes should withstand the applied pressure during separation processes. The diameter of the membrane limits application area of hollow fiber membrane regarding the mechanical strength of the membrane. The diameter of the membrane is an important criterion for the flow side of feed. When the membrane diameter ranges between 50  $\mu\text{m}$  and 200  $\mu\text{m}$ , feed fluid is applied to outside of the membrane and permeate is removed from the inner side of the hollow fiber membrane. [6].

### 2.1.2.1 Hollow Fiber Membrane Production

Hollow fiber membrane is one of the best suitable geometry for industrial applications regarding high surface area per unit volume [33]. Type of the polymers used for the production of hollow fiber membrane are summarized in Table 2.2.

Table 2.2. Type of polymer used for production of hollow fiber membrane [6,34]

<b>Polymer Type</b>		<b>Polymer Type</b>	
Cellulose Acetate	CA	Polypropylene	PP
Polyvinylidene fluoride	PVDF	Torlon	-
Polyethersulfone	PES	Matrimid	-
Polybenzimidazole	PBI	Polyether ketone	PEK
Polyetherimide	PEI	Surface Modification Macromolecules	SMM
Ultem	-	Silicon rubber	SR
Polydimethylsiloxane	PDMS	Poly(ethylene-co-vinyl alcohol)	EVOH
Polyaniline	PAni	Polyacrylonitrile	PAN
Chitosan	Ch	Poly(4-vinylpyridine)	P4VP
Polytetrafluoraethylene	PTFE	Poly(vinylidene fluoride-co- hexafluoropropylene)	PVDF- HFP

Chemical, mechanical and thermal properties of polymers affect the membrane gas separation performance, dope liquid preparation conditions and membrane production method [34]. Melt spinning and solution spinning methods are used for production of hollow fiber membranes. Melt spinning is based on extrusion of melting polymer from a mold. Hollow fiber membranes produced by this method having lower flux due to their denser structure compared to those produced by solution spinning method. This method is specifically suitable for non-soluble polymers [6]. Dry-wet spinning method is the most widely used method for the production of asymmetric hollow fiber membranes. In this method, polymer is dissolved in a convenient solvent, then asymmetric hollow fiber membranes are produced by using a twin orifice spinneret with suitable configuration of dope liquid and bore liquid [6]. Dry spinning and wet spinning are two important steps of this method. In dry spinning step, solvent is partially evaporated. This step enables the formation of a dense layer resulted from the evaporation of the solvent. This step is followed by wet spinning step where coagulation of dope liquid occurs by using a proper non-solvent which has low solvent strength [35]. In the literature, water is generally preferred as a coagulant when its availability and non-toxic properties are taken into account. In this step, solvent exchange between non-solvent coagulant and solvent used for preparation of dope liquid enables formation of porous support layer. In this step, dense layer formation may occur with delayed demixing process. Production steps of dry wet spinning process was shown in Figure 2.3.

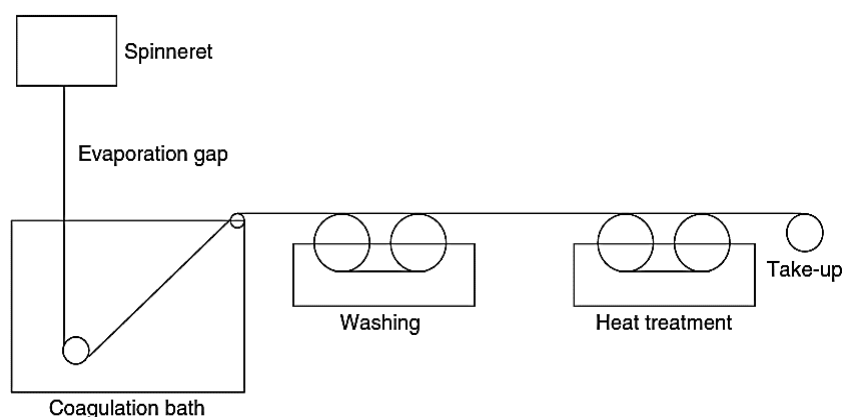


Figure 2.3: Production steps of dry-wet spinning of hollow fiber membranes [6]

Dope liquid and bore liquid solution are pumped with specified flow rates flow through spinneret with a suitable configuration. Hollow fiber is exposed to dry-wet phase inversion process throughout air gap followed by wet phase inversion process in a coagulation bath. Hollow fiber membranes could also be produced by free fall method inside a coagulation bath or taken up by using a wheel with specified take-up rate. Washing step is used for removing residual solvent from hollow fiber membranes. This step could be followed by solvent exchange step regarding of the type of solvent used in coagulation bath. Heat treatment step is applied for removing residual solvent completely [6].

#### **2.1.2.2 The Effect of Spinning Conditions on Membrane Gas Separation Performance**

Spinning conditions including composition and types of bore liquid, composition of dope liquid and types of polymer, additives, flow rate of dope liquid and bore liquid, inside and outside diameter of spinneret orifice, air gap height, dope liquid temperature, types of coagulation bath fluid and hollow fiber take up rate affect the hollow fiber membrane gas separation performance [6,34,36].

Composition and type of bore liquid affect the mass transfer resistance during spinning of hollow fiber membranes. This causes defect formation on the membrane surface, which results in a dramatic decrease in the membrane gas separation performance. Ismail et.al. (1999) showed that addition of salt to the water used as bore liquid decrease the water strength, this resulted in an increase in the selectivity by changing the membrane morphology. Kapantaikadis et al. (2002) demonstrated that increase in the solvent composition in the bore liquid resulted in increase in the membrane permeance without lowering selectivity. Types of bore liquid indicates the side of selective layer based on the type of coagulation bath liquid [6,39,40]. The effect of composition and types of bore liquid on the PES hollow fiber membrane gas separation performance were tabulated in Table 2.3.

Table 2.3: The effect of composition and types of bore liquid on the gas permeance and selectivities

Bore liquid	Gas Permeance (GPU)			Ideal Selectivity			Reference
	He	CO <sub>2</sub>	O <sub>2</sub>	He/N <sub>2</sub>	CO <sub>2</sub> /N <sub>2</sub>	O <sub>2</sub> /N <sub>2</sub>	
2-PrOH	1.8	0.4	0.11	17.0	3.8	2.0	[41]
EtOH	88	26.6	6.3	64	19.3	4.6	
50 % 2PrOH/H <sub>2</sub> O	202.8	81.9	17.6	81.2	27.9	5.67	

Phase inversion kinetics, interactions between dope liquid and coagulation bath liquids affect asymmetric membrane formation mechanism. Addition of non-solvent liquid into the dope liquid leads to increase in coagulation rate by decreasing coagulation value. Selective layer formation is a result of increasing local polymer concentration due to evaporation of solvent and solvent component of the dope liquid during dry phase inversion processes. Surface tension of the solvent in the dope liquid affects the surface porosity and formation of the selective layer by affecting capillary pressure on the membrane surface [42].

The structure of the selective layer is affected from the ratio of the rate of coagulation bath liquid flowing inside to the rate of non-solvent liquid flowing outside during wet phase inversion processes. Clausi and Koros (2000) stated that usage of volatile solvent for the preparation of the dope liquid affects phase inversion rate. This enables control of phase inversion rate by using different volatile solvent having unique volatility. The rate of dry and wet phase inversion processes have influence on membrane gas separation performance by affecting membrane morphology as tabulated in Table 2.4.

Table 2.4: The effect of non-solvent addition to spinning dope liquid on the PES hollow fiber membrane gas separation performance

Membrane Code	Gas Permeance (GPU)				Ideal Selectivity			Reference
	He	CO <sub>2</sub>	O <sub>2</sub>	N <sub>2</sub>	He/N <sub>2</sub>	CO <sub>2</sub> /N <sub>2</sub>	O <sub>2</sub> /N <sub>2</sub>	
without addition of non-solvent (PNo-4)	284	103	100	107	2.65	0.96	0.93	[42]
non-solvent: EtOH (Pet-4)	122	41	35	45	2.71	0.91	0.78	
non-solvent: 2-PrOH (PPr-4)	1587	741	757	816	1.94	0.91	0.93	

Morphology of the selective layer changes with the polymer composition of the dope liquid and types of the polymer. This changes the local polymer composition, which influences the membrane gas separation performance. The effects of polymer composition of dope liquid on membrane gas separation performance was tabulated in Table 2.5.

Table 2.5: Effect of the dope liquid polymer composition on the membrane gas separation performance

Polymer composition (wt. %)	Gas Permeance (GPU)	Ideal Selectivity	Reference
25 (Matrimid 5218)	1.0 (O <sub>2</sub> )	6.8 (O <sub>2</sub> /N <sub>2</sub> )	[44]
22 (Matrimid 5218)	1.7 (O <sub>2</sub> )	6.4 (O <sub>2</sub> /N <sub>2</sub> )	
PI: PES 20:80 (Dope A)	40 (CO <sub>2</sub> )	40 (CO <sub>2</sub> /N <sub>2</sub> )	[38]
PI: PES 50:50 (Dope B)	31 (CO <sub>2</sub> )	35 (CO <sub>2</sub> /N <sub>2</sub> )	
PI: PES 80:20 (Dope C)	60 (CO <sub>2</sub> )	39 (CO <sub>2</sub> /N <sub>2</sub> )	

Design of the spinneret shown in Figure 2.4 affects flow dynamics of the dope liquid inside the orifice. Elongation and shear rate influences membrane morphology by changing molecular order and bond intensity.

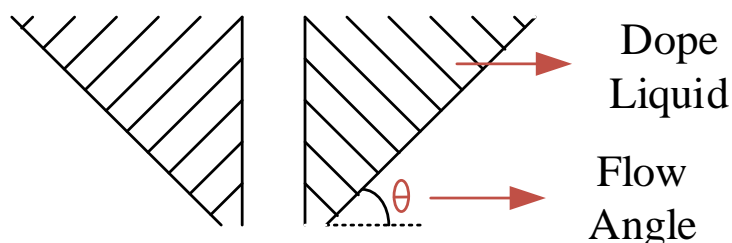


Figure 2.4. Schematic diagram of spinneret indicating flow angle

The effect of different flow angles ( $\theta = 60^\circ, 75^\circ, 90^\circ$ ), affecting elongation and shear rate, on gas separation performance was tabulated in Table 2.6.

Table 2.6: The effect of different flow angles on PES hollow fiber membrane gas separation performance

Gas Permeance (O <sub>2</sub> ) (GPU)			O <sub>2</sub> /N <sub>2</sub> Selectivity			Reference
60 °	75 °	90 °	60 °	75 °	90 °	
4.21	4.63	4.75	6.18	6.10	4.76	[45]
3.08	2.68	3.75	5.50	6.33	4.70	

Hollow fiber membranes could be produced by free-fall or pulling with the help of take up wheel from coagulation bath. Elongation rate difference between those two methods affects the membrane gas separation performance implicitly as shown in Table 2.7.

Table 2.7: The effect of take up wheel on the dual layer hollow fiber membrane gas separation performance containing poly[2,2'-(1,3-phenylene)-5,5'-bibenzimidazole(PBI)/Matrimid and polysulfone (PS) layers

Take-up speed (cm/min)	Method	Permeance (GPU)			Selectivity		Reference
		H <sub>2</sub>	CH <sub>4</sub>	CO <sub>2</sub>	H <sub>2</sub> /CO <sub>2</sub>	CO <sub>2</sub> /CH <sub>4</sub>	
371	Free Fall	30.9	3.542	4.90	6.18	1.38	[46]
681	Elongational draw	39.0	0.527	5.76	6.77	10.93	

Air gap height between spinneret and coagulation bath is critical in terms of membrane pore formation and pore structure [6]. This affects the membrane gas separation performance. The effect of the air gap height on the gas permeance is controversial issue regarding different researches as tabulated in Table 2.8 due to uncontrolled spinning conditions like relative humidity.

Table 2.8: The effect of air gap height on the membrane gas separation performance

Membrane Code	Air Gap Height (cm)	Gas Permeance (GPU)	Reference
PI: PES 20:80 (Dope A)	1	57 (CO <sub>2</sub> )	[38]
	10	130 (CO <sub>2</sub> )	
PES:NMP 29.4:70.6 (PN <sub>0</sub> )	0	103 (CO <sub>2</sub> )	[42]
	22	42 (CO <sub>2</sub> )	
PES:NMP:MeOH 29.4:51.65:18.95 (PMe)	0	387 (CO <sub>2</sub> )	
	22	837 (CO <sub>2</sub> )	
PES:NMP:H <sub>2</sub> O 25:66.98:8.02 (RHo1)	5	81.1 (CO <sub>2</sub> )	[41]
	15	97.9 (CO <sub>2</sub> )	
PES:NMP:H <sub>2</sub> O 27:65.20:7.80 (Rho2)	5	88.6 (CO <sub>2</sub> )	
	15	74.9 (CO <sub>2</sub> )	
PES:NMP 30:70	0	75.8 (O <sub>2</sub> )	[39]
	14.4	22.9 (O <sub>2</sub> )	
PEI:NMP:EtOH 30:59.38:10.62 (PEI1)	0	367 (He)	[48]
	30	462.6 (He)	
PEI:NMP:EtOH 25:62.36:12.64 (PEI2)	2	780 (He)	
	10	5570 (He)	
Matrimid:NMP:EtOH 26.2:58.9:14.9 (M1)	2.5	33.7 (O <sub>2</sub> )	[43]
	18.5	11.2 (O <sub>2</sub> )	
Matrimid:NMP:EtOH:THF 26.2:55.9:14.9:3.0 (M2)	2.5	19.9 (O <sub>2</sub> )	
	11.5	9.4 (O <sub>2</sub> )	
Matrimid:NMP:EtOH:THF 26.2:53.0:14.9:5.9 (M3)	0.1	33 (O <sub>2</sub> )	[49]
	40	2.2 (O <sub>2</sub> )	

### 2.1.2.3 Hollow Fiber Membrane Coating

Hollow fiber membranes are formed as a module to increase membrane area per unit volume. These membranes located inside the module must have high mechanical strength to resist high pressure applied to one side of the membrane for higher membrane permeance. In order to produce defect-free membranes, improve mechanical strength of membranes, overcome trade-off between membrane permeance and selectivity, hollow fiber membranes are coated [6,40,41]. Chen et al. reported that defect-free selective layer could not be formed without PDMS coating as a gutter layer which was also used for minimizing penetration of coating solution into the membrane pores and decreasing the surface roughness. This group coated substrate with non-spinnable PEBAX 1657 solution in order to enhance CO<sub>2</sub> separation performance of the hollow fiber membrane [40]. Kapantaidakis et al. showed that PDMS coating enhanced CO<sub>2</sub>/N<sub>2</sub> selectivity of hollow fiber membranes [41]. Table 2.9 shows the effect of coating of hollow fiber membranes on the gas separation performance of the membrane

Table 2.9 : The effect of coating of hollow fiber membranes to the gas separation performance of the membrane

Membrane code	Gas permeance (GPU)		Ideal Selectivity of CO <sub>2</sub> /N <sub>2</sub>	Reference
	CO <sub>2</sub>	N <sub>2</sub>		
PDMS/PAN	2151.7	228.1	9.43	[40]
PDMS/PAN/PEBAX	481.5	11.5	42.0	
PES:PI 80:20 Uncoated Dope A fiber (Air gap 10cm)	100	50	2	[47]
PES:PI 80:20 PDMS Coated Dope A fiber (Air gap 10cm)	40	1	40	

Gas separation performance of the hollow fiber membranes is directly related to the polymer type used for preparation of the membrane. Their performance could be enhanced by coating with different types of polymer. The CO<sub>2</sub> permeance and CO<sub>2</sub>/CH<sub>4</sub> ideal selectivity of Matrimid hollow fiber membranes ranges from 8.5 GPU to 14.7 GPU and 37 to 59.6, respectively [24,50]. Gas separation performance of the Fluorinated polyimides (6FDA) have the highest CO<sub>2</sub> permeance compared to other polyimides. The CO<sub>2</sub> permeance and CO<sub>2</sub>/CH<sub>4</sub> ideal selectivity of PDMS coated 6FDA-2,6-DAT hollow fiber membrane are 76 GPU and 63, respectively [50]. The CO<sub>2</sub> permeance and CO<sub>2</sub>/CH<sub>4</sub> ideal selectivity of PDMS coated 6FDA-Durane hollow fiber membrane are 373 GPU and 19.7, respectively [51].

Ismail research group produced pure PSF hollow fiber membranes. The CO<sub>2</sub> permeance and CO<sub>2</sub>/CH<sub>4</sub> ideal selectivity of these hollow fiber membranes ranges from 54.8 GPU to 88.2 GPU and 1.63 to 4.15, respectively. The CO<sub>2</sub> permeance and CO<sub>2</sub>/CH<sub>4</sub> ideal selectivity of PDMS coated hollow fiber membranes ranges from 38.1 GPU to 58.1 GPU and 13.6 to 41.5, respectively [13].

The Magueijo research group produced PSF hollow fiber membranes. The CO<sub>2</sub> permeance value and CO<sub>2</sub>/CH<sub>4</sub> ideal selectivity of pure PSF hollow fiber membrane 187 GPU and 1, respectively. The CO<sub>2</sub> permeance value and CO<sub>2</sub>/CH<sub>4</sub> ideal selectivity of PDMS coated PSF hollow fiber membrane are 85 GPU and 40.3, respectively. The CO<sub>2</sub> permeance value and CO<sub>2</sub>/CH<sub>4</sub> ideal selectivity of PSF mixed matrix hollow fiber membrane containing 5% xerogel 262 GPU and 0.83, respectively. The CO<sub>2</sub> permeance value and CO<sub>2</sub>/CH<sub>4</sub> ideal selectivity of PDMS coated this PSF mixed matrix hollow fiber membrane are 103 GPU and 33, respectively [52].

#### **2.1.2.4 Mixed Matrix Hollow Fiber Membranes**

Ceramic membranes and zeolite membranes have higher selectivity compared to polymeric gas separation membranes. However, production of mixed matrix membranes is more advantageous when the production cost and production difficulties of ceramic and zeolite membranes are taken into account. Mixed matrix membranes enables to combine the higher selectivity of porous fillers and the ease

of production of polymeric membranes. Zeolites, non-porous materials, carbon nano tubes, metal oxides and metal organic frameworks are different types of fillers used in the production of mixed matrix membranes. Fillers help increase membrane flux [53]. Homogeneous dispersion of the filler inside the polymer matrix and compatibility between filler and polymer matrix are critical problems confronted during the production of mixed matrix membranes. Surface modification is suitable for the solution of compatibility problem between organic and inorganic phases. Metal organic frameworks are more suitable for surface modifications thus; they are more preferable as filler [54,55]. According to type of filler used in different polymeric membranes, permeability and selectivity values were tabulated in Table 2.10.

Table 2.10: The effect of filler type to the gas separation performance of different types of polymeric membranes

<b>Polymer Type</b>	<b>Filler Type</b>	<b>Permeability/ Permeance (CO<sub>2</sub>)</b>	<b>Ideal Selectivity of CO<sub>2</sub>/CH<sub>4</sub></b>	<b>Reference</b>
Matrimid 5218	-	4.45 Barrer	37	[56]
	Zeolite 4A	5.98 Barrer	43	
	CMS	4.76 Barrer	48	
P84	-	0.83 Barrer	7	
	CNT	1.09 Barrer	11	
Matrimid 5218	-	11.3 Barrer	35	[55]
	GT 4A	9.17 Barrer	41.2	
Ultem	-	1.535 Barrer	37.9	[57]
	ZIF-8	11.1 Barrer	40.4	
PSF	-	65.24 GPU	17.15	[58]
	GO	74.47 GPU	29.90	
PI	-	87.6 GPU	12.8	[59]
	3% m Cu <sub>3</sub> (BTC) <sub>2</sub>	64.9 GPU	7.7	
	6% m Cu <sub>3</sub> (BTC) <sub>2</sub>	37.2 GPU	8.6	

Polysulfone (PSF) is widely used polymer for the production of biogas separation membranes. The performance of the polysulfone was improved by using filler. The Magueijo research group produced PSF hollow fiber membranes using carbon xerogel as filler. The CO<sub>2</sub> permeance and CO<sub>2</sub>/CH<sub>4</sub> ideal selectivity of pure PSF hollow fiber membrane are 187 GPU and 1, respectively. Addition of 5 % carbon xerogel increases CO<sub>2</sub> permeance to 262 but it decreases CO<sub>2</sub>/CH<sub>4</sub> ideal selectivity to 0.83 [52].

Koros research group produced asymmetric polyetherimide (ULTEM-100) hollow fiber membranes by dry-jet-wet quenching method. The CO<sub>2</sub> permeance is 14 GPU

for pure ULTEM -1000 hollow fiber membrane and 26 GPU for mixed matrix ULTEM -1000 hollow fiber membrane containing 17 % ZIF-8, respectively [60].



## CHAPTER 3

### EXPERIMENTAL METHODOLOGY

#### 3.1 Preparation of Pure PI Hollow Fiber Membranes

##### 3.1.1 Materials of PI Hollow Fiber Membranes

Polyimide resin (PI) was provided by Alfa Aesar Inc. The glass transition temperature, density and molecular weight are 305°C, 1.2 g/cm<sup>3</sup> and 80000 g/mol, respectively. Polyimide resins were dried in an oven at 80°C overnight prior to use for removal of moisture absorbed.

N,N-Dimethylformamide (DMF) (>99% purity) was purchased from Sigma Aldrich Inc. Tetrahydrofuran (THF) (>99.9% purity), ethanol (EtOH) (absolute for analysis) were purchased from Merck Inc. All chemicals were used as received without further purification.

##### 3.1.2 Preparation of Hollow Fiber Membranes

Dope solution was prepared by dissolving polyimide in the solvent mixture at 60°C by priming. In order to prepare 100 g PI dope solution with a composition of 30 PI:7 THF: 63 DMF (wt.%), 70 g solvent mixture was prepared than 5 g PI was added to 30 g once every two hours and stirred continuously with a magnetic stirrer overnight. Dope solution was degassed for 2 h at 60°C and stored at 60°C overnight before spinning. Bore liquid solution was prepared by mixing 90 wt. % of DMF and 10 wt. % distilled water. Pure PI hollow fiber membranes were prepared by dry/wet solution spinning process by using twin orifice spinneret as shown in Figure 3.1.

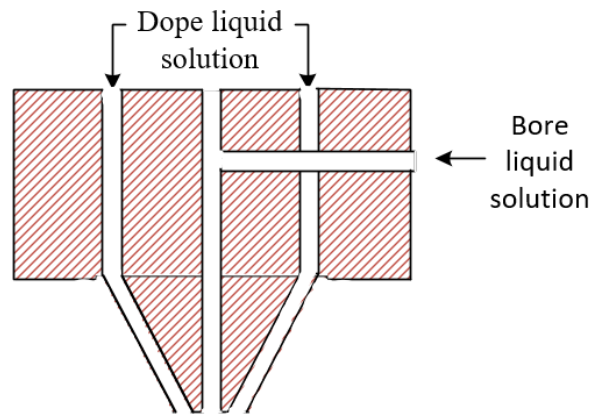


Figure 3.1. Schematic view of twin orifice spinneret

The spinneret was made by Yener Makina, OSTİM, Ankara. The inner and outer diameter of the spinneret were 0.3 mm and 1.2 mm, respectively. The bore liquid enters the spinneret through the inner channel and forms the bore part of the hollow fiber membrane. The dope liquid enters the spinneret through the annulus without contacting bore liquid until the spinneret outlet. Experimental set-up for hollow fiber spinning system was shown in Figure 3.2.

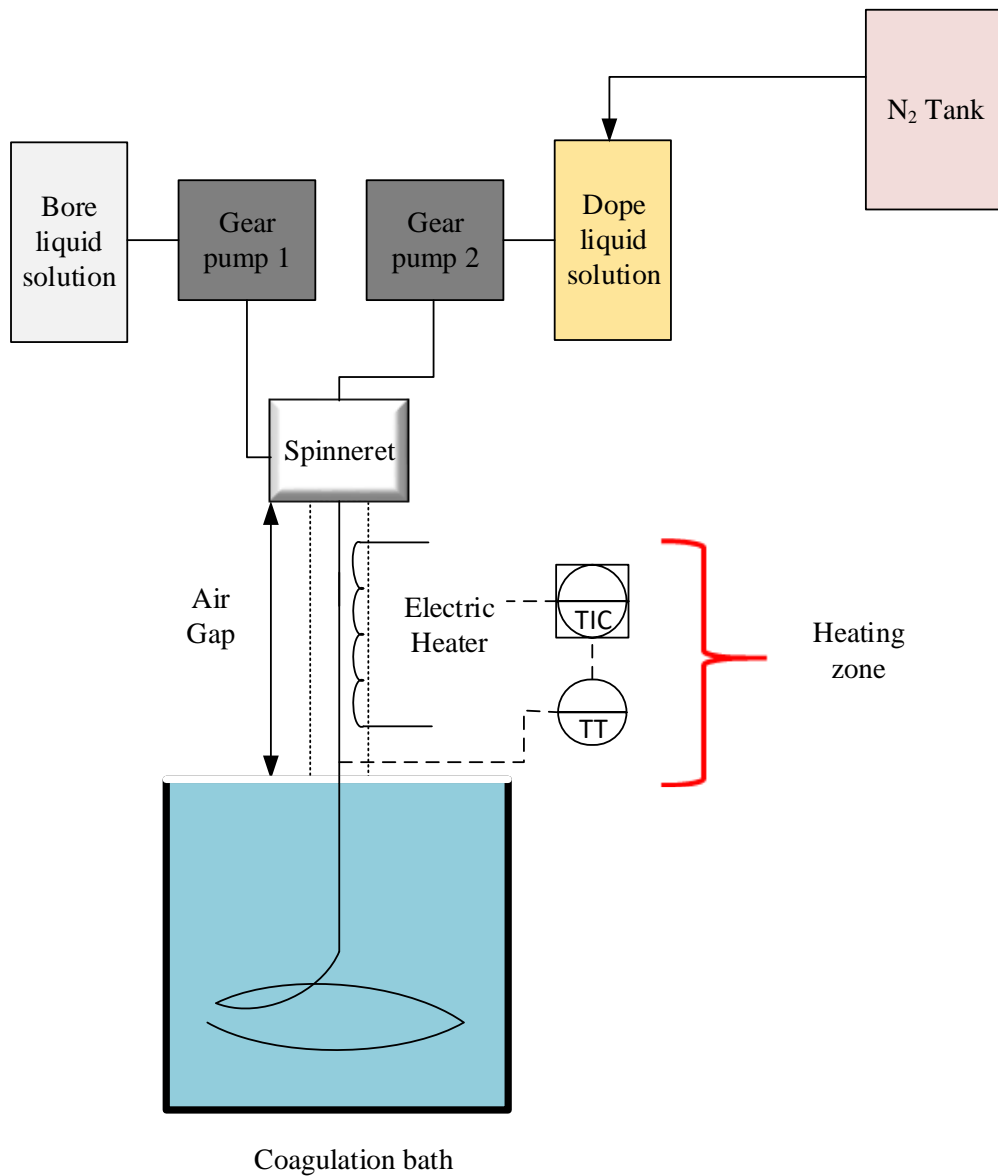


Figure 3.2. The schematic view of hollow fiber spinning system based on the free fall method

Dope liquid solution was pressurized to 1 bar g by using pressurized nitrogen (N<sub>2</sub>) gas. Dope and bore liquid solutions were pumped to the spinneret by using gear pumps whose speed could be controlled to adjust flow rates of the solutions as shown in Table 3.1. At the spinneret exit, hollow fiber membranes flowed through the air gap where the dry phase inversion occurs and into the coagulation bath where the wet phase inversion occurs. The heater was placed between spinneret and

coagulation bath in order to adjust heating zone temperature to 15°C or 35°C based on the selected spinning conditions.

Hollow fiber membranes produced by free fall method were washed with renewed distilled water for two days to remove residual solvent. Solvent exchange method was applied by using methanol for 1 h followed and fibers were dried at 120°C under vacuum for 12 h.

The bore liquid had a composition of 90 wt. % DMF and 10 wt. % distilled water throughout the study. The non-solvent in the coagulation bath was tap water and the bath temperature was 15±2°C.

The effect of dope liquid flow rate, bore liquid flow rate, air gap height, THF content of dope liquid and the temperature of the convective heating zone on the hollow fiber membrane morphology and gas separation performance were examined. According to the spinning parameters, membrane codes were shown as PI.BX.DY.AGZ where B, D, AG indicates bore flow rate, dope flow rate and air gap, respectively. X and Y showed the pump settings. The real flow rates corresponding the pump settings were shown in Table 3.1.

Table 3.1 Real flow rates corresponding the pump settings used for defining membrane codes

<b>Pump Adjustment</b>	<b>Real Flow rate (g/min)</b>
B20	0.50
B30	0.75
B40	1.00
D30	1.0
D100	2.6

For instance, PI.B20.D30.AG6 membrane code used for defining PI hollow fiber membrane prepared by adjusting bore flow rate to 0.50 g/min, dope flow rate to 1.0 g/min, and air gap height to 6 cm.

### 3.1.3 Hollow Fiber Membrane Coating Methodology

In order to seal membrane defects and enhance membrane selectivity, hollow fiber membrane was coated with Pure PEBAX 1657 solution by dip coating method. The composition of coating solution was shown in Table 3.2. Hollow fiber membrane was soaked into the coating solution for 10 s, then placed into 60°C oven for 8 h.

## 3.2 Preparation of PEBAX 1657 Membranes, Flat Sheet PES Support Membranes, and PEBAX 1657 and PEBAX 1657/ZIF-8 coated PES Support Membranes

### 3.2.1 Materials for Flat Sheet Membrane Preparation

Ultrason E6020P Polyethersulfone (PES) was provided by BASF Inc. The glass transition temperature, apparent density and molecular weight are 225°C, 0.25 g/cm<sup>3</sup> and 75000 g/mol, respectively. The simple structure of PES was shown in Figure 3.3.

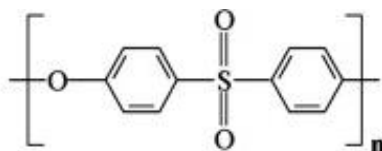


Figure 3.3. Structural formula of PES [61]

PEBAX (®) MH 1657 resin consisting of 60 wt.% PEO and 40 wt.% PA6 was purchased from Arkema Inc. The glass transition temperature and density are -40°C and 1.14 g/cm<sup>3</sup> respectively. The simple repeating unit of PEBAX 1657 was shown in Figure 3.4 where x and y are equal to 0.6 and 0.4, respectively. Polymer resins were dried in the oven at 80°C overnight prior to use for removal of moisture absorbed.

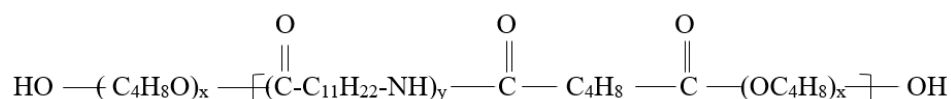


Figure 3.4. Structural formula of PEBAX 1657 [28]

Zinc nitrate hexahydrate ( $\text{Zn}(\text{NO}_3)_2 \cdot 6\text{H}_2\text{O}$ , 98%) and sodium hydroxide pellets were purchased from Acros Inc. Methanol ( $\text{CH}_3\text{OH}$ ) and isopropyl alcohol (IPA) were obtained from Sigma Aldrich Inc. 2-methylimidazole ( $\text{H}_{\text{mim}}$ , 99 %) was purchased from Merck Inc. 4-Nitroanilin (PNA) (>99.9 % purity) was purchased from Aldrich Inc. All chemicals were used as received.

### 3.2.2 Synthesis Method of ZIF-8 crystals

ZIF-8 crystals were synthesized with molar composition of  $1\text{Zn}^{2+} : 7.9 \text{H}_{\text{mim}} : 695 \text{CH}_3\text{OH}$  as explained in Keser Demir et al., 2014 [62]. According to this molar composition, zinc nitrate hexahydrate and 2-methylimidazole solutions were prepared by dissolving them in methanol separately. Solutions were mixed rapidly in a sealed batch reactor. The synthesis was completed by stirring at 300 rpm for 1h at room conditions. ZIF-8 crystals were precipitated from reaction mixture by centrifuging at 6000 rpm for 5 min. Recovered crystals were washed with methanol twice in order to remove unreacted reactants by centrifuging at 6000 rpm for 20 min. Purified ZIF-8 crystals were stored in methanol to prevent agglomeration of crystals during addition of them to membrane casting solution.

### 3.2.3 Preparation of Flat Sheet Membranes

The flat membranes were prepared by solution-casting method. In order to produce PEBAX 1657 based flat membranes, ethanol/water (70/30 wt. %) mixture was used as solvent. The composition of casting solution is shown in Table 3.2. The weight percent of ZIF-8 crystal and PNA was adjusted based on the PEBAX 1657 amount in the solution.

Table 3.2. The recipe for flat membrane preparation

<b>Membrane Code</b>	<b>PEBAX 1657 (wt. % of solvent)</b>	<b>ZIF-8 (wt. % of PEBAX 1657)</b>	<b>PNA (wt. % of PEBAX 1657)</b>
Pure PEBAX 1657	4	0	0
PEBAX 1657/ZIF-8	4	10	0
PEBAX 1657/PNA	4	0	4
PEBAX 1657/ZIF-8/PNA	4	10	4

For the preparation of PEBAX 1657 based flat membrane casting solution, PEBAX 1657, ZIF-8 and PNA were dissolved in the solvent at 60°C regarding compositions shown in Table 3.2. The solution was vigorously stirred for 12 h at 60°C and ultrasonicated for 2 h. 25 ml solution was casted onto disposable weighing pan with a diameter of 10 cm. The solvent was evaporated in 60°C oven for 8 h. The resulting membrane was peeled off and stored in dry ambient conditions.

In order to prepare flat sheet PES membrane solution, PES were dissolved in DMF at 60°C by priming. In order to prepare 10 g PES flat sheet membrane solution, 0.5 g PES were added initially to 7 g DMF portion-wise up to 3 g and stirred continuously with a magnetic stirrer overnight to obtain a 30 wt. % PES solution. The homogenous solution was ultra-sonicated for 2 h and kept at ambient conditions overnight. PES solution was cast onto glass plate by using a 500- $\mu$ m-casting knife. The prepared polymeric films were placed into coagulation bath overnight in order to prepare asymmetric flat sheet membranes similar to structure of prepared hollow fiber membranes. Considering the composition of non-solvent in the coagulation bath, membranes code were labeled as shown in Table 3.3.

Table 3.3. Membrane codes based on coagulation bath compositions

<b>Membrane Code</b>	<b>Non-solvent composition (IPA/ Water wt. %)</b>
PES/IPA	100 wt. % IPA/ 0 wt. % Water
PES/IPA/Water	50 wt. % IPA/ 50 wt. % Water
PES/ Water	0 wt. % IPA/ 100 wt. % Water

The membrane was soaked into distilled water bath overnight to remove IPA and DMF from the pores of the membrane and then was dried in a vacuum oven at 120°C, under vacuum for 24 h.

### **3.2.4 Coating of Flat Sheet PES membranes by PEBAX 1657 and PEBAX 1657/ZIF-8 solution**

In order to imitate coating of the hollow fiber membranes to enhance their membrane gas separation performance, PES flat sheet membranes were coated with Pure PEBAX 1657 and PEBAX 1657/ZIF-8 solution by dip coating method due to complex geometry of hollow fiber membranes. PES flat sheet membrane was soaked into coating solution for 10 s, then placed into 60°C oven for 8 h.

## **3.3 Characterization of Pure and Mixed Matrix Membranes and ZIF-8 Crystals**

### **3.3.1 Fourier Transform Infrared Spectroscopy (FTIR)**

FTIR spectra of PEBAX 1657 based membranes were scanned at 450-4000  $\text{cm}^{-1}$  with attenuated total reflection technique by FTIR spectrometer (EQUINOX 55).

### **3.3.2 N<sub>2</sub> Adsorption Desorption Isotherms**

The N<sub>2</sub> adsorption-desorption isotherms were obtained using Micromeritics Tristar II equipment at 77 K. In order to prepare ZIF-8 samples, they were degassed at 135°C for 24 h under vacuum. According to microstructural characteristic of ZIF-8 crystals, the BET surface area was calculated.

### **3.3.3 Thermal Gravimetric Analysis (TGA)**

The thermal stabilities of the membranes were examined by thermal gravimetric analysis. Shimadzu DTG-60H was used to examine the weight changes as a function of temperature over time in air with heating rate of 10°C/min from 50°C to 650°C.

### **3.3.4 Scanning Electron Microscopy (SEM)**

The morphology of the ZIF-8 crystals, pure and mixed matrix membranes were observed by using SEM in METU Central Laboratory with a QUANTA 400F Field Emission series scanning device. The membranes were fractured by tweezers under liquid nitrogen to prevent stretching of the membrane cross section. The membrane samples and ZIF-8 crystals were sputter-coated with thin film of gold-palladium.

### **3.3.5 X-ray Diffraction (XRD)**

Rigaku MiniFlex X-ray powder diffractometer with a radiation source of Cu-K $\alpha$  at a scan rate of 2°/min was used for phase identification of solid products. XRD pattern of synthesized solid products were compared with the one belonging to ZIF-8 crystal given in the literature [62]. Area under the characteristic peaks of ZIF-8 at Bragg angles between 0°-40° which belongs the planes of (011), (002), (112), (022), (013), (222), (114), and (134) were calculated to analyze reproducibility of the crystallinity of the synthesized ZIF-8 crystals.

## **3.4 Gas Permeation Measurements**

The gas permeation properties of hollow fiber membranes and flat membranes for single gases including H<sub>2</sub> (Linde, 99.99 %), N<sub>2</sub> (Linde, 99.99 %), CO<sub>2</sub> (Linde, 99.9 %), and CH<sub>4</sub> (Linde, 99.9 %) were determined using a constant volume variable pressure method. The schematic diagram of the test setup which is made up of a vacuum pump, a pressure gauge, a membrane cell, a pressure transducer, a computer with suitable electrical connections and pneumatic fittings (6 mm) was shown in Figure 3.5.

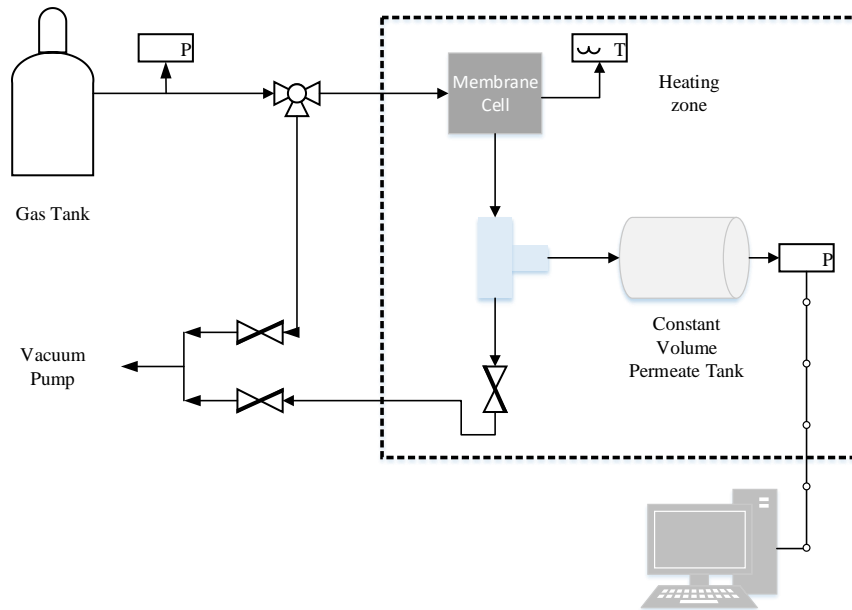


Figure 3.5. The schematic diagram of the gas permeation test setup

A stainless steel membrane cell for flat membranes gas permeation test shown in Figure 3.6 was made in the Chemical Engineering Department Machine Shop. The effective membrane area was  $13.2 \text{ cm}^2$ . The volume of the permeate tank was  $30.64 \text{ cm}^3$ .

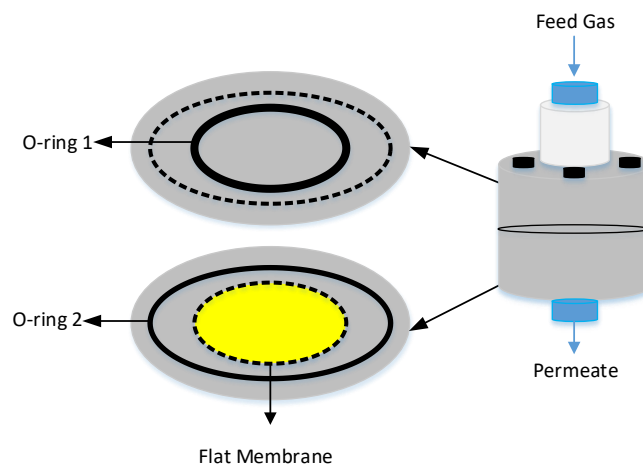


Figure 3.6. Schematic view of membrane cell for the flat sheet membrane gas permeation test

Two Viton O-rings were located inside the membrane cell to prevent any gas leakage from both the feed side and permeate side during gas permeation test. The design of the membrane cell for gas permeation test of hollow fiber membranes were different than the one for flat membranes as shown in Figure 3.6 and Figure 3.7.

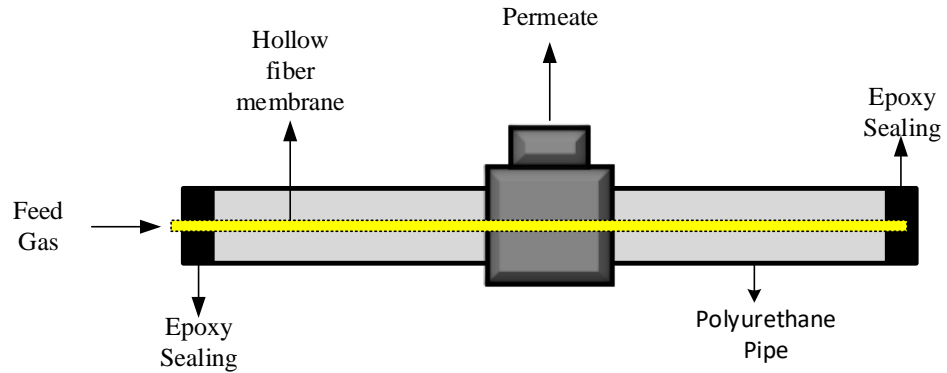


Figure 3.7: Schematic view of membrane cell for the hollow fiber membrane gas permeation test

Hollow fiber membrane was located inside the polyurethane pipe. The one side of the hollow fiber membrane was completely sealed with epoxy. Test gas was fed to the bore side of the hollow fiber by sealing shell side of the membrane with epoxy.

Gas permeation tests were carried out under 3 bar trans membrane pressure (TMP) and 35°C. In order to initialize membrane gas permeation test, the feed and the permeate side of the membrane was vacuumed for 2 h by using vacuum pump as shown in Figure 3.5 to remove gas molecules remaining inside the pipes and membrane structure. The feed pressure of the membrane module was kept constant during gas separation performance tests. The pressure at the permeate side was recorded as a function of time by using a pressure transducer connected to constant volume permeate tank and computer by using Opik04 program. A sample calculation for membrane gas permeation test was given in Appendix A.



## **CHAPTER 4**

### **RESULTS AND DISCUSSION**

#### **4.1 Characterization of ZIF-8 crystals**

##### **4.1.1 X-ray Diffraction (XRD)**

Phase identification of synthesized solid particles was carried out by X-ray powder diffractometer. Synthesized particles were dried at 80°C oven overnight to remove any residual solvent. Dry crystals were ground and activated at 180°C for 12 h. X-ray patterns of the reference and synthesized particles were shown in Figure 4.1 [62]. As a sample code, synthesis 1 and synthesis 2 indicate synthesized particles at different batches.

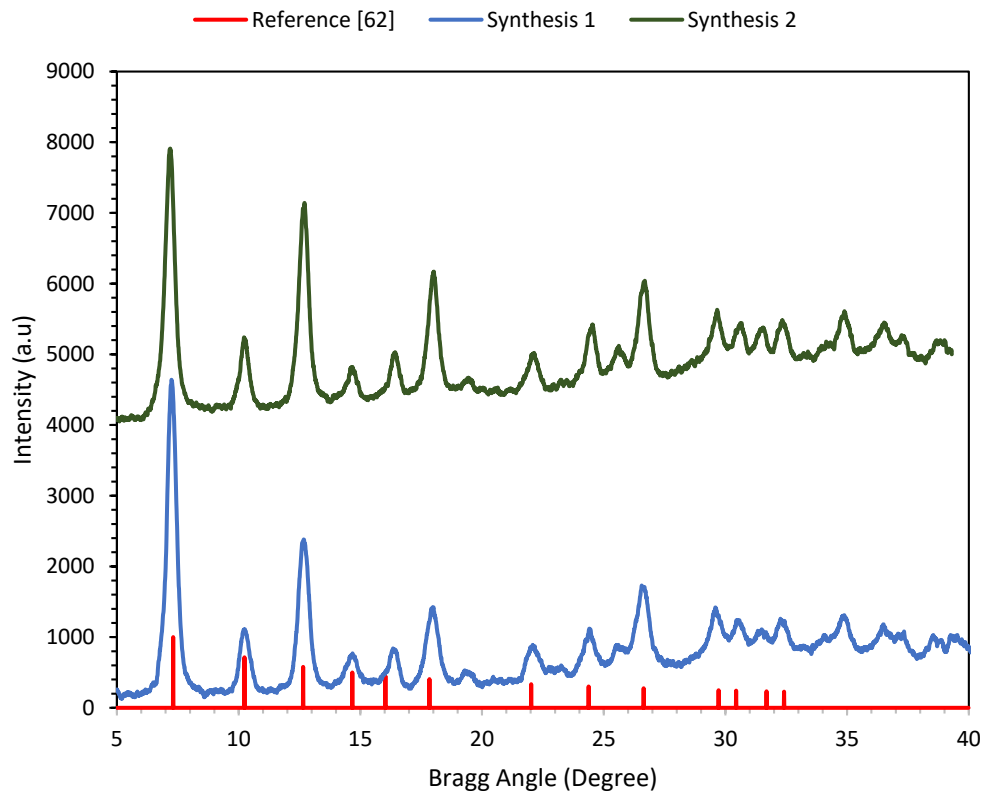


Figure 4.1. X-ray pattern of ZIF-8 crystals

The characteristic peaks of synthesized crystals matched with those of reference ZIF-8 crystals, indicating that ZIF-8 crystals were synthesized successfully. In order to analyze reproducibility of the crystallinity of synthesized ZIF-8 crystals, the area under the diffraction peaks on the patterns of synthesized ZIF-8 crystals were calculated (Table 4.1).

Table 4.1. Total peak area under the characteristic peaks of synthesized ZIF-8 crystals

Planes of Peaks	Peak areas	
	Synthesized 1	Synthesized 2
(011)	1500	1333
(002)	281	293
(112)	726	980
(022)	76	121
(013)	111	152
(222)	362	572
(114)	30	59
(134)	416	447
<b>Total Peak Area</b>	<b>3502</b>	<b>3957</b>

Those samples were analyzed in different days, hence the difference in peak areas can be attributed to the sample preparation for XRD analysis, determination of background radiation, beginning and final points of a peak and to the slight changes in the XRD settings especially voltage and current. Therefore, it could be concluded that ZIF-8 was reproducibly synthesized with high crystallinity.

#### 4.1.2 Scanning Electron Microscopy (SEM)

The morphology of ZIF-8 crystals was determined by SEM analysis (Figure 4.2) ZIF-8 crystals were well dispersed and have hexagonal shape coherent with the literature. The average particle size of ZIF-8 crystals was measured as  $69 \pm 14$  nm by counting 50 particles. The average particle size was similar to the size of ZIF-8 crystals synthesized by Keser et. al [62] from synthesis solution with a molar composition of  $1\text{Zn}^{2+}: 7.9 \text{H}_{\text{mim}}: 695 \text{CH}_3\text{OH}$ .

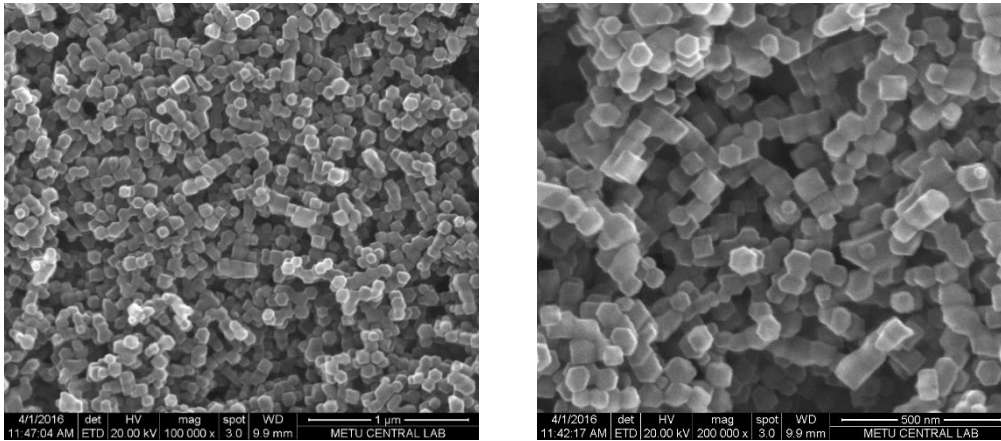


Figure 4.2. SEM micrographs of ZIF-8 crystals

### 4.1.3 N<sub>2</sub> Adsorption Desorption Isotherms

The N<sub>2</sub> adsorption-desorption isotherms, which were obtained using Micromeritics Tristar II equipment at 77 K, are shown in Figure 4.3. Prior to adsorption measurements, ZIF-8 crystals were degassed at 135 °C for 24 h under vacuum.

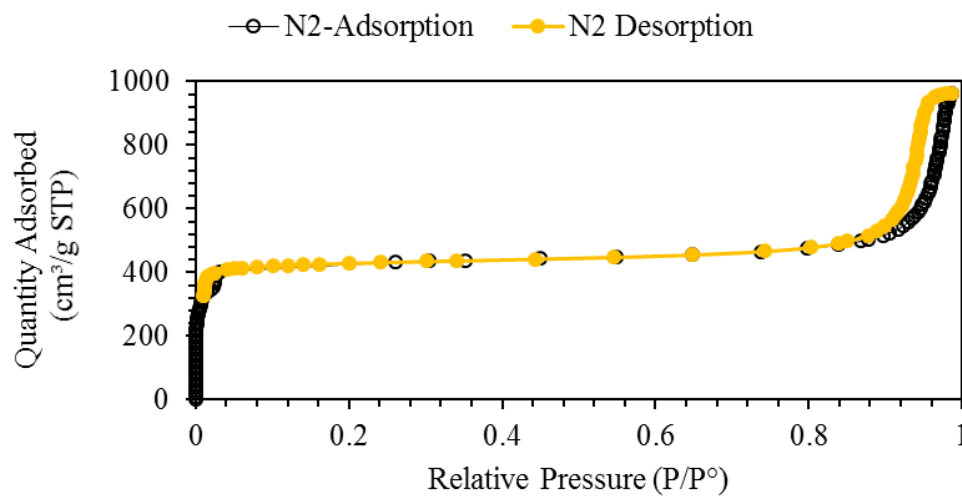


Figure 4.3. N<sub>2</sub> adsorption-desorption isotherms of synthesized ZIF-8 crystals

Figure 4.3 shows that ZIF-8 has Type I  $N_2$  adsorption isotherm and no hysteresis was observed in the desorption. This behavior is characteristic to microporous materials [62]. The BET surface area, which was found as  $1349 \text{ m}^2/\text{g}$  is similar to literature values. The BET surface area of ZIF-8 crystals reported in the literature varies between  $744 \text{ m}^2/\text{g}$  and  $1630 \text{ m}^2/\text{g}$  [62]. The high BET surface area of synthesized ZIF-8 crystals also showed that they were well crystallized.

## 4.2 Selection of the Type of Polymer for the Preparation of Membranes

Types of the polymer used for membrane preparation influences the gas separation performance of the membrane since permeability and selectivity are intrinsic material properties of the polymers [4,6]. The Robeson plot for  $\text{CO}_2/\text{CH}_4$  pair (Figure 4.4) shows the gas separation performance of polymers used in this study.

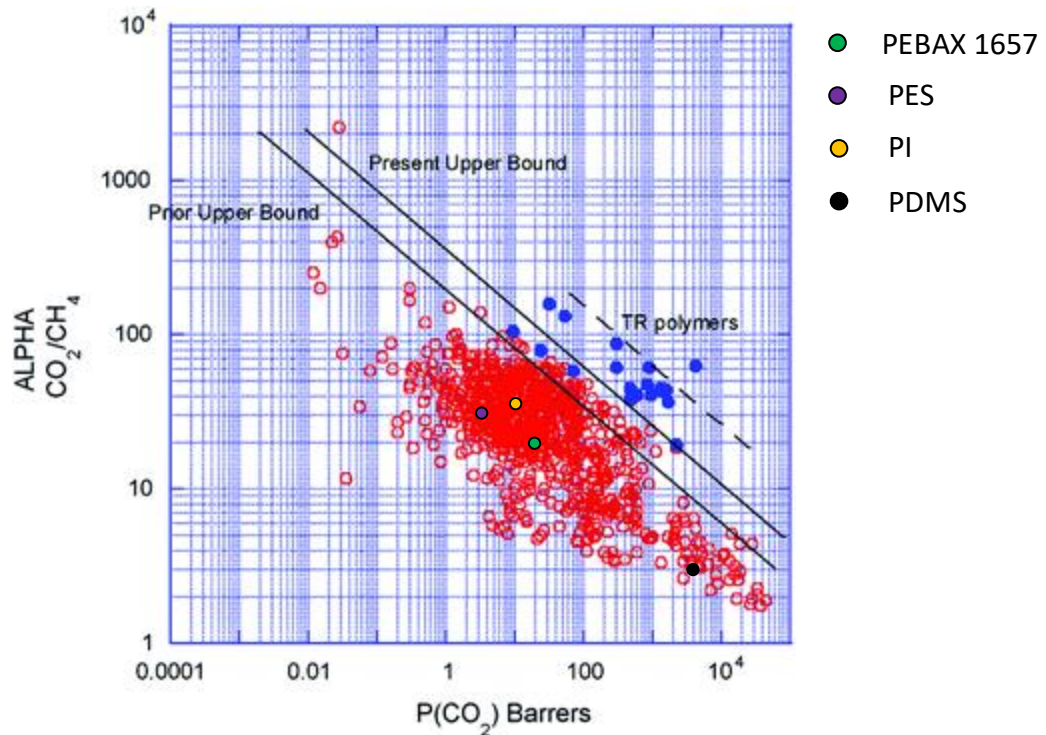


Figure 4.4. Comparison of  $\text{CO}_2/\text{CH}_4$  ideal selectivity and  $\text{CO}_2$  permeability for different types polymeric membranes compared to Robeson upper bound [16,63,64]

Nearly, 80 % of the biogas refining membranes are made of polyimide and cellulose acetate due to their high permeability and selectivity values [5,7]. In order to prepare hollow fiber membrane, spinnable polymers should be selected. Both polyimide and cellulose acetate are spinnable polymers but polyimide shows better gas separation performance [4]. Therefore, polyimide was used for the preparation of hollow fiber membranes.

For the preparation of mechanical support, PES is widely used since it can be easily manufactured in various configurations with a wide range of pore sizes and structures [25]. Besides, PES have good chemical and thermal stability [24]. Therefore, as an economical polymer with desired properties, PES was used for the preparation of support membranes.

As a high flux rubbery polymer, it was possible to use PDMS for sealing membrane defects in order to enhance the gas separation performance of membranes [13,51,52]. The main objective of biogas refining processes is to separate CO<sub>2</sub> from CH<sub>4</sub> to increase calorific value and decrease transportation cost [4]. PEBAX 1657 has high CO<sub>2</sub> affinity, which increases CO<sub>2</sub>/CH<sub>4</sub> selectivity of the membranes [14]. Therefore, PEBAX 1657 was used for coating of the membranes in order to enhance CO<sub>2</sub> separation performance of them.

### **4.3 Characterization and Gas Separation Performance of Polyimide Hollow Fiber Membranes**

In this study, pure PI hollow fiber membranes were prepared by dry/wet spinning and the effect of spinning conditions on the morphology of membranes was investigated. The spinning conditions were dope solution flow rate, bore liquid flow rate, addition of more volatile solvent (THF) to dope solution, air gap height, and heating zone temperature.

The morphology of the hollow fiber membranes was compared based on the bore diameter, membrane outside diameter and selective layer thickness, which were measured by a software called Image J. The effect of spinning conditions on the type of macrovoids and the number of macrovoids on the supporting layer were reported

semi-quantitatively. Figure 4.5 shows the SEM image of a hollow fiber membrane prepared from a dope solution with a composition of 30% PI:7% THF: 63% DMF (all percentages are by weight). The properties used for morphological analysis were shown on the Figure 4.5.

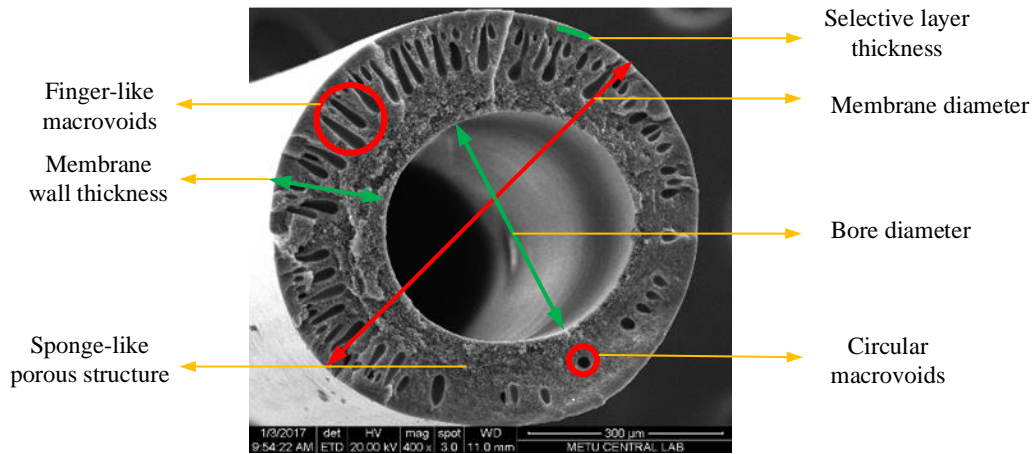


Figure 4.5. The SEM images of hollow fiber membrane produced by using 35°C convective heating zone with the mass ratio of 30 PI: 7 THF: 63 DMF PI.B20.D30.AG 6

As shown in Figure 4.5, the bore (tube inside) and membrane (outside) diameters were assessed as a morphological property. Although the membranes were prepared using the same spinneret with inner and outer orifice diameters of 300 and 1200 μm, respectively the membrane diameter of hollow fibers changed between 608 μm and 1182 μm depending on the spinning conditions as shown in the SEM images between Appendices F and J. Besides, the hollow fiber membranes do not have perfect circular cross-section due to asymmetry in the spinneret.

The most important morphological property is apparently the skin layer thickness, which is a dense layer responsible from the selective permeation of gas molecules through the membrane. The skin layer can be formed either on the outer surface or on the inner surface of membrane by arranging the spinning conditions, besides the

thickness of skin layer depends on the spinning conditions, as well. In the present study, the skin layer was formed on the outer surface, and the parameters influencing the thickness and compactness of skin layer was investigated. For morphological analysis of membranes, bore and membrane diameters and the skin layer thickness were measured at least 10 different points and averaged to report.

A gas separation membrane is exposed to high-pressure gases for higher membrane fluxes. A hollow fiber membrane composed of a dense skin layer and a supporting porous layer underneath the skin layer. Although the main function of supporting layer is to provide mechanical stability, it should also show low resistance to gas permeation. A membrane with a selective skin layer is expected to have highly permeable support layer. On the other hand, Brown et al. suggested a membrane having a support layer consisting of sponge-like structured closed pores. The wall of closed pores exhibits the properties of the skin layer and contribute to the gas separation. On the other hand, large interconnected voids with finger-like or circular shape are not desired since they decrease the mechanical strength of the membrane. Besides, finger-like voids provide additional gas transfer resistance if they have skin layer [65]. This morphology suggested by Brown et al. could be useful if there is no selective skin layer on the membrane surface. All the membranes prepared in the present study had sponge-like pore structure with some finger-like or circular macrovoids. The number of macrovoids on the supporting layer was determined semi-quantitatively based on SEM images. The scale has 3 grades as “high”, “medium” and “low” for a membrane with many, some and few macrovoids based on their covered area of the supporting layer, respectively. In addition, the number of finger-like macrovoids was analyzed semi-quantitatively with a 3-grade scale as follows: “majority” indicating that most of the macrovoids are finger-like, “equality” indicating that the number of finger-like and circular macrovoids are similar and “minority” indicating that most of the macrovoids are circular.

#### **4.3.1 Change of Membrane Dimensions with Spinning Conditions**

Hollow fiber membranes were prepared using two different spinning conditions, which includes dope and bore liquid flow rates, THF content of the dope solution, air gap height, and heating zone temperature. Figure 4.6 and Figure 4.7 show that

the maximum membrane diameter was 1182  $\mu\text{m}$ , which was obtained when the respective bore and dope solution flowrates were 0.75 and 1 g/min, 12 cm air gap height, dope solution contains no THF and the heating zone temperature was 15°C. On the other hand, the minimum membrane diameter was 608  $\mu\text{m}$ , which was obtained if the respective bore and dope solution flowrates were 0.5 and 1 g/min, air gap height was 20 cm, no THF exists in the dope solution and the heating zone temperature was 35°C.

The results indicate that the effectiveness level of those variables on the membrane diameter decreases in the order of temperature>air gap height>bore and dope solution flow rates> THF content. As the heating zone temperature or air gap height decreased, membrane diameter increased, whereas addition of THF to the dope solution had an inverse effect on the diameter. Membranes produced from dope solutions containing THF has smaller diameter than those prepared without THF.

The results also suggest that bore and dope solution flow rates should be considered together to evaluate the effect of them on the membrane diameter. If spinning is carried out at a high dope or low bore flow rates, a change in the bore or dope flow rate, respectively, has no effect on the membrane diameter. On the other hand, if the spinning is carried out at low dope and high bore flow rates, change in the dope or bore flow rate affect the membrane diameter with an opposite trend. Figure 4.6 and Figure 4.7 also show the bore diameter of membranes. The effect of spinning conditions on the bore diameter are more clear than that on the membrane diameter. As the temperature was decreased and bore flow rate was increased, membranes with larger bore diameter were obtained. Similarly, membranes with larger bore diameter were obtained from dope solutions, which does not contain THF. No effect of dope solution flow rate was observed on the bore diameter.

All those parameters, especially temperature and THF content may have strong influences on the viscosity and die-swell of dope solution at the exit of spinneret, which may cause an extension or shrinkage on the diameters. Increase in air gap height increases the length of the hollow fiber membranes suspended from spinneret. Gravitational force exerted on the nascent hollow fiber membrane causes higher stretching, which influences the spinning rate of the hollow fiber membrane.

Reduction in the membrane diameter with increasing air gap height could be explained by a result of higher spinning rate of the nascent hollow fiber membrane [66,67,68].

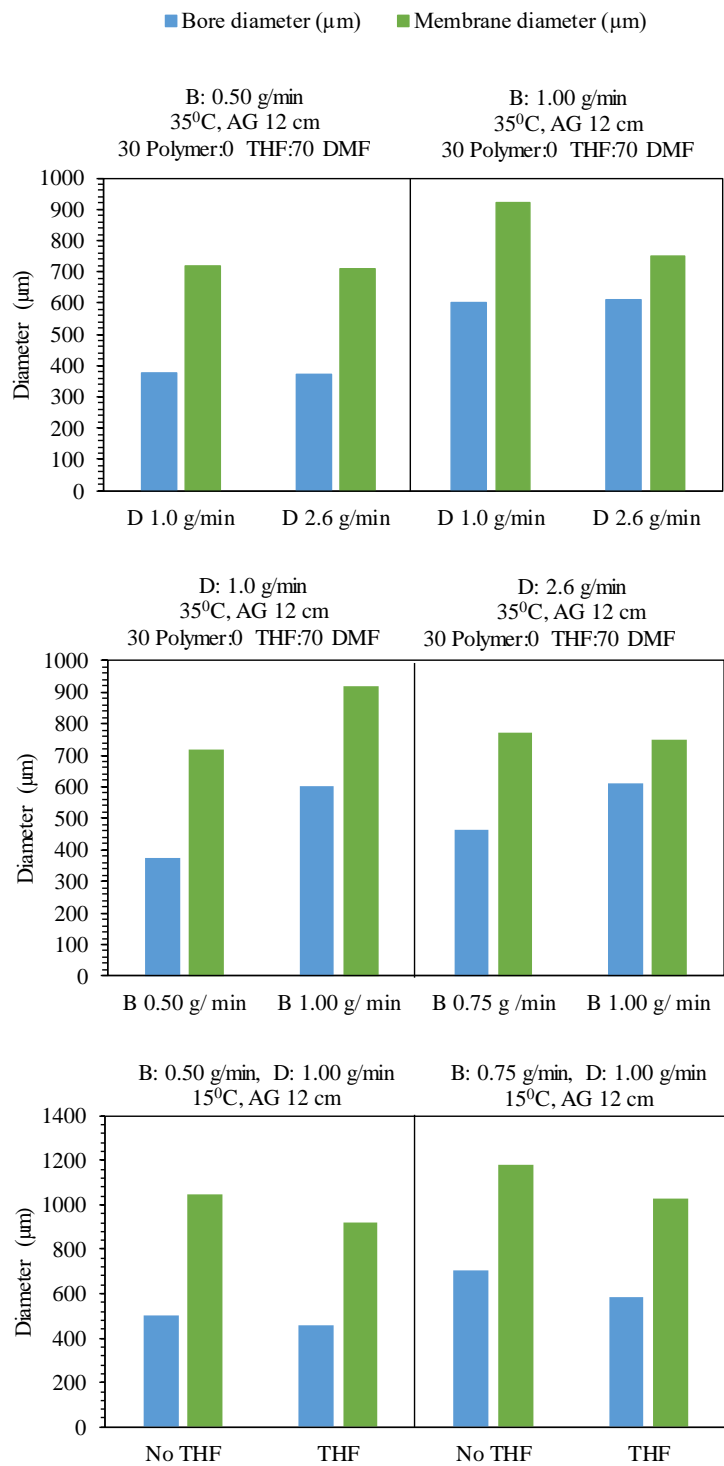


Figure 4.6. The effect of dope and bore flow rate, and THF content of the dope solution on the bore and membrane diameter

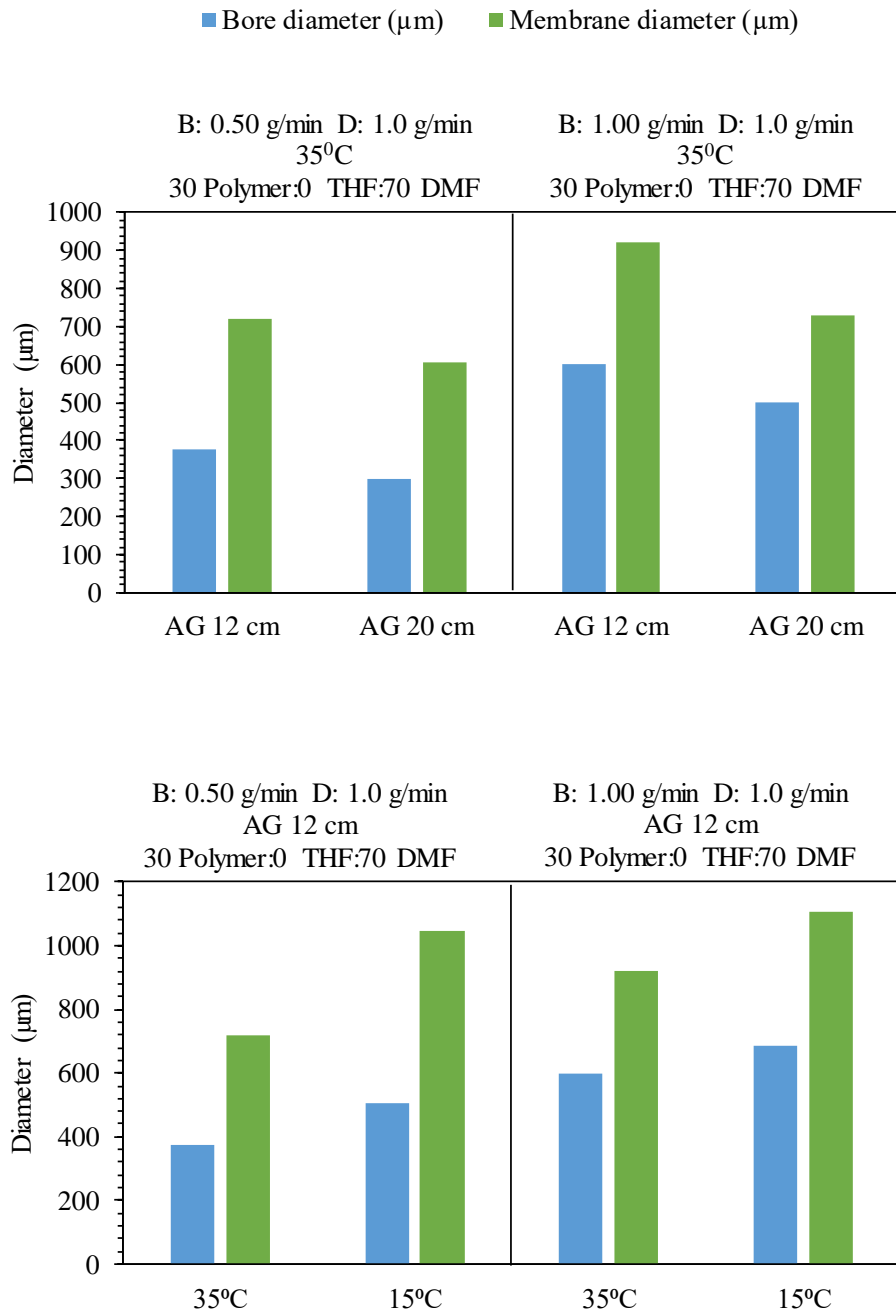


Figure 4.7. The effect of air gap height and temperature on the bore and membrane diameter

### 4.3.2 Change of skin layer thickness with spinning conditions

Hollow fiber membranes were prepared with different bore and dope flow rates, air gap height, heating zone temperature and THF contents. Figure 4.8 and Figure 4.9 show the change of skin layer thickness with those spinning conditions. A membrane with the thickest skin layer was 21  $\mu\text{m}$ , which was obtained from spinning with respective bore and dope solution flow rates of 0.5 and 1 g/min, air gap height of 12 cm, heating zone temperature of 15°C. There was THF in the dope solution. On the other hand, most of the other spinning conditions yielded membranes with a skin layer of  $4\pm 2$   $\mu\text{m}$ .

The results clearly indicate that temperature and THF content have strong influence on the skin layer thickness. THF (tetrahydrofuran) is a more volatile solvent with a boiling point of 66°C than DMF, which has a boiling point of 153°C. THF addition leads to fast evaporation from the dope solution causing difference in local polymer concentration and delayed liquid-liquid demixing in phase inversion [65,66], which is expected to result in formation of a denser layer and thicker skin layer. The experiments investigating the effect of THF showed that there is a limiting bore flow rate. During the spinning with low bore flow rate, membrane prepared from dope with THF had a skin layer thickness of 21  $\mu\text{m}$ , whereas at high bore flow rate, membranes had a skin layer thickness of only 1  $\mu\text{m}$  regardless of THF content.

Behind all the discussion on the effect of THF, the relative humidity of ambient air, which cannot be controlled, should also be considered since ambient conditions might change the membrane formation mechanism. Water vapor may penetrate into the dope solution and cause phase inversion during dry-spinning. Therefore, the effect of THF may be obscured by the high humidity of ambient air.

Temperature of heating zone is likely to have a similar effect, that is, evaporation of solvent and delayed liquid-liquid demixing. Our experiments carried out at different temperatures without using THF in the dope solution showed that membrane prepared at 15 and 35°C have skin layer thicknesses of 2 and 6  $\mu\text{m}$ , respectively.

The bore and dope flow rates should again be considered together to evaluate the effect of them on the skin layer thickness. The results suggested that at high dope and bore flow rates, thicker membranes were obtained, but at low dope and bore flow rates, the skin layer thickness was small.

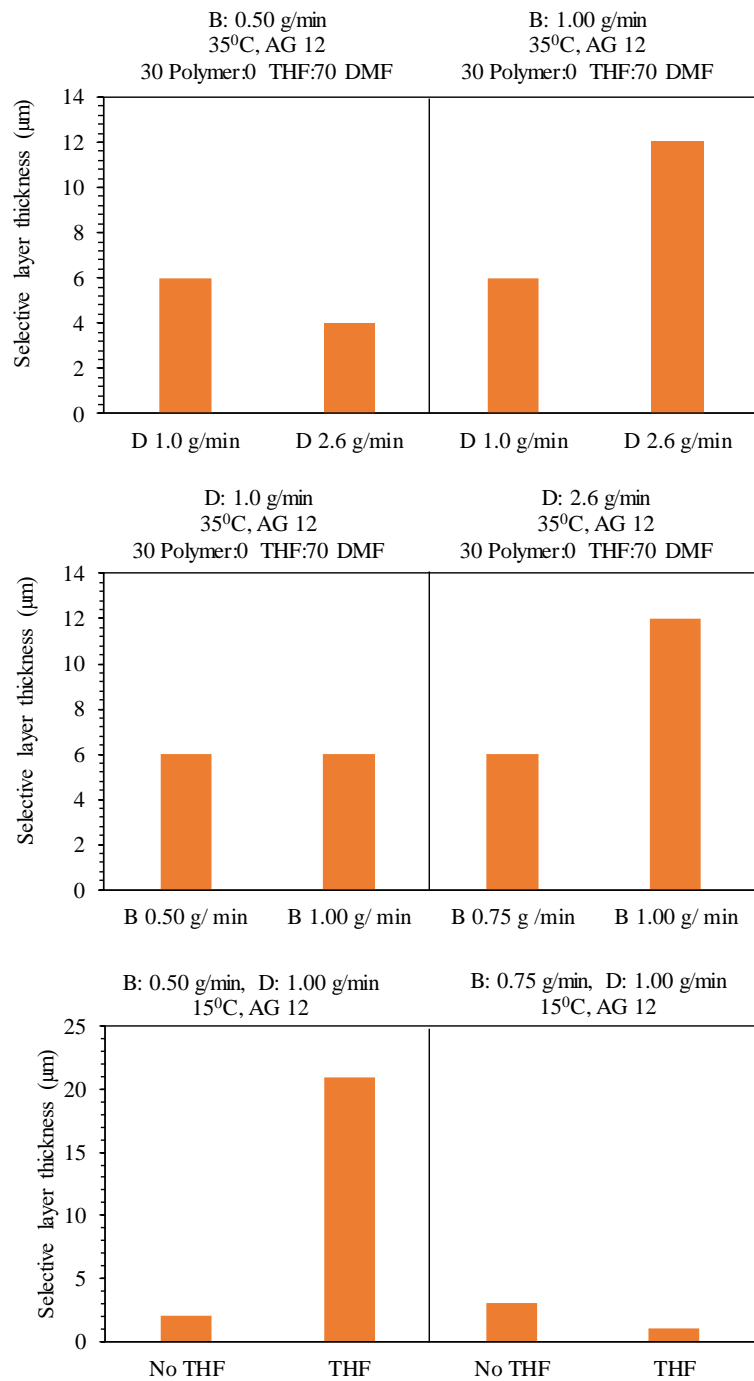


Figure 4.8. The effect of dope and bore flow rate, and THF content of the dope solution on the selective layer thickness

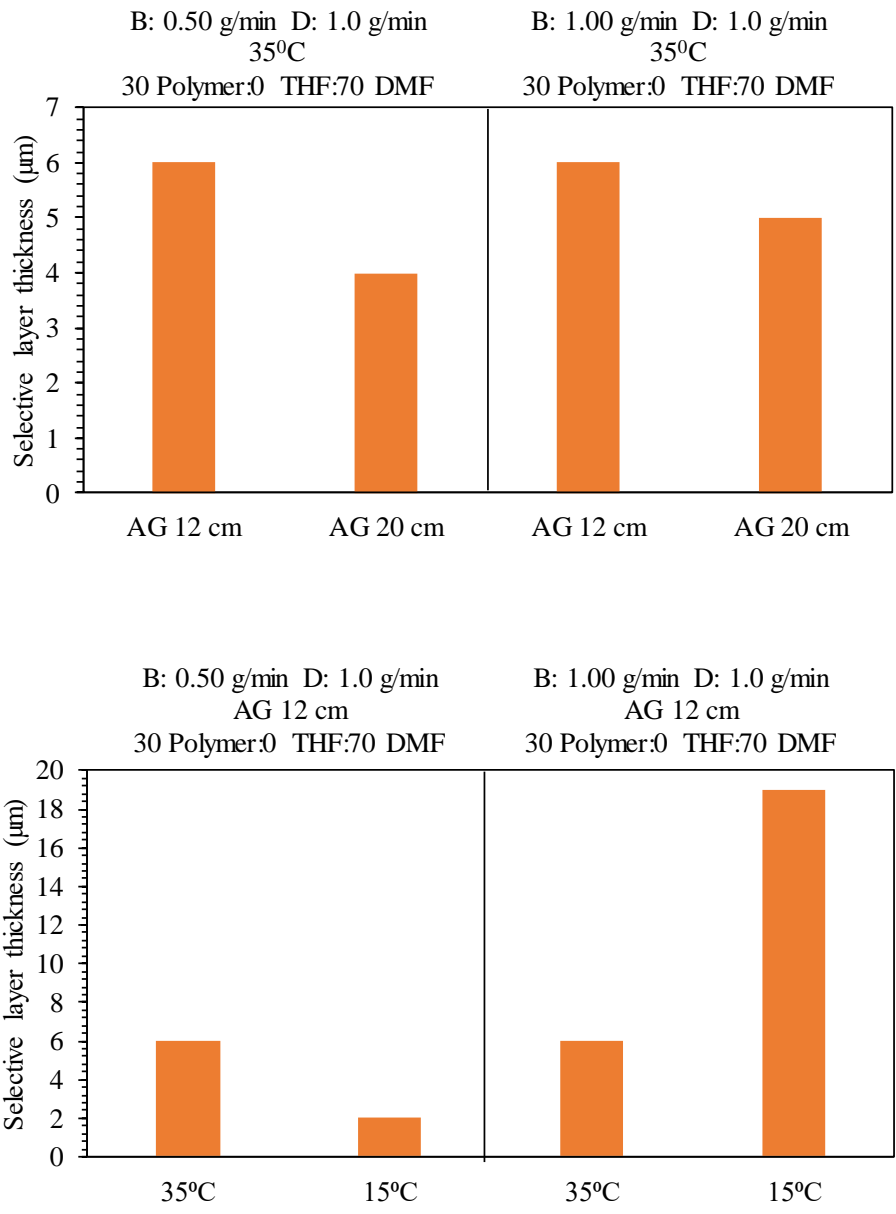


Figure 4.9. The effect of air gap height and temperature on the selective layer thickness

### 4.3.3 The Effect of Spinning Conditions on the Macrovoid Structure of Membranes

Table 4.2-Table 4.6 show the effect of spinning parameters on the void structure of the membranes. Bore liquid flow rate has no substantial influence on the macrovoid formation. At all bore liquid flow rates, the membrane had a lot of finger-like macrovoids. Although the dope flow rate did not change the macrovoid structure, mostly finger-like, the number of macrovoids decreased with increasing dope flow rate. The results inspecting the effect of bore and dope solution flow rates suggested that all membrane had many macrovoids mostly in finger-like shape regardless of dope and bore liquid flow rates. Similarly, as the air gap was increased or THF was added to the dope solution, a decrease in the number of macrovoids was observed, which was coherent with the literature [66]. Although air gap has a limited effect on the macrovoid structure, most of the macrovoids formed at all air gaps were finger-like, the number of finger-like voids decreased in the presence of THF.

Table 4.2. The effect of dope solution flow rate on the number of finger-like macrovoids compared to circular-shaped macrovoids and the covered area of those structures on the supporting layer [35°C, AG 12, 30 Polymer:0 THF:70 DMF ]

<b>Dope liquid flow rate</b>	<b>Bore liquid flow rate</b>	<b>Comparative number of Finger-like macrovoids</b>	<b>Covering area of macrovoid structures</b>
D 1.0 g/min	0.50	Majority	High
D 2.6 g/min	0.50	Majority	Low
D 1.0 g/min	1.00	Majority	High
D 2.6 g/min	1.00	Minority	Low

Table 4.3. The effect of bore solution flow rate on the number of finger-like macrovoids compared to circular-shaped macrovoids and the covered area of those structures on the supporting layer [35°C, AG 12, 30 Polymer:0 THF:70 DMF ]

<b>Bore liquid flow rate (g/min)</b>	<b>Dope liquid flow rate (g/min)</b>	<b>Comparative number of Finger-like macrovoids</b>	<b>Covering area of macrovoid structures</b>
0.50	1.0	Majority	High
1.00	1.0	Majority	High
0.75	2.6	Majority	High
1.00	2.6	Minority	Low

Table 4.4. The effect of THF addition on the number of finger-like macrovoids compared to circular-shaped macrovoids and the covered area of those structures on the supporting layer [15°C, AG 12, D 1.0 g/min]

<b>THF addition</b>	<b>Bore liquid flow rate (g/min)</b>	<b>Comparative number of Finger-like macrovoids</b>	<b>Covering area of macrovoid structures</b>
-	0.50	Majority	High
THF	0.50	Equality	Medium
-	0.75	Majority	High
THF	0.75	Minority	Medium

Table 4.5. The effect of air gap height on the number of finger-like macrovoids compared to circular-shaped macrovoids and the covered area of those structures on the supporting layer [35°C, D 1.0 g/min, 30 Polymer:0 THF:70 DMF]

<b>Air gap height</b>	<b>Bore liquid flow rate (g/min)</b>	<b>Comparative number of Finger-like macrovoids</b>	<b>Covering area of macrovoid structures</b>
12	0.50	Majority	High
20	0.50	Majority	Medium
12	1.00	Majority	High
20	1.00	Equality	Medium

Table 4.6. The effect of temperature on the number of finger-like macrovoids compared to circular-shaped macrovoids and the covered area of those structures on the supporting layer (Dope liquid composition 30 PI:0 THF: 70 DMF)

<b>Membrane code</b>	<b>Temperature (°C)</b>	<b>Comparative number of Finger-like macrovoids</b>	<b>Covering area of macrovoid structures</b>
PI.B20.D30.AG12	35	Majority	High
PI.B20.D30.AG12	15	Majority	High
PI.B40.D30.AG12	35	Majority	High
PI.B40.D30.AG12	15	Majority	High

#### 4.3.4 Gas Permeation through Hollow Fiber Membranes

In order to investigate effect of spinning conditions on the hollow fiber membrane gas permeation results, uniformity of the hollow fiber membrane was controlled by measuring gas permeation of different parts of the membrane prepared at the same batch. The membrane samples having different spinning conditions were taken from

the similar location of the prepared hollow fiber membranes. According to those results given in the Appendix E, prepared hollow fiber membranes were not uniform. The effect of spinning parameters on the gas permeation results of the hollow fiber membranes having highest CO<sub>2</sub>/CH<sub>4</sub> ideal selectivity was shown in Table 4.7 to Table 4.11 . Although, selective dense layer was differentiated at the outer surface of hollow fiber membranes, their gas separation performance was not satisfying for biogas refining processes. The best membrane had a H<sub>2</sub>/CH<sub>4</sub> and CO<sub>2</sub>/CH<sub>4</sub> ideal selectivity of 37.07 and 13.15, whereas it was reported PI hollow fiber membranes with CO<sub>2</sub>/CH<sub>4</sub> ideal selectivity of 37 to 59.6 [24,50]. The best membrane prepared in this study was obtained by using the following spinning conditions: bore and dope flow rate were 1 and 1 g/min, air gap height was 12 cm, there was no THF in dope solution and temperature of heating zone was 35°C.

It was difficult to explain the individual effect of spinning condition studied in this thesis. However, it was clear that temperature of the heating zone has strong influence on the quality of membranes. Hollow fiber membranes prepared at 35°C has substantially higher ideal selectivities than those prepared at 15°C. For instance, two membranes prepared with dope and bore flow rate of 1 and 1 g/min, air gap height of 12 cm, without THF has CO<sub>2</sub>/CH<sub>4</sub> ideal selectivity of 1.04 at 15°C and 13.15 at 35°C as shown in Table 4.11.

Table 4.7. The effect of dope solution flow rate on the hollow fiber membrane gas separation performance (convective heating zone temperature 35°C and Dope liquid composition 30 PI:0 THF: 70 DMF, B20: 0.50 g/min, B40:1.00 g/min, D30: 1.0 g/min, D100: 2.6 g/min)

Membrane code	Gas Permeance (GPU)			Ideal Selectivity		
	H <sub>2</sub>	CO <sub>2</sub>	CH <sub>4</sub>	H <sub>2</sub> /CO <sub>2</sub>	H <sub>2</sub> /CH <sub>4</sub>	CO <sub>2</sub> /CH <sub>4</sub>
PI.B20.D30.AG12	8.43	2.43	0.34	3.47	24.81	7.14
PI.B20.D100.AG12	6.22	2.19	0.31	2.83	20.00	7.06
PI.B40.D30.AG12	14.90	5.28	0.40	2.82	37.07	13.15
PI.B40.D100.AG12	11.11	5.33	0.47	2.08	23.69	11.37

Table 4.8. The effect of bore solution flow rate on the hollow fiber membrane gas separation performance (convective heating zone temperature 15°C and Dope liquid composition 30 PI:0 THF: 70 DMF, B20: 0.50 g/min, B30:0.75 g/min, B40: 1.00 g/min, D30:1.0 g/min)

Membrane code	Gas Permeance (GPU)			Ideal Selectivity		
	H <sub>2</sub>	CO <sub>2</sub>	CH <sub>4</sub>	H <sub>2</sub> /CO <sub>2</sub>	H <sub>2</sub> /CH <sub>4</sub>	CO <sub>2</sub> /CH <sub>4</sub>
PI.B20.D30.AG6	2.20	0.75	0.18	2.93	12.28	4.19
PI.B30.D30.AG6	2.19	0.72	0.18	3.02	12.13	4.02
PI.B20.D30.AG12	3.68	0.38	0.27	9.58	13.49	1.41
PI.B40.D30.AG12	3.22	0.41	0.39	7.90	8.26	1.04

Table 4.9. The effect of more volatile solvent addition to dope solution on the hollow fiber membrane gas separation performance (convective heating zone temperature 15°C, B20: 0.50 g/min, D30: 1.0 g/min)

Membrane code	Dope liquid composition (PI: THF: DMF) (w/w)	Gas Permeance (GPU)			Ideal Selectivity		
		H <sub>2</sub>	CO <sub>2</sub>	CH <sub>4</sub>	H <sub>2</sub> /CO <sub>2</sub>	H <sub>2</sub> /CH <sub>4</sub>	CO <sub>2</sub> /CH <sub>4</sub>
PI.B20.D30. AG 12	30:0:70	3.68	0.38	0.27	9.58	13.49	1.41
PI.B20.D30. AG 12	30:7:63	6.37	2.54	0.52	2.51	12.33	4.92

Table 4.10. The effect of air gap height between spinneret and coagulation bath on the hollow fiber membrane gas separation performance (convective heating zone temperature 15°C and Dope liquid composition 30 PI:0 THF: 70 DMF, B20: 0.50 g/min, B30:0.75 g/min, D30: 1.0 g/min)

Membrane code	Gas Permeance (GPU)			Ideal Selectivity		
	H <sub>2</sub>	CO <sub>2</sub>	CH <sub>4</sub>	H <sub>2</sub> /CO <sub>2</sub>	H <sub>2</sub> /CH <sub>4</sub>	CO <sub>2</sub> /CH <sub>4</sub>
PI.B20.D30.AG 6	2.20	0.75	0.18	2.93	12.28	4.19
PI.B20.D30.AG12	3.68	0.38	0.27	9.58	13.49	1.41
PI.B30.D30.AG 6	2.19	0.72	0.18	3.02	12.13	4.02
PI.B30.D30.AG 12	5.09	1.43	0.39	3.56	13.21	3.71

Table 4.11. The effect of temperature on the hollow fiber membrane gas separation performance (Dope liquid composition 30 PI:0 THF: 70 DMF, B20: 0.50 g/min, B40: 1.00 g/min, D30:1.0 g/min)

Membrane code	Temperature (°C)	Gas Permeance (GPU)			Ideal Selectivity		
		H <sub>2</sub>	CO <sub>2</sub>	CH <sub>4</sub>	H <sub>2</sub> /CO <sub>2</sub>	H <sub>2</sub> /CH <sub>4</sub>	CO <sub>2</sub> /CH <sub>4</sub>
PI.B20.D30.AG12	35	8.43	2.43	0.34	3.47	24.81	7.14
PI.B20.D30.AG12	15	3.68	0.38	0.27	9.58	13.49	1.41
PI.B40.D30.AG 12	35	14.90	5.28	0.40	2.82	37.07	13.15
PI.B40.D30.AG 12	15	3.22	0.41	0.39	7.90	8.26	1.04

Hollow fiber membrane spinning process for gas separation applications have wide range of spinning conditions such as composition and types of bore liquid, composition of dope liquid and types of polymer, usage of additives, flow rate of

dope liquid and bore liquid solution, spinneret design, air gap height, dope liquid temperature, non-solvent type used in coagulation bath, and take-up rate. Spinning conditions influence hollow fiber membrane morphology and gas separation performance by affecting thermodynamic and kinetic factors of phase inversion processes. In order to prepare defect free hollow fiber membranes, those five spinning conditions were investigated with different combinations. Hollow fiber membranes with defects and showing low gas separation performance could be enhanced by coating the membrane surface with a rubbery polymer. The following section describes the preparation of hollow fiber membranes coated with PEBAX 1657.

#### **4.3.5 The Effects of PEBAX 1657 Coating on the Membrane Morphology and Gas Separation Performance**

Membrane defects cause to decrease gas separation performance of a membrane dramatically. The gas separation performance could be enhanced by coating with a high flux rubbery polymer. Coating layer of high flux polymer like PDMS does not behave as a selective barrier. Sealing membrane defects helps to decrease non-diffusive gas flow, which enhance gas separation performance of the membrane [6]. For biogas refining processes, the main objective is to separate CO<sub>2</sub> from CH<sub>4</sub>. PEBAX 1657 has high CO<sub>2</sub> affinity, which increases CO<sub>2</sub>/CH<sub>4</sub> selectivity of the membranes [14]. Besides, PEBAX 1657 has desired properties such as economical feasibility, easy film formation, high mechanical strength and good temperature resistance [5]. Therefore, hollow fiber membranes having surface defects were coated with PEBAX 1657 due to its possible contribution to CO<sub>2</sub>/CH<sub>4</sub> selectivity of the membranes. PEBAX coating was performed on 15-cm PI hollow fibers by dip-coating.

The effect of PEBAX 1657 coating on the hollow fiber membrane gas separation performance was shown in Table 4.12. A membrane coated with PEBAX was indicated by a black box at left end of the table. The uncoated counterpart of this membrane was also shown in the preceding row.

Table 4.12. The effect of PEBAX 1657 coating on the hollow fiber membrane gas separation performance (convective heating zone temperature 35°C and Dope liquid composition 30 PI:0 THF: 70 DMF, B20:0.50 g/min, B40:1.00 g/min, D30:1.0 g/min, D100:2.6 g/min)

Membrane code	Gas Permeance (GPU)			Ideal Selectivity		
	H <sub>2</sub>	CO <sub>2</sub>	CH <sub>4</sub>	H <sub>2</sub> /CO <sub>2</sub>	H <sub>2</sub> /CH <sub>4</sub>	CO <sub>2</sub> /CH <sub>4</sub>
PI.B20.D30. AG12	7.70	2.31	0.42	3.32	18.13	5.45
PEBAX 1657 coated PI.B20.D30. AG12	6.58	2.71	0.22	2.42	30.15	12.44
PI.B20.D100. AG12	6.22	2.19	0.31	2.83	20.00	7.06
PEBAX 1657 coated PI.B20.D100. AG12	5.31	2.07	0.18	2.57	28.82	11.23
PI.B40.D30. AG12	8.72	5.40	0.44	1.62	19.89	12.31
PEBAX 1657 coated PI.B40.D30.AG12	6.80	2.73	0.20	2.50	33.76	13.53
PI.B40.D100. AG12	11.11	5.33	0.47	2.08	23.69	11.37
PEBAX 1657 coated PI.B40.D100.AG12	9.79	3.82	0.27	2.56	36.28	14.17

According to Table 4.12, gas separation performance of hollow fiber membrane was enhanced by coating when the gas separation performance of virgin membranes compared with coated ones. PEBAX 1657 coating mostly decreased the gas permeances since the membrane thickness increased by coating. This polymer has CO<sub>2</sub> affinity thus the decrease in CO<sub>2</sub> permeance was lower than the permeances of the other gases [14]. Therefore, ideal selectivity of coated hollow fiber membranes was higher than virgin ones’.

Coating enables to seal defects where gas molecules could flow convectively. Therefore, it was expected that gas separation performance of coated membranes should be closer to pure PI hollow fiber membranes used for biogas refining.

According to Table 4.12, coated hollow fiber membranes did not show the ideal CO<sub>2</sub>/CH<sub>4</sub> selectivity of PI membranes which is between 37 and 59.6 [24,50]. The ideal selectivity of dense pure PEBAX 1657 membrane was reported as 19.4±0.1 [31]. This showed that PEBAX 1657 coating layer not only seals the membrane defects but also behaves as the main selective barrier instead of PI hollow fiber membrane. This could be explained by high membrane defect area compared to total membrane surface area and coating defects [6]. Therefore, it was concluded that PEBAX 1657 coated hollow fiber membranes showed the gas separation performance of PEBAX 1657/PI composite hollow fiber membrane instead of sealed PI membrane.

In order to investigate the adhesion between PEBAX 1657 coating layer and PI hollow fiber membrane, SEM images of PEBAX 1657 coated membranes were analyzed. The SEM images of PEBAX 1657 coated hollow fiber membranes was shown in Figure 4.10. In this figure, border of coating layer was indicated with red lines.

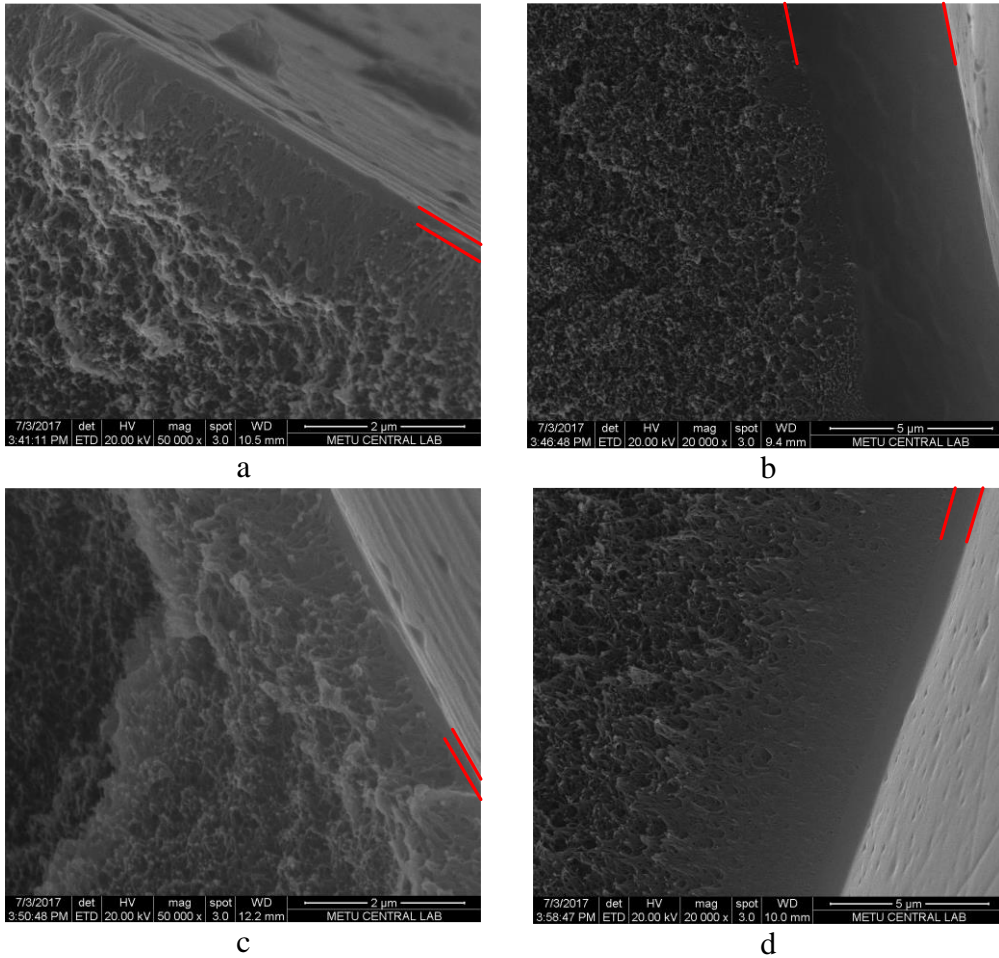


Figure 4.10. The SEM images of PEBA 1657 coated hollow fiber membranes produced by using 35°C convective heating zone with the mass ratio of 30 PI: 0 THF: 70 DMF a) PI.B20.D100.AG12 b) PI.B40.D100.AG12 c) PI.B20.D30.AG12 d) PI.B40.D30. AG12

As shown in Figure 4.10, PEBA 1657 coating layer was differentiated at the outer layer of hollow fiber membranes without any void between coating layer and the membrane. This showed that PEBA 1657 is compatible with PI and an acceptable material to prepare composite hollow fiber membrane.

#### **4.4 Characterization and Gas Separation Performance of Flat Sheet Membranes**

The defects on a hollow fiber membrane can be sealed by coating the membrane with a rubbery polymer and to enhance gas separation performance. The hollow fiber membranes produced in this study exhibited low permselectivities indicating the presence of many defects, which has to be sealed for an efficient gas separation.

Hollow fiber membranes may not be convenient to investigate the success of coating process due to their geometry and difficulty of preparation. For this purpose, it was decided to study the effect of coating on flat membranes, which can be prepared more easily than hollow fiber membranes.

The flat membrane should, therefore be porous in order to imitate hollow fiber membranes with surface defects. For this purpose, porous PES flat sheet membranes were prepared by using different coagulation bath compositions as shown in Table 3.3. The non-solvent induced phase separation is a common method to produce porous membranes. PES was studied instead of PI due to the its low price and easiness of PES membrane preparation.

In order to investigate gas separation performance of PEBAX 1657 polymer and compatibility between PEBAX 1657 polymer matrix and ZIF-8 crystals, PEBAX 1657, PEBAX 1657/ZIF-8, PEBAX 1657/PNA, PEBAX 1657/ZIF-8/PNA flat sheet membranes were prepared by solvent evaporation. PEBAX 1657 based flat sheet membranes had nonporous dense structure as shown in Figure 4.11.

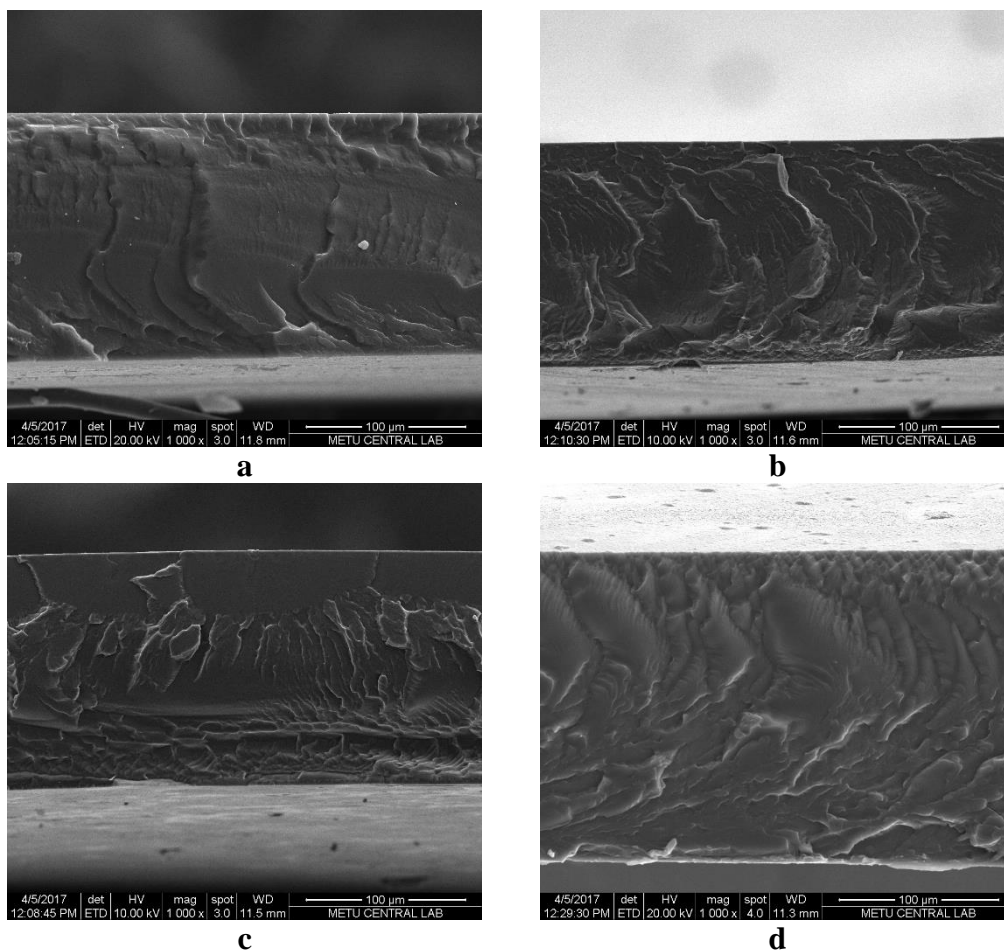


Figure 4.11. The SEM images of a) pure PEBAX 1657 b) PEBAX 1657/ZIF-8 c) PEBAX 1657/PNA d) PEBAX 1657/ZIF-8/PNA flat sheet membranes

Compatibility between polymer matrix and inorganic fillers is important for gas separation performance of the mixed matrix membrane. In order to alleviate compatibility problem, low molecular additives are incorporated to membrane casting solution. PNA was used as a compatibilizer for the preparation of mixed matrix membranes.

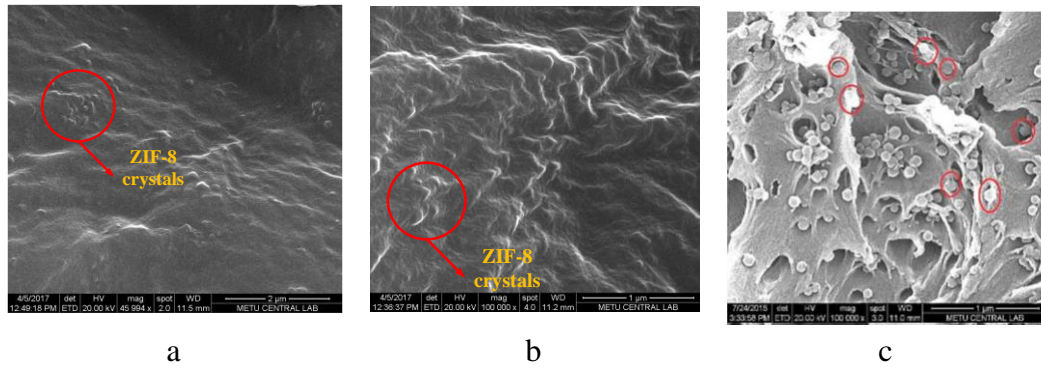


Figure 4.12. The SEM image of ZIF-8 crystals distributed in polymer matrix a) PEBAX 1657/ZIF-8 b) PEBAX 1657/ZIF-8/PNA flat sheet membranes c) PES/PI/ZIF-8 20/80/10 membrane (not compatible ZIF-8 crystals with PES/PI polymer matrix) [64]

Figure 4.12 a and b shows that no interfacial void has formed around the ZIF-8 crystals, which suggests that ZIF-8 crystals are compatible with PEBAX 1657 matrix and there is no need for a third component as a compatibilizer during the membrane preparation. The gas separation performance of PEBAX 1657 and PEBAX 1657/ZIF-8 flat sheet membranes and their performance reported in the literature [31] are shown in Table 4.13.

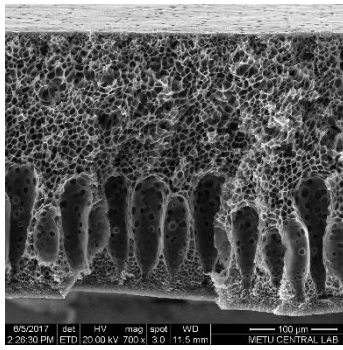
Table 4.13. The gas separation performance of pure PEBAX 1657 and PEBAX 1657/ZIF-8 flat sheet membranes

Membrane Code	Permeability (Barrer)			Ideal Selectivity	
	N <sub>2</sub>	CO <sub>2</sub>	CH <sub>4</sub>	CO <sub>2</sub> /N <sub>2</sub>	CO <sub>2</sub> /CH <sub>4</sub>
Pure PEBAX 1657	8.35	190.87	18.21	22.86	10.48
PEBAX 1657/ZIF-8	9.08	325.63	12.56	35.85	25.93
PEBAX 1657/ZIF-8 /PNA	6.85	153.36	14.67	22.39	10.46
Pure PEBAX 1657 [31]	-	10	-	-	19.4±0.1
PEBAX 1657/ZIF-8 [31]	-	200	-	-	15.1±0.2

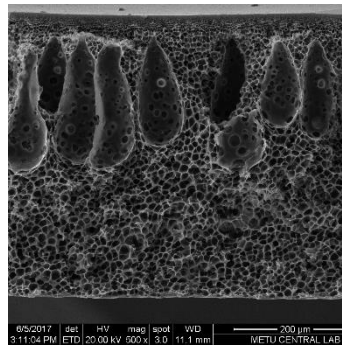
According to Table 4.13, the incorporation of ZIF-8 into membrane formulation did not change in N<sub>2</sub> and CH<sub>4</sub> permeabilities significantly, but CO<sub>2</sub> permeability increased by almost 50%. Consequently, CO<sub>2</sub>/N<sub>2</sub> and CO<sub>2</sub>/CH<sub>4</sub> ideal selectivities almost doubled. This could be attributed partly to the adsorption affinity of ZIF-8 to CO<sub>2</sub>. McEwen et al. showed that adsorption selectivity of CO<sub>2</sub> over N<sub>2</sub> and CH<sub>4</sub> is approximately 4 and 8, respectively, based on single gas adsorption measurements. Therefore, substantial increase in the CO<sub>2</sub>/N<sub>2</sub> and CO<sub>2</sub>/CH<sub>4</sub> ideal selectivities are likely due to the molecular sieving effect of ZIF-8 and well adhesion between ZIF-8 crystals and PEBAX matrix [69]. ZIF-8 is of a pore aperture of 0.34 nm, which is greater than the kinetic diameter of CO<sub>2</sub> (0.33nm) but smaller than the kinetic diameters of N<sub>2</sub> (0.36 nm) and CH<sub>4</sub> (0.38 nm). Hence, CO<sub>2</sub> may permeate through ZIF-8, while the others are rejected [5,16].

On the other hand, Sutrisna et al. [31] reported that incorporation of ZIF-8 crystals decreased ideal selectivity of CO<sub>2</sub>/CH<sub>4</sub> as given in Table 4.13. This was explained by the possible formation of non-selective voids around the crystals [31]. In addition to morphological examination of PEBAX 1657/ ZIF-8 membrane, the enhanced gas separation performance of this membrane verified the compatibility between ZIF-8 crystals and PEBAX 1657 polymer matrix. As shown in Table 4.13, incorporation of PNA did not enhance gas separation performance of the membrane.

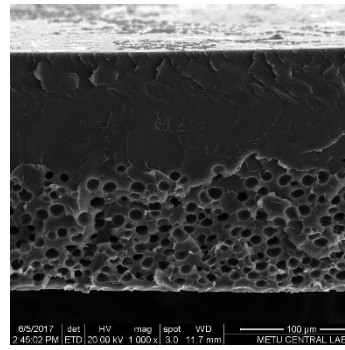
The SEM images of PES flat sheet membranes were analyzed in order to investigate the effect of non-solvent used in the coagulation bath. Coagulant influences the precipitation path and precipitation rate of the membrane casting solution, which affects the membrane formation mechanism [6]. PES flat sheet membranes were coagulated in pure water bath, 50 wt. % water / 50 wt. % IPA bath and pure IPA bath. Immersion precipitation method (non-solvent induced phase separation) is used for the preparation of asymmetric membranes. The effect of coagulant on the membrane morphology was shown in Figure 4.13. In those figures, overall view of membrane and both side of the membrane at higher magnifications were given.



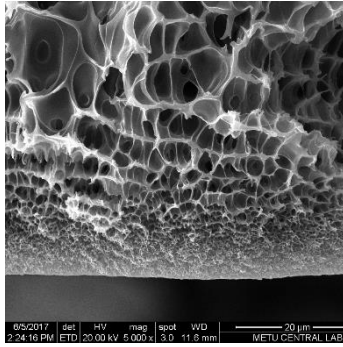
overall view



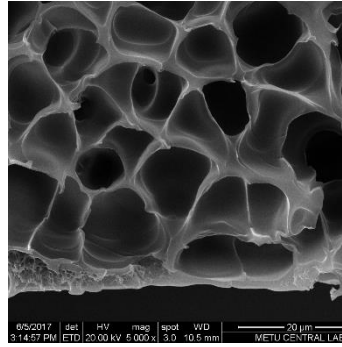
overall view



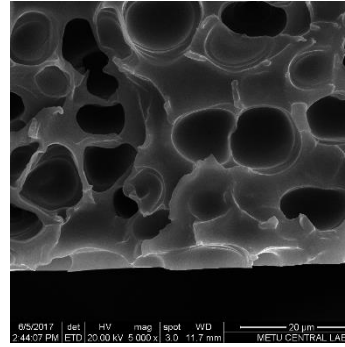
overall view



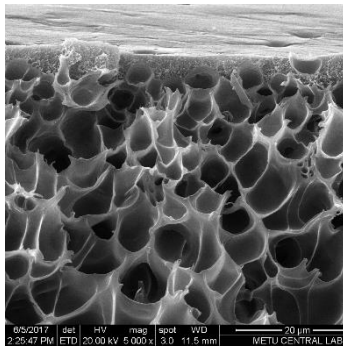
air side



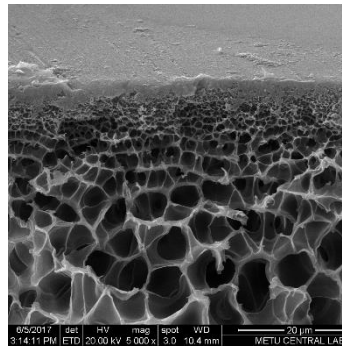
glass plate side



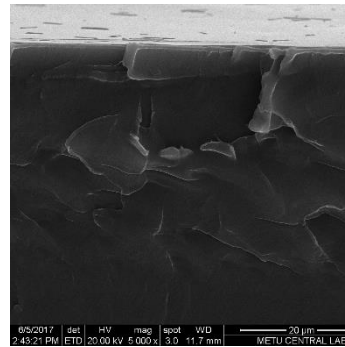
glass plate side



glass plate side



air side



air side

**a**

**b**

**c**

Figure 4.13. The SEM images of PES flat sheet membranes coagulated by using different types of non-solvent a) Pure water b) 50 wt. % water / 50 wt. % IPA c) pure IPA

According to Figure 4.13 a and b, the PES flat sheet membranes coagulated in pure water and 50 wt. % water / 50 wt. % IPA mixture have similar morphology with the PI hollow fiber membranes. The membrane has a thin skin layer, expectedly dense, over a thick porous substructure. Finger-like-pores were also observed in the flat

membranes. On the other hand, PES flat sheet membranes coagulated in pure IPA consisted of a thicker dense selective layer supported by substructure with low porosity (Figure 4.13c). This was explained by the delayed liquid-liquid phase separation process due to effect of IPA on the local polymer concentration based on interactions between solvent, non-solvent and polymer. This leads to formation of concentrated polymer layer at the interface [70]. Table 4.14 shows the gas permeation performances of PES flat sheet membranes prepared by using different coagulants.

Table 4.14. The gas separation performance of PES flat sheet membranes [Knudsen selectivity for CO<sub>2</sub>/N<sub>2</sub> and CO<sub>2</sub>/CH<sub>4</sub> is 0.80 and 0.60, respectively]

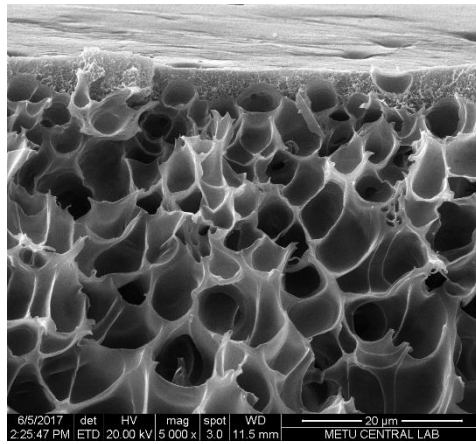
Membrane Code	Permeance (GPU)			Ideal Selectivity	
	N <sub>2</sub>	CO <sub>2</sub>	CH <sub>4</sub>	CO <sub>2</sub> /N <sub>2</sub>	CO <sub>2</sub> /CH <sub>4</sub>
<b>PES/Water</b>	7.41	26.18	9.27	3.53	2.82
<b>PES/IPA/Water</b>	23.50	22.33	32.61	0.95	0.68
<b>PES/IPA</b>	4.85E-03	4.56E-02	2.62E-03	9.40	17.42

According to Table 4.14, PES/IPA membrane showed lower gas permeances compared to the others, which was expected results regarding the membrane morphologies shown in Figure 4.13. Ideal selectivity of CO<sub>2</sub>/CH<sub>4</sub> was reported as 33.9±3.4 for dense PES flat sheet membrane [64]. Theoretical values of the Knudsen diffusion selectivity calculated by using Equation 4.1 [6], for CO<sub>2</sub>/N<sub>2</sub> and CO<sub>2</sub>/CH<sub>4</sub> are 0.80 and 0.60, respectively. Knudsen diffusion selectivity of the gases is inversely proportional with the square root of their molecular weights (MW).

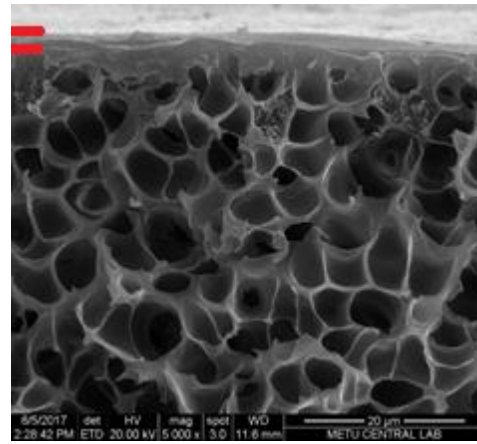
$$\alpha_{i/j} = \sqrt{\frac{MW(j)}{MW(i)}} \quad \text{Equation 4.1}$$

The ideal CO<sub>2</sub>/CH<sub>4</sub> selectivity of PES/IPA membrane was higher than the Knudsen diffusion selectivity but lower than the reported value for dense PES flat sheet membrane. This means that pore size of the membrane was in the range of transient zone between pore flow and solution diffusion pores [6]. The ideal selectivity of CO<sub>2</sub>/N<sub>2</sub> and CO<sub>2</sub>/CH<sub>4</sub> for PES/Water and PES/IPA/Water membranes was higher than theoretical Knudsen diffusion selectivity values. This indicated that membrane has a porous structure whose pore size is smaller than the mean free path of penetrant gas molecules [6]. For the imitation of hollow fiber membranes having surface defects, it was decided to use 50 wt. % IPA and 50 wt. % water mixture and pure water as a coagulant for the preparation of ultrafiltration PES flat sheet membranes regarding the morphology and gas separation performance of PES/Water and PES/IPA/Water membranes.

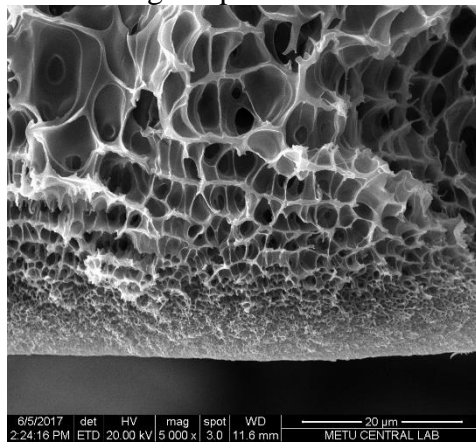
Figure 4.14 and Figure 4.15 shows the SEM images of PEBAX 1657 coated PES/Water and PES/IPA/Water membranes. In those figures, both side of the membrane were shown and border of coating layer was indicated with red lines.



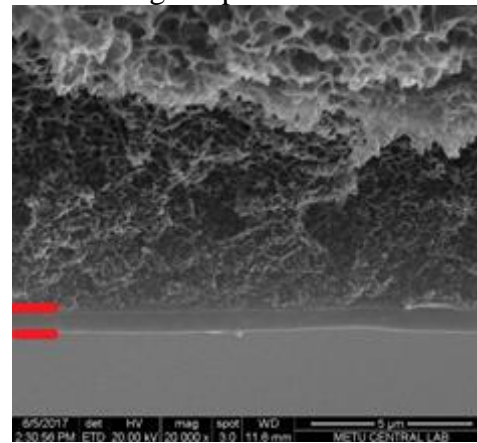
glass plate side



glass plate side



air side



air side

**a**

**b**

Figure 4.14. The SEM images of PES/Water flat sheet membranes a) virgin PES/Water flat sheet membranes b) PEBA 1657 coated PES/Water flat sheet membranes



on the gas separation performance of the PES/Water and PES/IPA/Water flat sheet membrane was shown in Table 4.15.

Table 4.15. The gas separation performance of prepared virgin PES/Water and PES/IPA/Water flat sheet membranes and PEBAX 1657 coated PES/Water and PES/IPA/Water flat sheet membranes

Membrane Code	Permeance (GPU)			Ideal Selectivity	
	N <sub>2</sub>	CO <sub>2</sub>	CH <sub>4</sub>	CO <sub>2</sub> /N <sub>2</sub>	CO <sub>2</sub> /CH <sub>4</sub>
<b>PES/Water</b>	7.41	26.18	9.27	3.53	2.82
<b>PEBAX 1657 coated PES/Water</b>	0.64	12.27	0.84	19.23	14.69
<b>PES/IPA/Water</b>	23.50	22.33	32.61	0.95	0.68
<b>PEBAX 1657 coated PES/IPA/Water</b>	0.94	8.42	0.89	8.99	9.44
<b>Literature [31] Dense PEBAX 1657</b>	-	-	-	-	19.4±0.1

The gas separation performance of PES/Water and PES/IPA/Water flat sheet membranes were enhanced by PEBAX 1657 coating. Prepared asymmetric composite flat sheet membranes should show the gas separation performance of the dense PEBAX 1657 membrane. Although, coating layer was differentiated at the both surface of the membrane, the ideal selectivity of them was lower than the one reported in the literature [31]. On the other hand, prepared asymmetric composite flat sheet membranes showed similar ideal selectivity with the prepared pure PEBAX 1657 membranes. This may be resulted from the differences in the membrane preparation conditions.

Mixed matrix membranes enables to combine higher gas permeance value of inorganic membranes and ease of formation of polymeric membranes. Therefore, ZIF-8 crystals were incorporated to PEBAX 1657 coating solution for the further enhancement of asymmetric composite membrane gas separation performance. The effect of incorporation of ZIF-8 crystals to coating solution on the morphology of the PES/Water and PES/IPA/Water flat sheet membrane was shown in Figure 4.16 and Figure 4.17.

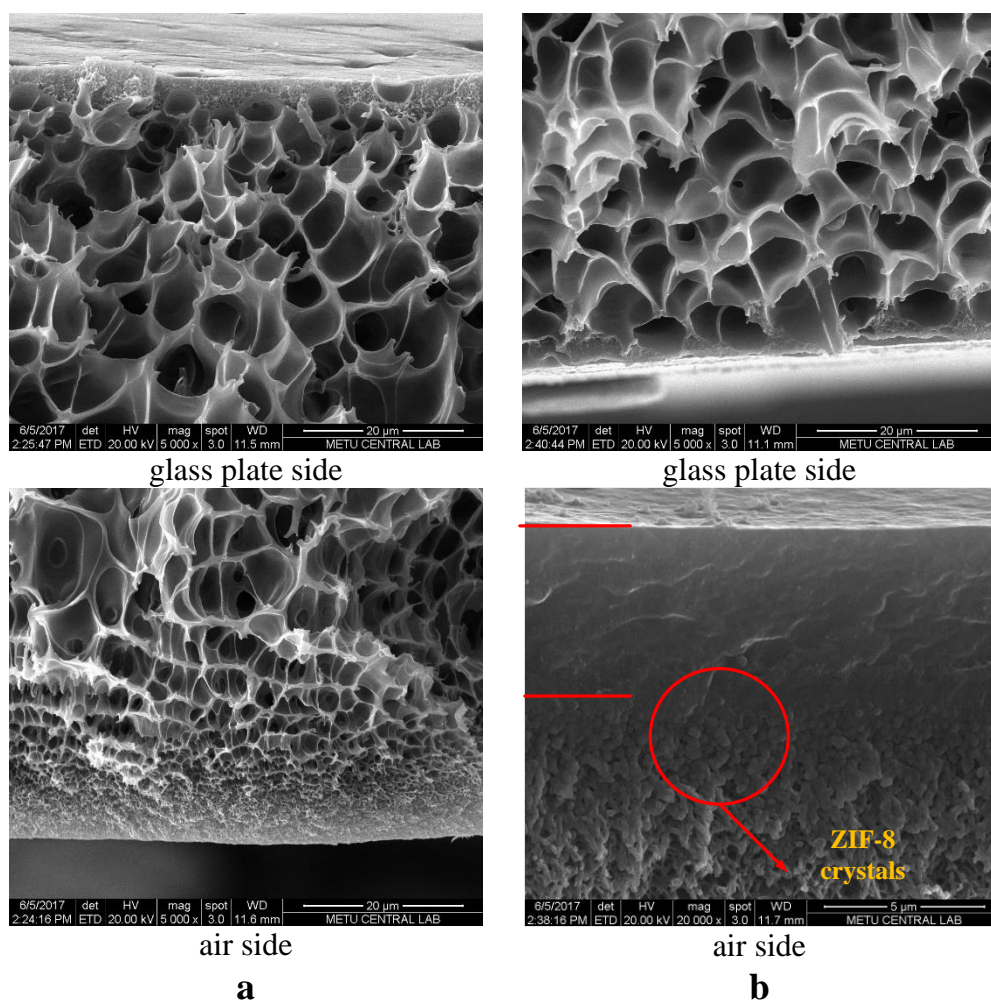


Figure 4.16. The SEM images of PES/Water flat sheet membranes a) virgin PES/Water flat sheet membranes b) PEBAX 1657/ZIF-8 coated PES/Water flat sheet membranes

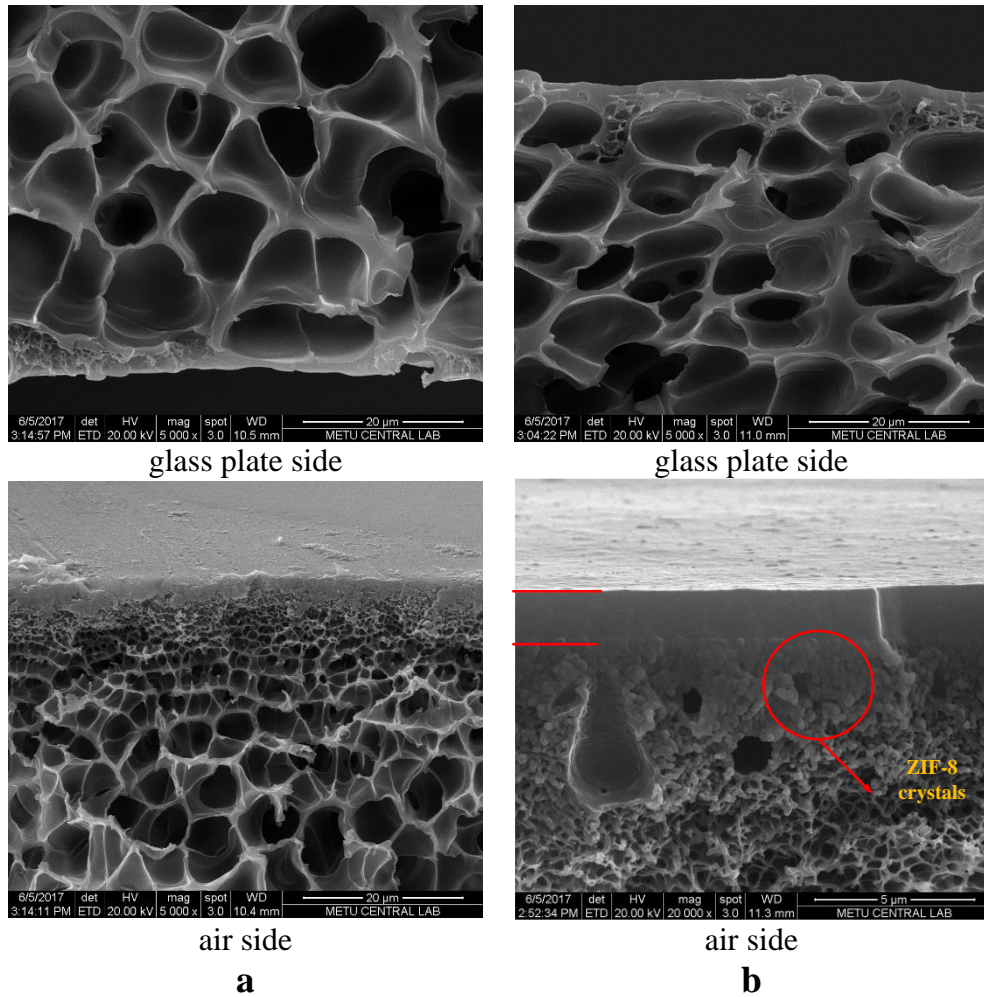


Figure 4.17. The SEM images of PES/IPA/Water flat sheet membranes a) virgin PES/IPA/Water flat sheet membranes b) PEBAX 1657/ZIF-8 coated PES/IPA/Water flat sheet membranes

According to Figure 4.16 and Figure 4.17, PEBAX 1657/ZIF-8 coating layer could be differentiated at both of the surfaces of the coated membrane but coating layer thickness was distinctive for the different surface of the membranes. Coating layer thickness was higher for the surface supported by fine porous structure compared to the one supported by coarse porous structure. In addition, ZIF-8 crystals were not differentiated at the surface supported by coarse porous structure. This might be explained by the penetration of coating solution and ZIF-8 crystals through coarse

pore structure. The effect of PEBAX 1657/ZIF-8 coating on the gas separation performance of the PES/Water and PES/IPA/Water flat sheet membrane was shown in Table 4.16.

Table 4.16. The gas separation performance of prepared virgin PES/Water and PES/IPA/Water flat sheet membranes and PEBAX 1657/ZIF-8 coated PES/Water and PES/IPA/Water flat sheet membranes

Membrane Code	Permeance (GPU)			Ideal Selectivity	
	N <sub>2</sub>	CO <sub>2</sub>	CH <sub>4</sub>	CO <sub>2</sub> /N <sub>2</sub>	CO <sub>2</sub> /CH <sub>4</sub>
<b>PES/Water</b>	7.41	26.18	9.27	3.53	2.82
<b>PEBAX 1657/ZIF-8 coated PES/Water</b>	3.82	6.73	4.65	1.76	1.45
<b>PES/IPA/Water</b>	23.50	22.33	32.61	0.95	0.68
<b>PEBAX 1657/ZIF-8 coated PES/IPA/Water</b>	0.74	4.67	0.88	6.34	5.32

According to Table 4.15 and Table 4.16, incorporation of ZIF-8 crystals did not enhance gas separation performance of PEBAX 1657 coated PES/Water and PES/IPA/Water flat sheet membranes. Li et al. reported that addition of ZIF-8 crystals decreased the total crystallinity of the coating layer of the selective layer, which results in higher free volume and greater chain mobility of the membrane [5]. According to this report, incorporation of ZIF-8 should enhance gas diffusion in contrast to gas permeation test results shown in Table 4.15 and Table 4.16. The decrease in the gas permeance of PEBAX 1657/ZIF-8 coated PES/Water and PES/IPA/Water flat sheet membranes may be explained by variable coating layer thickness of coated membranes. Incorporation of ZIF-8 crystals should also increase

ideal selectivity of CO<sub>2</sub>/N<sub>2</sub> and CO<sub>2</sub>/CH<sub>4</sub> regarding ZIF-8 pore aperture and kinetic diameter of CO<sub>2</sub>, N<sub>2</sub>, and CH<sub>4</sub>, which were explained above. According to Table 4.16, ideal selectivity of CO<sub>2</sub>/N<sub>2</sub> and CO<sub>2</sub>/CH<sub>4</sub> PEBAX 1657/ZIF-8 coated PES/Water and PES/IPA/Water flat sheet membranes did not increase in contrast to expectations. Ismail et al. reported that this may be explained by partial blockage of the pores and limited contact area between the particle and polymer matrix due to larger clustered ZIF-8 particles as shown in Figure 4.18 [71].

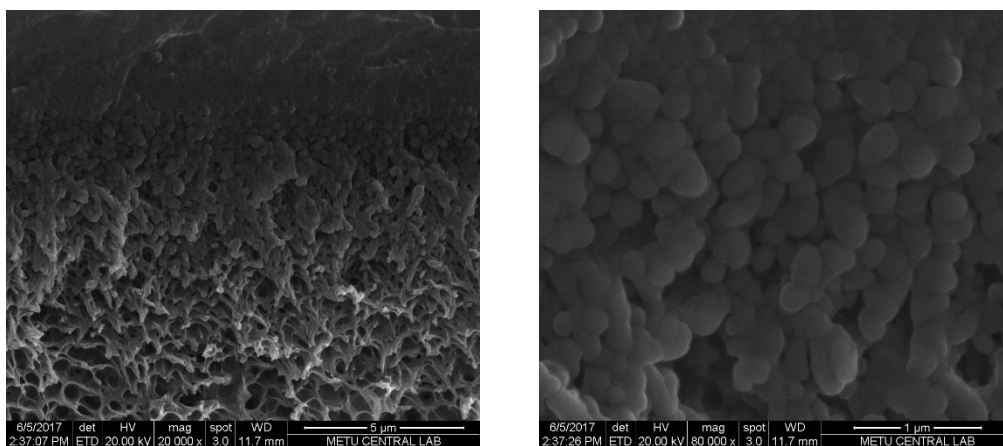


Figure 4.18. The SEM image of ZIF-8 crystals distributed in polymer matrix

The average particle size and shape of the ZIF-8 crystals incorporated PEBAX 1657 coating solution was  $69 \pm 14$  nm and rhombic dodecahedron, respectively as shown in Figure 4.2. This specific morphology of ZIF-8 crystals could not be differentiated through membrane structures shown in Figure 4.18. This may be resulted from clustered ZIF-8 crystals, which decreased the membrane gas separation performance.

#### 4.4.1 Fourier Transform Infrared Spectroscopy (FTIR)

Regarding Figure 4.11, PEBAX 1657, ZIF-8, and PNA are compatible materials since no phase separation was observed in those SEM micrographs. In order to analyze possible interactions between PEBAX 1657, ZIF-8, and PNA, pure PEBAX

1657, PEBAX 1657/PNA, PEBAX1657/ZIF-8, PEBAX/PNA/ZIF-8 membranes, PNA and ZIF-8 were analyzed by FTIR (Figure 4.19).

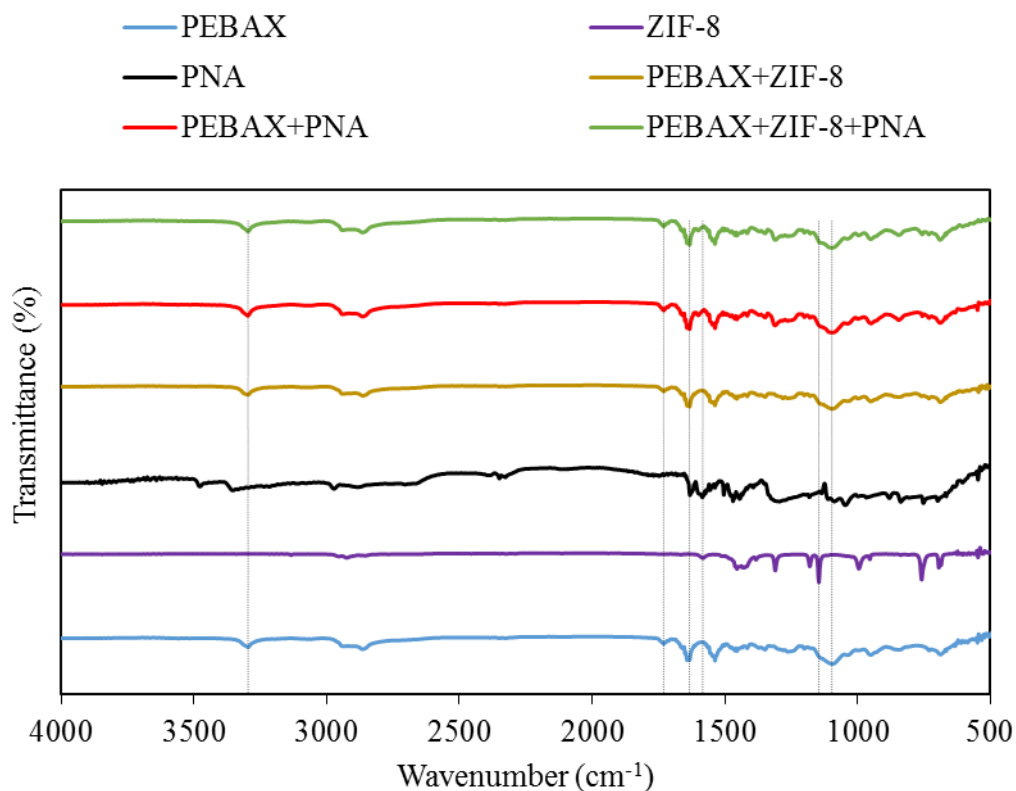


Figure 4.19. FTIR spectra of pure PEBAX 1657, PEBAX 1657/PNA, PEBAX/ZIF-8, PEBAX/PNA/ZIF-8 membranes and PNA and ZIF 8 solids

The characteristic peaks of PEBAX 1657 and ZIF-8 crystals were shown by dashed lines based on those peaks reported by Sutrisna et al. and Zhang et al [5,31]. The characteristic peak of PEO segments of PEBAX 1657 membranes is at about 1096 cm<sup>-1</sup>, which is attributed to the stretching vibration of C-O-C group. The characteristic peaks of hard polyamide segment are at about 3297, 1633, and 1731 cm<sup>-1</sup>, which are the stretching vibrations of -N-H-, H-N-C=O, and O-C=O groups, respectively [5,31]. The characteristic peaks of ZIF-8 crystals are at around 1583, 1146 cm<sup>-1</sup> which are attributed to C=N, and C-N groups.

Sutrisna et al. reported that addition of ZIF-8 into polymer matrix, even at small percentages like 3 wt. % ZIF-8, causes a shift in the wavenumber of characteristic peaks of hard polyamide segment. They suggested that this showed the formation of hydrogen bonds between polyamide segment and ZIF-8 crystals [31]. On the other hand, Zhang et al. did not observe a shift on the peaks of PEBAX/ZIF-8 (15 wt. %) membrane [5]. In the current study, similar to Zhang et al. [5], no change was observed in the peaks of neither ZIF-8 nor PEBAX 1657, suggesting that ZIF-8 and PEBAX 1657 formed a physical blend without a strong interaction. Nevertheless, SEM micrographs and gas permeation properties of PEBAX 1657/ZIF-8 membranes suggest good compatibility and well adhesion probably owing to weak interactions between ZIF-8 crystals and polymer matrix [72].

#### **4.4.2 Thermal Gravimetric Analysis (TGA)**

The membranes were also analyzed by Thermal Gravimetric Analysis (TGA). The amount of residual solvent in the membranes, and temperature and weight of decomposition reactions were investigated based on thermograms of PES, and PEBAX 1657 based membranes shown in Figure 4.20. As a result of decomposition of ZIF-8 crystals, the theoretical weight loss was calculated as 97.28 % which is close to calculated % weight loss from thermograms as shown in Appendix C.

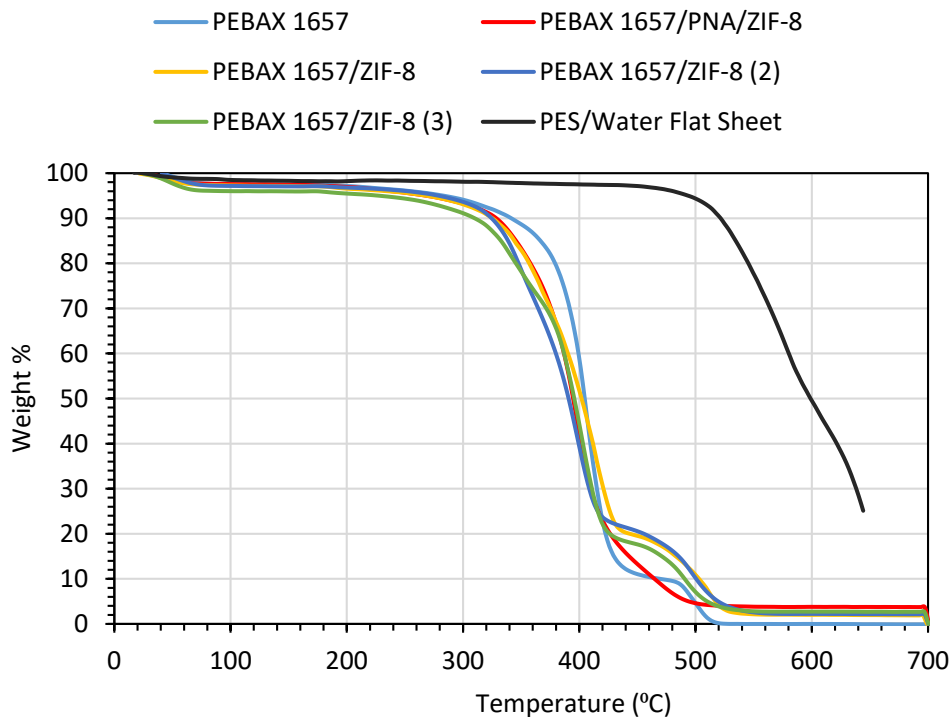


Figure 4.20. TGA results of PEBAX 1657 based membranes

According to Figure 4.20, % weight loss of different parts of the same PEBAX 1657/ZIF-8 membrane indicated as PEBAX 1657/ ZIF-8, PEBAX 1657/ ZIF-8 (2) and PEBAX 1657/ ZIF-8 (3) were similar. This showed almost uniform distribution of ZIF-8 crystals through the membrane. The increase in the slope of weight loss curve for ZIF-8 incorporated membranes indicated the formation of ZnO as the decomposition product [73]. The weight loss of PEBAX 1657 based membranes up to 320°C was insignificant. The major weight loss of PES membrane was significant above 490°C. Thermal decomposition temperature of PEBAX 1657 based membranes were higher than 400°C, which is coherent with the product specifications. Thermal decomposition temperature of PES and were 581.49°C, which are coherent with the product specifications.

As a conclusion, selection of coagulant influenced the membrane morphology and gas separation performance of the PES flat sheet membranes. PEBAX 1657 coated PES/Water and PES/IPA/Water flat sheet membranes showed better gas separation

performance compared to virgin ones. PEBAX 1657/ZIF-8 coated PES/Water flat sheet membranes showed lower gas separation performance than virgin ones. On the other hand, PEBAX 1657/ZIF-8 coating enhanced gas separation performance of virgin PES/IPA/Water membranes. Although composite structure of PEBAX 1657 coated PES flat sheet membranes was differentiated in SEM images, PEBAX 1657 based flat sheet membranes showed better gas separation performance compared to them. This may be explained by the penetration of the coating solution into the membrane pores. This could be prevented by pre-coating of PES flat sheet membranes with high flux rubbery polymer such as PDMS. Since, gutter layer helps to decrease possible penetration of the coating solution and surface roughness, which mitigates surface coating problems [74].



## CHAPTER 5

### CONCLUSIONS

In this study, the effect of spinning conditions including dope solution flow rate, bore liquid flow rate, addition of more volatile solvent to dope solution, air gap height, and temperature on the membrane morphology and gas separation performance was investigated. The single gas permeances of H<sub>2</sub>, CO<sub>2</sub> and CH<sub>4</sub> at 3 bar TMP and 35°C of the hollow fiber membranes were measured to investigate their ideal gas separation performance. The effect of PEBAX 1657 coating of PI hollow fiber membrane gas separation performance and the morphology was investigated whether it enhances gas separation performance of virgin hollow fiber membranes. For the further investigation of gas separation performance of PEBAX 1657, PEBAX 1657 based membranes without PES supports were also prepared. Into the formulation of those membranes, p-nitroaniline (PNA) and microporous ZIF-8 crystals were incorporated to analyze compatibility of ZIF-8 crystals with PEBAX 1657 polymer matrix. The effect of PEBAX 1657 coating on the membrane performance was investigated using flat sheet ultrafiltration membranes to imitate surface defects of the hollow fiber membrane since it has simpler geometry compared to other. The flat polyethersulfone (PES) membranes prepared by using different coagulation bath composition of water and IPA were coated with PEBAX 1657 and PEBAX 1657/ZIF-8. The gas separation performance of flat sheet membranes was characterized by measuring single gas permeances of N<sub>2</sub>, CO<sub>2</sub> and CH<sub>4</sub> at 3 bar TMP, 35°C. The conclusions were listed below:

1. Although selective dense layer was differentiated at the outer surface of the PI hollow fiber membranes, gas separation performance of those membranes was not sufficiently high for biogas refining. Spinning conditions influenced hollow fiber membrane morphology simultaneously. Therefore, the individual effect of spinning conditions changed with the other spinning parameters.

2. PEBAX 1657 coating of PI hollow fiber membranes enhanced the gas separation performance of hollow fiber membranes.
3. ZIF-8 crystals were compatible with PEBAX 1657 polymer addition without addition of compatibilizer (PNA) when SEM image of PEBAX 1657/ZIF-8 flat sheet membranes were investigated. There was no void around ZIF-8 crystals which were distributed through polymer matrix uniformly.
4. PEBAX 1657/ZIF-8 flat sheet membranes showed better gas separation performance compared to Pure PEBAX 1657 membranes, since incorporation of ZIF-8 crystals did not influence  $N_2$  and  $CH_4$  permeability but it increases  $CO_2$  permeability significantly. Therefore, ideal gas selectivity of  $CO_2/N_2$  and  $CO_2/CH_4$  increased.
5. PES/IPA flat sheet membranes showed better ideal gas selectivity of  $CO_2/N_2$  and  $CO_2/CH_4$  compared to PES/Water and PES/IPA/Water membranes, since PES/IPA membranes had thick dense selective layer supported by porous structure but the others had porous structure. This structure increased gas permeance and decreased ideal gas selectivity of the PES/Water and PES/IPA/Water membranes for all gases.
6. PES/Water and PES/IPA/Water flat sheet membranes having ideal selectivity of  $CO_2/N_2$  and  $CO_2/CH_4$  higher than Knudsen diffusion selectivity were coated with PEBAX 1657 and PEBAX 1657/ZIF-8 solution in order to imitate coating of hollow fiber membranes having microporous surface defects. PEBAX 1657 coating enhanced both PES/Water and PES/IPA/Water flat sheet membrane gas separation performance. PEBAX 1657/ZIF-8 coating decreased both ideal selectivity and gas permeance of PES/Water flat sheet membrane. On the other hand, PEBAX 1657/ZIF-8 coating increased the ideal selectivity of the PES/IPA/Water flat sheet membrane while decreasing gas permeances.

## REFERENCES

- [1] Blok, K., & Nieuwlaar, E. (2016). *Introduction to Energy Analysis* (2nd ed.)
- [2] Achinas, S., & Euverink, G. J. (2016). Theoretical analysis of biogas potential prediction from agricultural waste. *Resource-Efficient Technologies*, 2(3), 143-147. doi:10.1016/j.reffit.2016.08.001
- [3] Kalambe, S., Sapkal, R. S., & Sapkal, V. S. (2012). Low Pressure Separation Technique of Biogas into CH<sub>4</sub> and CO<sub>2</sub> employing PDMS membrane. *International Journal of Advanced Engineering Technology*, 3(1)
- [4] Falbo, F., Brunetti, A., Barbieri, G., Drioli, E., & Tasselli, F. (2016). CO<sub>2</sub>/CH<sub>4</sub> separation by means of Matrimid hollow fibre membranes. *Applied Petrochemical Research*, 6(4), 439-450. doi:10.1007/s13203-016-0164-z
- [5] Li, M., Zhang, X., Zeng, S., Bai, L., Gao, H., Deng, J., ... Zhang, S. (2017). Pebax-based composite membranes with high gas transport properties enhanced by ionic liquids for CO<sub>2</sub> separation. *RSC Adv*, 7(11), 6422-6431. doi:10.1039/c6ra27221e
- [6] Baker, R. W. (2004). *Membrane technology and applications* (2nd ed.). Chichester: J. Wiley.
- [7] Figoli, A., Cassano, A., & Basile, A. (2016). Membrane technologies for biorefining.
- [8] Hunger, K., Schmeling, N., Jeazet, H. B., Janiak, C., Staudt, C., & Kleinermanns, K. (2012). Investigation of Cross-Linked and Additive Containing Polymer Materials for Membranes with Improved Performance in Pervaporation and Gas Separation. *Membranes*, 2(4), 727-763. doi:10.3390/membranes2040727
- [9] Iarikov, D. D., & Ted Oyama, S. (2011). Review of CO<sub>2</sub>/CH<sub>4</sub> Separation Membranes. *Inorganic Polymeric and Composite Membranes - Structure, Function and Other Correlations*, 91-115. doi:10.1016/b978-0-444-53728-7.00005-7

- [10] Koolivand, H., Sharifa, A., Chehrazi, E., Kashani, M. R., & Paran, S. M. (2016). Mixed-matrix membranes comprising graphene-oxide nanosheets for CO<sub>2</sub>/CH<sub>4</sub> separation: A comparison between glassy and rubbery polymer matrices. *Polymer Science Series A*, 58(5), 801-809. doi:10.1134/s0965545x16050084
- [11] Ahmadi Feijani, E., Tavasoli, A., & Mahdavi, H. (2015). Improving Gas Separation Performance of Poly(vinylidene fluoride) Based Mixed Matrix Membranes Containing Metal–Organic Frameworks by Chemical Modification. *Industrial & Engineering Chemistry Research*, 54(48), 12124-12134. doi:10.1021/acs.iecr.5b02549
- [12] Yuan, H., Yu, B., Cong, H., Peng, Q., Yang, R., Yang, S., ... Li, Z. (2016). MODIFICATION PROGRESS OF POLYMER MEMBRANES FOR GAS SEPARATION. *Rev.Adv.Mater.Sci*, 44.
- [13] Chung, T. S., Teoh, S. K., & Hu, X. (1997). Formation of ultrathin high-performance polyethersulfone hollow-fiber membranes. *Journal of Membrane Science*, 133(2), 161-175. doi:10.1016/s0376-7388(97)00101-4
- [14] Zhao, D., Ren, J., Li, H., Li, X., & Deng, M. (2014). Gas separation properties of poly(amide-6-b-ethylene oxide)/amino modified multi-walled carbon nanotubes mixed matrix membranes. *Journal of Membrane Science*, 467, 41-47. doi:10.1016/j.memsci.2014.05.009
- [15] Abdul Wahab, M. S., Abdul Rahman, S., & Ahmad, A. L. (2017). Biomethane Purification Using PVDF/Pebax 1657 Thin Film Composite Membrane. *Journal of Physical Science*, 28(Suppl. 1), 39-51. doi:10.21315/jps2017.28.s1.3
- [16] Surya Murali, R., Ismail, A., Rahman, M., & Sridhar, S. (2014). Mixed matrix membranes of Pebax-1657 loaded with 4A zeolite for gaseous separations. *Separation and Purification Technology*, 129, 1-8. doi:10.1016/j.seppur.2014.03.017
- [17] Sridhar, S., Bee, S., & Bhargava, S. (2014). Membrane-based Gas Separation: Principle, Applications and Future Potential. *chemical industry digest*.
- [18] Bernardo, P., & Clarizia, G. (2013). 30 Years of Membrane Technology for Gas Separation. *CHEMICAL ENGINEERING TRANSACTIONS*, 32. doi:10.3303/CET1332334

- [19] Mulder, M. (2010). *Basic principles of membrane technology*.
- [20] Ismail, A. F., & Yean, L. P. (2003). Review on the development of defect-free and ultrathin-skinned asymmetric membranes for gas separation through manipulation of phase inversion and rheological factors. *Journal of Applied Polymer Science*, 88(2), 442-451. doi:10.1002/app.11744
- [21] Yilmaz, L., & McHUGH, A. J. (1985). Analysis of Nonsolvent-Solvent-Polymer Phase Diagrams and Their Relevance to Membrane Formation Modelling. *Applied Polymer Science*.
- [22] Bernardo, P., Drioli, E., & Golemme, G. (2009). Membrane Gas Separation: A Review/State of the Art. *Industrial & Engineering Chemistry Research*, 48(10), 4638-4663. doi:10.1021/ie8019032
- [23] Lu, G., Diniz da Costa, J., Duke, M., Giessler, S., Socolow, R., Williams, R., & Kreutz, T. (2007). Inorganic membranes for hydrogen production and purification: A critical review and perspective. *Journal of Colloid and Interface Science*, 314(2), 589-603. doi:10.1016/j.jcis.2007.05.067
- [24] Ismail, A., Rahim, R., & Rahman, W. (2008). Characterization of polyethersulfone/Matrimid® 5218 miscible blend mixed matrix membranes for O<sub>2</sub>/N<sub>2</sub> gas separation. *Separation and Purification Technology*, 63(1), 200-206. doi:10.1016/j.seppur.2008.05.007.
- [25] Tamime, A. Y. (2013). *Membrane processing: Dairy and beverage applications*. Chichester: Wiley-Blackwell.
- [26] Zhao, D., Ren, J., Wang, Y., Qiu, Y., Li, H., Hua, K., ... Deng, M. (2017). High CO<sub>2</sub> separation performance of Pebax®/CNTs/GTA mixed matrix membranes. *Journal of Membrane Science*, 521, 104-113. doi:10.1016/j.memsci.2016.08.061
- [27] Kim, J. H., & Lee, Y. M. (2001). Gas permeation properties of poly(amide-6-b-ethylene oxide)-silica hybrid membranes. *Journal of Membrane Science*, 193(2), 209-225. doi:10.1016/s0376-7388(01)00514-2
- [28] Murali, R. S., Sridhar, S., Sankarshana, T., & Ravikumar, Y. V. (2010). Gas Permeation Behavior of Pebax-1657 Nanocomposite Membrane Incorporated with Multiwalled Carbon Nanotubes. *Industrial & Engineering Chemistry Research*, 49(14), 6530-6538. doi:10.1021/ie9016495

- [29] Li, T., Pan, Y., Peinemann, K., & Lai, Z. (2013). Carbon dioxide selective mixed matrix composite membrane containing ZIF-7 nano-fillers. *Journal of Membrane Science*, 425-426, 235-242. doi:10.1016/j.memsci.2012.09.006
- [30] Jomekian, A., Behbahani, R. M., Mohammadi, T., & Kargari, A. (2016). CO<sub>2</sub>/CH<sub>4</sub> separation by high performance co-casted ZIF-8/Pebax 1657/PES mixed matrix membrane. *Journal of Natural Gas Science and Engineering*, 31, 562-574. doi:10.1016/j.jngse.2016.03.067
- [31] Sutrisna, P. D., Hou, J., Li, H., Zhang, Y., & Chen, V. (2017). Improved operational stability of Pebax-based gas separation membranes with ZIF-8: A comparative study of flat sheet and composite hollow fibre membranes. *Journal of Membrane Science*, 524, 266-279. doi:10.1016/j.memsci.2016.11.048
- [32] Wang, S., Liu, Y., Huang, S., Wu, H., Li, Y., Tian, Z., & Jiang, Z. (2014). Pebax-PEG-MWCNT hybrid membranes with enhanced CO<sub>2</sub> capture properties. *Journal of Membrane Science*, 460, 62-70. doi:10.1016/j.memsci.2014.02.036
- [33] Peng, N., & Chung, T. S. (2008). The effects of spinneret dimension and hollow fiber dimension on gas separation performance of ultra-thin defect-free Torlon® hollow fiber membranes. *Journal of Membrane Science*, 310(1-2), 455-465. doi:10.1016/j.memsci.2007.11.018
- [34] Feng, C., Khulbe, K., Matsuura, T., & Ismail, A. (2013). Recent progresses in polymeric hollow fiber membrane preparation, characterization and applications. *Separation and Purification Technology*, 111, 43-71. doi:10.1016/j.seppur.2013.03.017
- [35] JIANG, L. (2004). Fabrication of Matrimid/polyethersulfone dual-layer hollow fiber membranes for gas separation. *Journal of Membrane Science*, 240(1-2), 91-103. doi:10.1016/j.memsci.2004.04.015
- [36] Kaltalı, G. (2014). *FABRICATION OF POLYETHERSULFONE HOLLOW FIBERS FOR ULTRAFILTRATION* (Master's thesis, Middle East Technical University, Ankara, Turkey).
- [37] Ismail, A.F., Dunkin, I.R., Gallivan, S.L. and Shilton, S.J. 1999. Production of super selective polysulfone hollow fiber membranes for gas separation. *Polymer*, 40. 6499-6506.

- [38] Kapantaidakis, G., & Koops, G. (2002). High flux polyethersulfone–polyimide blend hollow fiber membranes for gas separation. *Journal of Membrane Science*, 204(1-2), 153-171. doi:10.1016/s0376-7388(02)00030-3
- [39] Chung, T., & Hu, X. (1997). Effect of air-gap distance on the morphology and thermal properties of polyethersulfone hollow fibers. *Journal of Applied Polymer Science*, 66(6), 1067-1077. doi:10.1002/(sici)1097-4628(19971107)66:6<1067::aid-app7>3.3.co;2-g
- [40] Chen, H. Z., Thong, Z., Li, P., & Chung, T. (2014). High performance composite hollow fiber membranes for CO<sub>2</sub>/H<sub>2</sub> and CO<sub>2</sub>/N<sub>2</sub> separation. *International Journal of Hydrogen Energy*, 39(10), 5043-5053. doi:10.1016/j.ijhydene.2014.01.047
- [41] Wang, D., Li, K., & Teo, W. (2000). Highly permeable polyethersulfone hollow fiber gas separation membranes prepared using water as non-solvent additive. *Journal of Membrane Science*, 176(2), 147-158. doi:10.1016/s0376-7388(00)00419-1
- [42] Wang, D., Li, K., & Teo, W. (1996). Polyethersulfone hollow fiber gas separation membranes prepared from NMP/alcohol solvent systems. *Journal of Membrane Science*, 115(1), 85-108. doi:10.1016/0376-7388(95)00312-6
- [43] Clausi, D. T., & Koros, W. J. (2000). Formation of defect-free polyimide hollow fiber membranes for gas separations. *Journal of Membrane Science*, 167(1), 79-89. doi:10.1016/s0376-7388(99)00276-8
- [44] Krol, J., Boerrigter, M., & Koops, G. (2001). Polyimide hollow fiber gas separation membranes: preparation and the suppression of plasticization in propane/propylene environments. *Journal of Membrane Science*, 184(2), 275-286. doi:10.1016/s0376-7388(00)00640-2
- [45] Cao, C., Chung, T., Chen, S. B., & Dong, Z. (2004). The study of elongation and shear rates in spinning process and its effect on gas separation performance of Poly(ether sulfone) (PES) hollow fiber membranes. *Chemical Engineering Science*, 59(5), 1053-1062. doi:10.1016/j.ces.2003.10.023
- [46] Hosseini, S. S., Peng, N., & Chung, T. S. (2010). Gas separation membranes developed through integration of polymer blending and dual-layer hollow fiber spinning process for hydrogen and natural gas enrichments. *Journal of Membrane Science*, 349(1-2), 156-166. doi:10.1016/j.memsci.2009.11.043

- [47] Kapantaidakis, G., Koops, G., & Wessling, M. (2002). Preparation and characterization of gas separation hollow fiber membranes based on polyethersulfone-polyimide miscible blends. *Desalination*, 145(1-3), 353-357. doi:10.1016/s0011-9164(02)00435-6
- [48] Wang, D., Li, K., & Teo, W. (1998). Preparation and characterization of polyetherimide asymmetric hollow fiber membranes for gas separation. *Journal of Membrane Science*, 138(2), 193-201. doi:10.1016/s0376-7388(97)00229-9
- [49] Carruthers, S. B., Ramos, G. L., & Koros, W. J. (2003). Morphology of integral-skin layers in hollow-fiber gas-separation membranes. *Journal of Applied Polymer Science*, 90(2), 399-411. doi:10.1002/app.12623
- [50] Cao, C., Wang, R., Chung, T. S., & Liu, Y. (2002). Formation of high-performance 6FDA-2,6-DAT asymmetric composite hollow fiber membranes for CO<sub>2</sub>/CH<sub>4</sub> separation. *Journal of Membrane Science*, 209(1), 309-319. doi:10.1016/s0376-7388(02)00359-9
- [51] Chung, T., Lin, W., & Vora, R. H. (2000). The effect of shear rates on gas separation performance of 6FDA-durene polyimide hollow fibers. *Journal of Membrane Science*, 167(1), 55-66. doi:10.1016/s0376-7388(99)00278-1
- [52] Magueijo, V., Anderson, L., Fletcher, A., & Shilton, S. (2013). Polysulfone mixed matrix gas separation hollow fibre membranes filled with polymer and carbon xerogels. *Chemical Engineering Science*, 92, 13-20. doi:10.1016/j.ces.2013.01.043
- [53] Kim, J., & Van der Bruggen, B. (2010). The use of nanoparticles in polymeric and ceramic membrane structures: Review of manufacturing procedures and performance improvement for water treatment. *Environmental Pollution*, 158(7), 2335-2349. doi:10.1016/j.envpol.2010.03.024
- [54] Zulhairun, A., Ng, B., Ismail, A., Surya Murali, R., & Abdullah, M. (2014). Production of mixed matrix hollow fiber membrane for CO<sub>2</sub>/CH<sub>4</sub> separation. *Separation and Purification Technology*, 137, 1-12. doi:10.1016/j.seppur.2014.09.014
- [55] Husain, S. (2006). *Mixed Matrix Dual Layer Hollow Fiber Membranes For Natural Gas Separation* (Doctoral dissertation).
- [56] Bakhtiari, O., Mosleh, S., Khosravi, T., & Mohammadi, T. (2011). Preparation, Characterization and Gas Permeation of Polyimide Mixed Matrix

Membranes. *Journal of Membrane Science & Technology*, 01(01). doi:10.4172/2155-9589.1000102

[57] Eiras, D., Labreche, Y., & Pessan, L. A. (2016). Ultem®/ZIF-8 Mixed Matrix Membranes for Gas Separation: Transport and Physical Properties. *Materials Research*, 19(1), 220-228. doi:10.1590/1980-5373-mr-2015-0621

[58] Zahri, K., Wong, K. C., Goh, P. S., & Ismail, A. F. (2016). Graphene oxide/polysulfone hollow fiber mixed matrix membranes for gas separation. *RSC Adv*, 6(92), 89130-89139. doi:10.1039/c6ra16820e

[59] Hu, J., Cai, H., Ren, H., Wei, Y., Xu, Z., Liu, H., & Hu, Y. (2010). Mixed-Matrix Membrane Hollow Fibers of Cu<sub>3</sub>(BTC)<sub>2</sub>MOF and Polyimide for Gas Separation and Adsorption. *Industrial & Engineering Chemistry Research*, 49(24), 12605-12612. doi:10.1021/ie1014958

[60] Dai, Y., Johnson, J., Karvan, O., Sholl, D. S., & Koros, W. (2012). Ultem®/ZIF-8 mixed matrix hollow fiber membranes for CO<sub>2</sub>/N<sub>2</sub> separations. *Journal of Membrane Science*, 401-402, 76-82. doi:10.1016/j.memsci.2012.01.044

[61] J. Han, W. Lee, J.M. Choi, R. Patel, B.R. Min, Characterization of polyethersulfone/polyimide blend membranes prepared by a dry/wet phase inversion: Precipitation kinetics, morphology and gas separation, *J. Memb. Sci.* 351 (2010) 141–148. doi:10.1016/j.memsci.2010.01.038

[62] Keser Demir, N., Topuz, B., Yilmaz, L., & Kalipcilar, H. (2014). Synthesis of ZIF-8 from recycled mother liquors. *Microporous and Mesoporous Materials*, 198, 291-300. doi:10.1016/j.micromeso.2014.07.052

[63] Chen, X. Y., Vinh-Thang, H., Ramirez, A. A., Rodrigue, D., & Kaliaguine, S. (2015). Membrane gas separation technologies for biogas upgrading. *RSC Adv*, 5(31), 24399-24448. doi:10.1039/c5ra00666j

[64] Karğılı, M. (2015). *POLYMER BLEND BASED MIXED MATRIX GAS SEPARATION MEMBRANES* (Master's thesis, MIDDLE EAST TECHNICAL UNIVERSITY )

[65] Brown, P. J., Ying, S., & Yang, J. (2002). MORPHOLOGICAL STRUCTURE OF POLYETHERKETONE MEMBRANES FOR GAS SEPARATION PREPARED BY PHASE INVERSION. *AUTEX Research Journal*, 2

- [66] Kamal, S. N., Leo, C. P., Ahmad, A. L., & Junaidi, M. U. (2013). Effects of THF as cosolvent in the preparation of polydimethylsiloxane/polyethersulfone membrane for gas separation. *Polymer Engineering & Science*, *54*(9), 2177-2186. doi:10.1002/pen.23767
- [67] Tasselli, F., Jansen, J. C., & Drioli, E. (2003). PEEKWC ultrafiltration hollow-fiber membranes: Preparation, morphology, and transport properties. *Journal of Applied Polymer Science*, *91*(2), 841-853. doi:10.1002/app.13207
- [68] Widjojo, N., Chung, T., Arifin, D. Y., Weber, M., & Warzelhan, V. (2010). Elimination of die swell and instability in hollow fiber spinning process of hyperbranched polyethersulfone (HPES) via novel spinneret designs and precise spinning conditions. *Chemical Engineering Journal*, *163*(1-2), 143-153. doi:10.1016/j.cej.2010.07.048
- [69] McEwen, J., Hayman, J., & Ozgur Yazaydin, A. (2013). A comparative study of CO<sub>2</sub>, CH<sub>4</sub> and N<sub>2</sub> adsorption in ZIF-8, Zeolite-13X and BPL activated carbon. *Chemical Physics*, *412*, 72-76. doi:10.1016/j.chemphys.2012.12.012
- [70] Lee, W., Kim, D., & Kim, J. (2000). Preparation and gas separation properties of asymmetric polysulfone membranes by a dual bath method. *Korean Journal of Chemical Engineering*, *17*(2), 143-148. doi:10.1007/bf02707135
- [71] Nordin, N. A., Ismail, A. F., Mustafa, A., Murali, R. S., & Matsuura, T. (2014). The impact of ZIF-8 particle size and heat treatment on CO<sub>2</sub>/CH<sub>4</sub> separation using asymmetric mixed matrix membrane. *RSC Adv*, *4*(94), 52530-52541. doi:10.1039/c4ra08460h
- [72] Ryu, S. R., Noda, I., & Jung, Y. M. (2010). What is the Origin of Positional Fluctuation of Spectral Features: True Frequency Shift or Relative Intensity Changes of Two Overlapped Bands? *Applied Spectroscopy*, *64*(9), 1017-1021. doi:10.1366/000370210792434396
- [73] Guo, J., & Peng, C. (2015). Synthesis of ZnO nanoparticles with a novel combustion method and their C<sub>2</sub>H<sub>5</sub>OH gas sensing properties. *Ceramics International*, *41*(2), 2180-2186. doi:10.1016/j.ceramint.2014.10.017
- [74] Dai, Z., Ansaloni, L., & Deng, L. (2016). Recent advances in multi-layer composite polymeric membranes for CO<sub>2</sub> separation: A review. *Green Energy & Environment*, *1*(2), 102-128. doi:10.1016/j.gee.2016.08.001

## APPENDICES

### APPENDIX A

#### CALCULATION OF SINGLE GAS PERMEANCE AND PERMEABILITY

Single gas permeance was calculated for asymmetric structured membranes. For symmetrical structured membranes, gas permeability was calculated. Permeate side of the membrane was kept under vacuum until the feed gas was pressurized to 2.1 bar g. Pressure increase in the permeate side was recorded with respect to time by using Opik 04 program. A sample rate of change in the permeate side pressure with respect to time was given in Figure A.1.

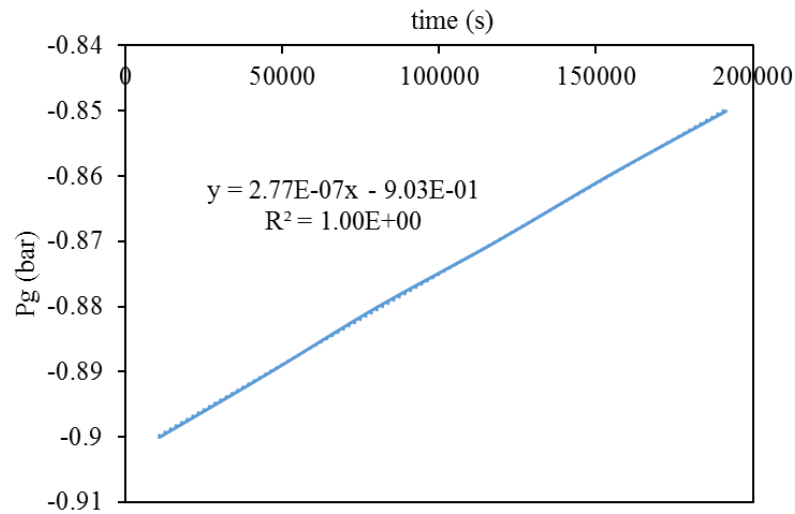


Figure A.1. The time (s) vs. permeate pressure (bar g) graph for CH<sub>4</sub> permeation test of PES/IPA membrane

In order to calculate membrane gas permeance, Equation A.1 was used.

$$\text{Permeance} = \frac{dn}{A \times dt \times TMP} \quad \text{Equation A.1}$$

Trans membrane pressure (TMP) was calculated by using Equation A.2. TMP was assumed constant for small increment of pressure with respect to time.

$$TMP = P_{feed} - P_{permeate} \quad \text{Equation A.2}$$

Membrane area (A) was calculated as 13.2 cm<sup>2</sup> for flat sheet membranes. In order to calculate dn/dt term, slope of the  $\Delta P$  vs t graph was used. CH<sub>4</sub> was assumed as an ideal gas at 3 bar and 35°C. By using ideal gas law dn/dt (mol/s) was calculated by Equation A.3.

$$\frac{dn}{dt} = \frac{V_{dead\ end}}{R \times T} \times \frac{dP}{dt} \quad \text{Equation A.3}$$

Gas permeation tests were conducted by using constant volume variable pressure module. Dead end volume ( $V_{dead\ end}$ ) was 30.64 cm<sup>3</sup>.

In order to calculate the gas permeability, Equation A.4 was used.

$$\text{Permeability} = \text{Permeance} \times \text{membrane thickness (l)} \quad \text{Equation A.4}$$

Membrane thickness were measured by using a micrometer.

## APPENDIX B

### AVERAGE PARTICLE SIZE OF THE ZIF-8 CRYSTALS

Particle size of ZIF-8 crystals was measured from SEM image of ZIF-8 crystals by using Image J software. Measured size of ZIF-8 crystals were shown in Table B.1.

Table B.1. Particle size measurement of different ZIF-8 crystals measured from SEM images

Particle #	Particle size (nm)	Particle #	Particle size (nm)	Particle #	Particle size (nm)
1	82	19	60	37	67
2	64	20	65	38	72
3	62	21	62	39	73
4	59	22	74	40	83
5	80	23	73	41	89
6	82	24	86	42	40
7	65	25	72	43	64
8	71	26	67	44	68
9	72	27	74	45	78
10	44	28	76	46	42
11	52	29	75	47	67
12	64	30	36	48	82
13	44	31	61	49	39
14	49	32	83	50	79
15	81	33	95		
16	87	34	94		
17	72	35	65		
18	86	36	79		
				<b>Mean</b>	<b>69 nm</b>
				<b>SD</b>	<b>14 nm</b>



## APPENDIX C

### TGA THERMOGRAMS OF THE PREPARED MEMBRANES

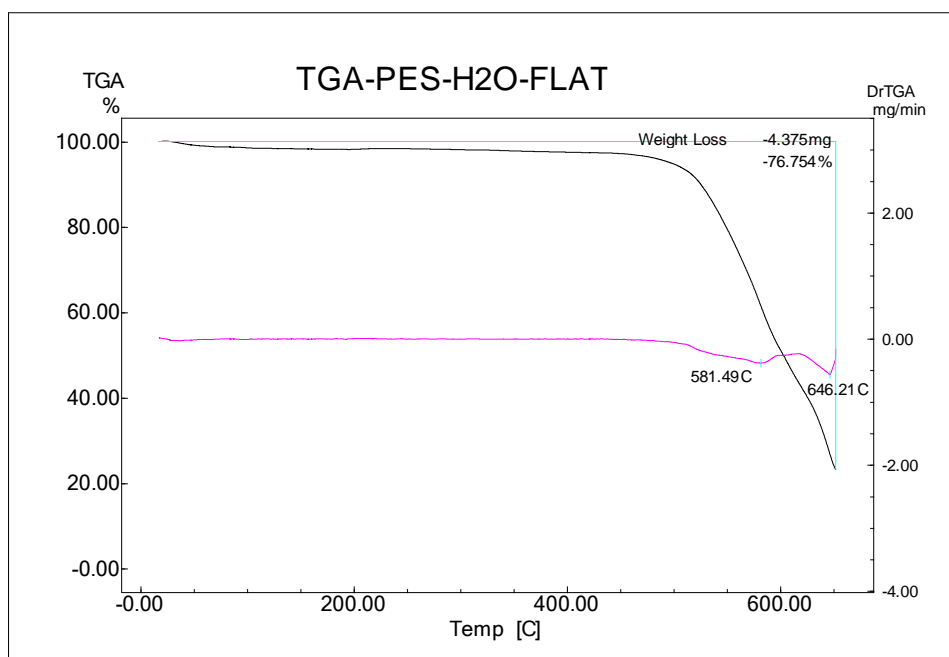


Figure C.1. The TGA thermogram of PES flat sheet membrane

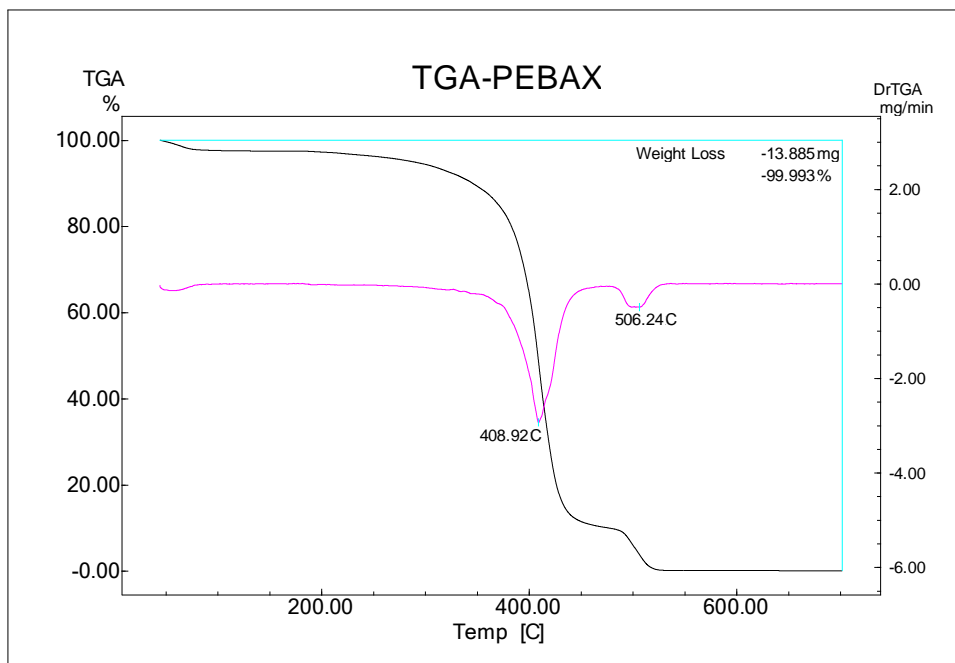


Figure C.2. The TGA thermogram of PEBAX 1657 flat sheet membrane

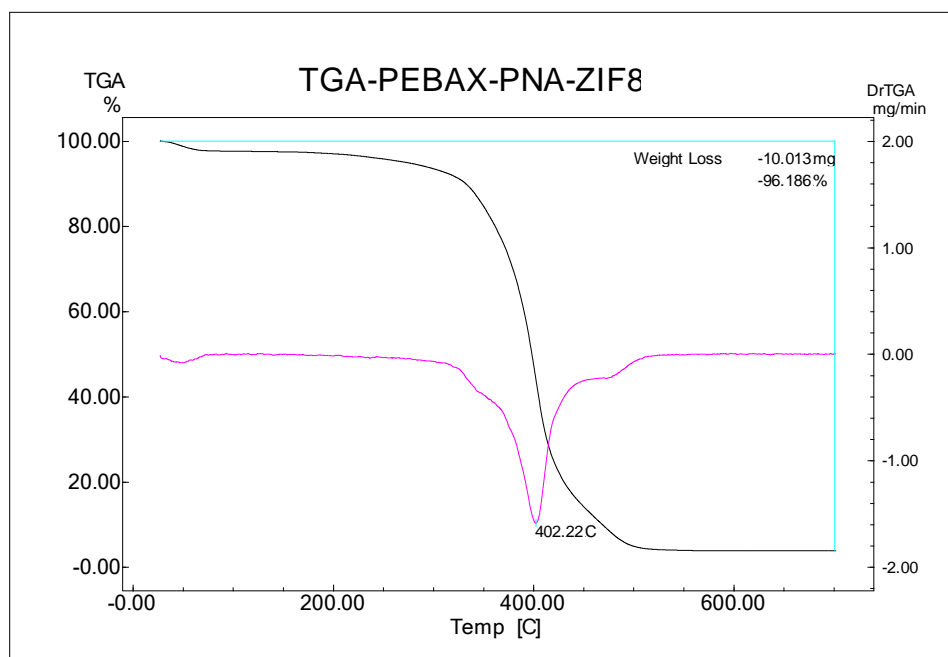


Figure C.3. The TGA thermogram of PEBAX 1657/PNAZIF-8 flat sheet membrane

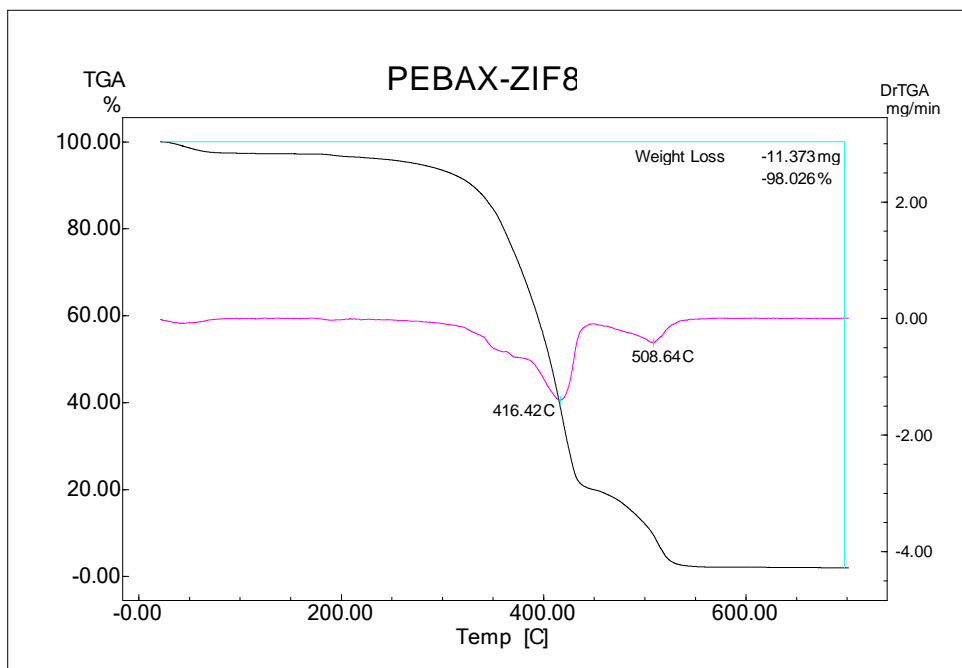


Figure C.4. The TGA thermogram of PEBAX 1657/ZIF-8 flat sheet membrane (part 1)

Sample calculation for expected theoretical weight loss for PEBAX 1657/ZIF-8 membrane was shown below:

Formula weight of ZIF-8 :1364.3 g/mol

Mass of ZnO as a decomposition product (1 mole ZIF-8 basis): 408.3 g

ZIF-8 weight: 9.09 g in 100 g membrane as a basis

$$\% \text{ ZnO (theoretical)} = \frac{9.09 \times 408.3}{1364.3} = 2.72 \%$$

$$\% \text{ weight loss (theoretical)} = 97.28 \%$$

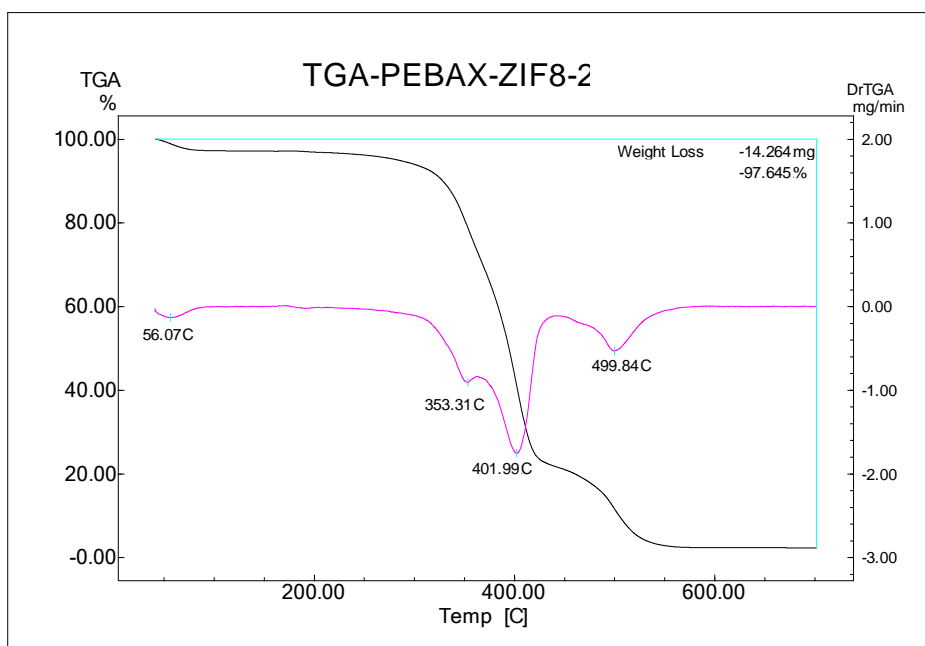


Figure C.5. The TGA thermogram of PEBAX 1657/ZIF-8 flat sheet membrane (part 2)

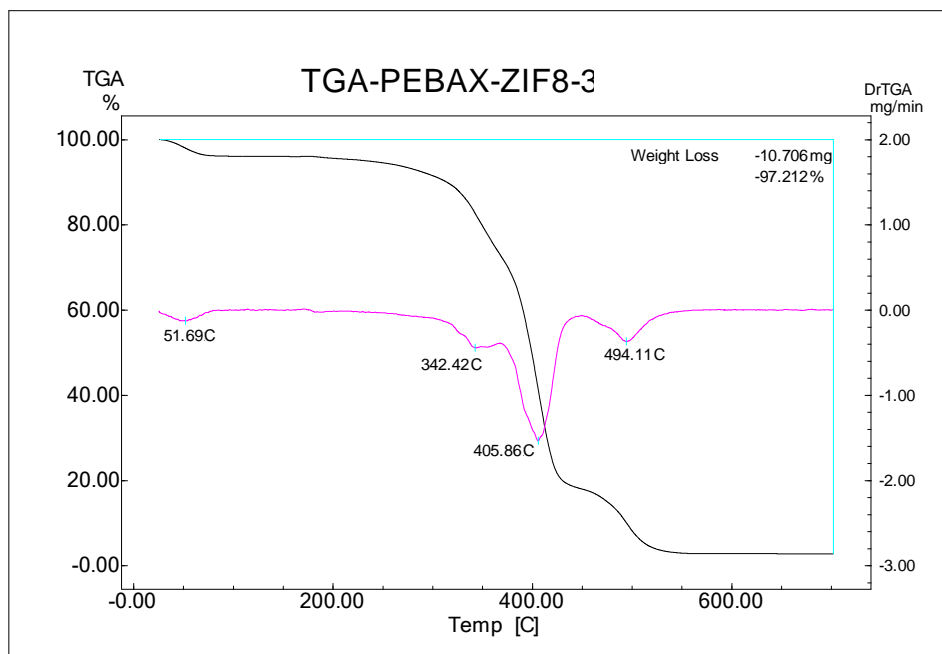


Figure C.6. The TGA thermogram of PEBAX 1657/ZIF-8 flat sheet membrane (part 3)

## APPENDIX D

### REPRODUCIBILITY OF THE FLAT SHEET MEMBRANE PREPARATION

The sample codes are shown as X.Y for prepared flat sheet membranes, where X represents batch numbers and Y represents membrane number obtained from batch X. For instances, PES/Water 3.1 shows that the third membrane prepared from the same composition and 1 indicates the piece of membrane obtained from this batch.

Table D.1. Reproducibility of the dense PEBAX 1657 membrane preparation

Membrane Code	Permeability (Barrer)			Ideal Selectivity	
	N <sub>2</sub>	CO <sub>2</sub>	CH <sub>4</sub>	CO <sub>2</sub> /N <sub>2</sub>	CO <sub>2</sub> /CH <sub>4</sub>
<b>Pure PEBAX 1657 No 8</b>	6.19	219.71	21.38	35.48	10.28
<b>Pure PEBAX 1657 No 10</b>	11.54	234.53	23.70	20.32	9.90
<b>Pure PEBAX 1657 No 27</b>	8.35	190.87	18.21	22.86	10.48
<b>Average</b>	8.69	215.04	21.10	26.22	10.22
<b>Std.Dev.</b>	2.20	18.13	2.25	6.63	0.24

Table D.2. Reproducibility of the dense PEBAX 1657/ZIF-8 membrane preparation

Membrane Code	Permeability (Barrer)			Ideal Selectivity	
	N <sub>2</sub>	CO <sub>2</sub>	CH <sub>4</sub>	CO <sub>2</sub> /N <sub>2</sub>	CO <sub>2</sub> /CH <sub>4</sub>
<b>PEBAX 1657/ZIF8 No 5</b>	9.08	325.63	12.56	35.85	25.93
<b>PEBAX 1657/ZIF8 No 15</b>	5.90	360.53	15.46	61.07	23.32
<b>PEBAX 1657/ZIF8 No 21</b>	13.01	300.90	29.72	23.14	10.13
<b>Average</b>	9.33	329.02	19.25	40.02	19.79
<b>Std.Dev.</b>	2.90	24.46	7.50	15.76	6.92

Table D.3. Reproducibility of the PES/Water membrane preparation

Membrane Code	Permeance (GPU)			Ideal Selectivity	
	N <sub>2</sub>	CO <sub>2</sub>	CH <sub>4</sub>	CO <sub>2</sub> /N <sub>2</sub>	CO <sub>2</sub> /CH <sub>4</sub>
<b>PES/Water 2.1</b>	7.41	26.18	9.27	3.53	2.82
<b>PES/Water 3.1</b>	8.40	26.09	11.17	3.11	2.34
<b>PES/Water 4.1</b>	8.35	15.73	11.14	2.01	1.41
<b>Average</b>	8.05	22.67	10.53	2.84	2.19
<b>Std.Dev.</b>	0.45	4.41	1.12	0.70	0.58

Table D.4. Reproducibility of the PES/IPA/Water membrane preparation

Membrane Code	Permeance (GPU)			Ideal Selectivity	
	N <sub>2</sub>	CO <sub>2</sub>	CH <sub>4</sub>	CO <sub>2</sub> /N <sub>2</sub>	CO <sub>2</sub> /CH <sub>4</sub>
<b>PES/IPA/WATER 4.1</b>	20.94	20.71	30.80	0.99	0.67
<b>PES/IPA/WATER 5.1</b>	22.58	21.42	34.46	0.95	0.62
<b>PES/IPA/WATER 7.1</b>	23.50	22.33	32.61	0.95	0.68
<b>Average</b>	22.34	21.49	32.62	0.96	0.66
<b>Std.Dev.</b>	1.06	0.67	1.50	0.02	0.03

Table D.5. Reproducibility of the PES/IPA membrane preparation

Membrane Code	Permeance (GPU)			Ideal Selectivity	
	N <sub>2</sub>	CO <sub>2</sub>	CH <sub>4</sub>	CO <sub>2</sub> /N <sub>2</sub>	CO <sub>2</sub> /CH <sub>4</sub>
<b>PES/IPA 1.1</b>	6.07E-03	8.99E-02	5.36E-03	14.80	16.77
<b>PES/IPA 4.1</b>	4.85E-03	4.56E-02	2.62E-03	9.40	17.42
<b>Average</b>	5.47E-03	7.22E-03	4.28E-03	12.10	17.10
<b>Std.Dev.</b>	6.13E-04	2.36E-03	1.47E-03	2.70	0.33

Table D.6. Reproducibility of the PEBAX 1657 coated PES/Water membrane preparation

Membrane Code	Gas Permeance (GPU)			Ideal Selectivity	
	N <sub>2</sub>	CO <sub>2</sub>	CH <sub>4</sub>	CO <sub>2</sub> /N <sub>2</sub>	CO <sub>2</sub> /CH <sub>4</sub>
<b>PEBAX 1657 coated PES/Water 2.1</b>	0.64	12.27	0.84	19.23	14.69
<b>PEBAX 1657 coated PES/Water 3.1</b>	0.37	6.48	0.64	17.75	10.13
<b>PEBAX 1657 coated PES/Water 4.3</b>	0.37	6.16	0.43	16.63	14.41
<b>Average</b>	0.46	8.30	0.63	17.87	13.08
<b>Std.Dev.</b>	0.13	2.81	0.17	1.07	2.09

Table D.7. Reproducibility of the PEBAX 1657 coated PES/IPA/Water membrane preparation

Membrane Code	Gas Permeance (GPU)			Ideal Selectivity	
	N <sub>2</sub>	CO <sub>2</sub>	CH <sub>4</sub>	CO <sub>2</sub> /N <sub>2</sub>	CO <sub>2</sub> /CH <sub>4</sub>
<b>PEBAX 1657 coated PES/IPA/Water 1.1</b>	0.94	8.42	0.89	8.99	9.44
<b>PEBAX 1657 coated PES/IPA/Water 2.1</b>	0.56	3.66	0.70	6.54	5.22
<b>PEBAX 1657 coated PES/IPA/Water 6.2</b>	0.30	3.21	0.46	10.57	7.00
<b>Average</b>	0.60	5.10	0.68	8.70	7.22
<b>Std.Dev.</b>	0.26	2.36	0.18	1.66	1.73

Table D.8. Reproducibility of the PEBAX 1657/ZIF-8 coated PES/Water membrane preparation

Membrane Code	Permeance (GPU)			Ideal Selectivity	
	N <sub>2</sub>	CO <sub>2</sub>	CH <sub>4</sub>	CO <sub>2</sub> /N <sub>2</sub>	CO <sub>2</sub> /CH <sub>4</sub>
<b>PEBAX 1657/ZIF-8 coated PES/Water</b>	3.82	6.73	4.65	1.76	1.45
<b>PEBAX 1657/ZIF-8 coated PES/Water</b>	0.99	6.22	4.77	6.28	1.30
<b>Average</b>	2.41	6.47	4.71	4.02	1.38
<b>Std.Dev.</b>	1.42	0.26	0.06	2.26	0.07

Table D.9. Reproducibility of the PEBAX 1657/ZIF-8 coated PES/IPA/Water membrane preparation

Membrane Code	Permeance (GPU)			Ideal Selectivity	
	N <sub>2</sub>	CO <sub>2</sub>	CH <sub>4</sub>	CO <sub>2</sub> /N <sub>2</sub>	CO <sub>2</sub> /CH <sub>4</sub>
<b>PEBAX 1657/ZIF-8 coated PES/IPA/Water</b>	0.81	4.64	0.90	5.72	5.18
<b>PEBAX 1657/ZIF-8 coated PES/IPA/Water</b>	0.74	4.67	0.88	6.34	5.32
<b>Average</b>	0.77	4.65	0.89	6.03	5.25
<b>Std.Dev.</b>	0.04	0.01	0.01	0.31	0.07



## APPENDIX E

### UNIFORMITY OF HOLLOW FIBER MEMBRANES THROUGHOUT THE SPINNING PROCESS

In each meter of hollow fiber, a sample was taken for gas permeation so that part 1 of PI.B20.D30 shows a sample taken from the 2<sup>nd</sup> m after spinning started and 2 of PI.B20.D30 shows the sample from 3<sup>rd</sup> m. (B20:0.50 g/min, B30:0.75 g/min, B40:1.00 g/min, D30:1.0 g/min, D100:2.6 g/min)

Table E.1. Uniformity of the prepared hollow fiber membranes with a 30 PI:7 THF:63DMF dope liquid composition and 15°C heating zone temperature

Membrane code	Gas Permeance (GPU)			Ideal Selectivity		
	H <sub>2</sub>	CO <sub>2</sub>	CH <sub>4</sub>	H <sub>2</sub> /CO <sub>2</sub>	H <sub>2</sub> /CH <sub>4</sub>	CO <sub>2</sub> /CH <sub>4</sub>
PI.B20.D30. AG 12 (part1)	6.37	2.54	0.52	2.51	12.33	4.92
PI.B20.D30. AG 12 (part2)	31.46	8.70	6.76	3.62	4.66	1.29

Table E.2. Uniformity of the prepared hollow fiber membranes with a 30 PI:0 THF: 70 DMF dope liquid composition and 15°C heating zone temperature

Membrane code	Gas Permeance (GPU)			Ideal Selectivity		
	H <sub>2</sub>	CO <sub>2</sub>	CH <sub>4</sub>	H <sub>2</sub> /CO <sub>2</sub>	H <sub>2</sub> /CH <sub>4</sub>	CO <sub>2</sub> /CH <sub>4</sub>
PI.B20.D30. AG6 (part1)	2.22	0.46	2.19	4.85	11.74	2.42
PI.B20.D30. AG6 (part2)	2.20	0.75	0.18	2.93	12.28	4.19
PI.B30.D30. AG6 (part1)	1.13	0.99	1.18	1.14	0.95	0.84
PI.B30.D30. AG6 (part2)	2.19	0.72	0.18	3.02	12.13	4.02
PI.B20.D30. AG12 (part1)	3.78	0.39	0.34	9.80	11.18	1.14
PI.B20.D30. AG12 (part2)	3.68	0.38	0.27	9.58	13.49	1.41
PI.B40.D30. AG12 (part1)	3.22	0.41	0.39	7.90	8.26	1.04
PI.B40.D30. AG12 (part2)	3.05	0.43	0.41	7.05	7.36	1.04
PI.B30.D30. AG 6 (part1)	1.13	0.99	1.18	1.14	0.95	0.84
PI.B30.D30. AG 6 (part2)	2.19	0.72	0.18	3.02	12.13	4.02
PI.B30.D30. AG 12 (part1)	5.09	1.43	0.39	3.56	13.21	3.71
PI.B30.D30. AG 12 (part2)	3.46	0.46	0.28	7.57	12.34	1.63

Table E.3. Uniformity of the prepared hollow fiber membranes with a 30 PI:0 THF: 70 DMF dope liquid composition and 35°C heating zone temperature

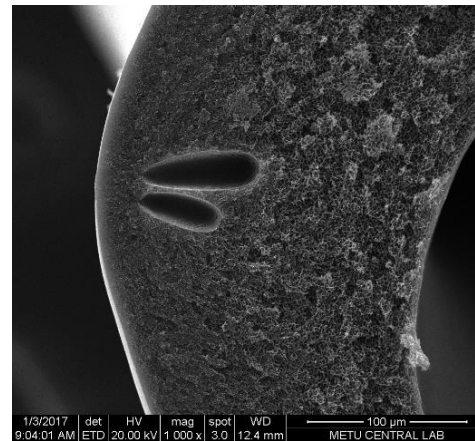
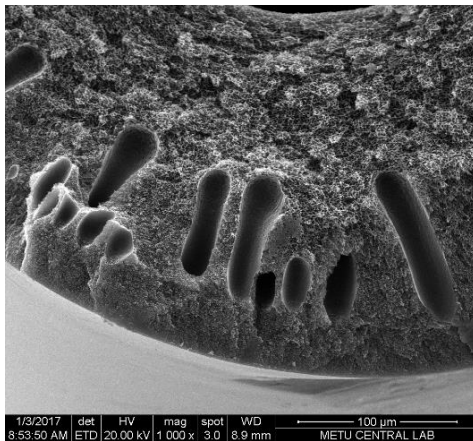
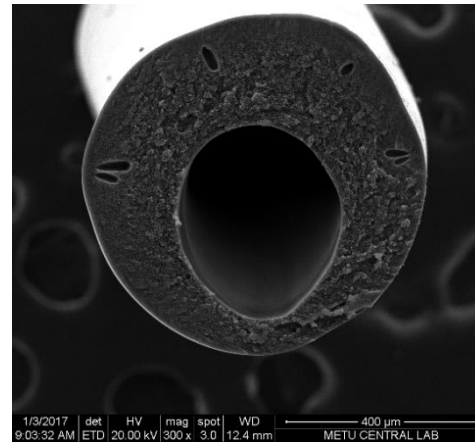
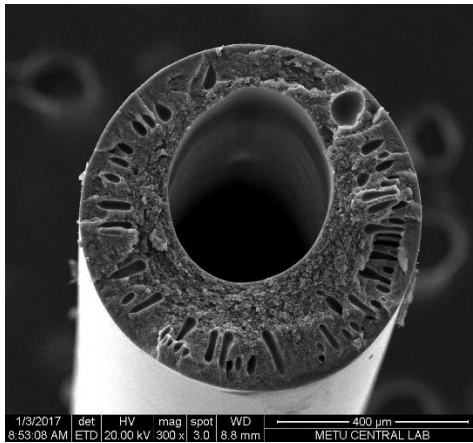
Membrane code	Gas Permeance (GPU)			Ideal Selectivity		
	H <sub>2</sub>	CO <sub>2</sub>	CH <sub>4</sub>	H <sub>2</sub> /CO <sub>2</sub>	H <sub>2</sub> /CH <sub>4</sub>	CO <sub>2</sub> /CH <sub>4</sub>
PI.B20.D30. AG12 (part1)	7.70	2.31	0.42	3.32	18.13	5.45
PI.B20.D30. AG12 (part2)	8.43	2.43	0.34	3.47	24.81	7.14
PI.B20.D100. AG12 (part1)	6.22	2.19	0.31	2.83	20.00	7.06
PI.B20.D100. AG12 (part2)	9.14	4.63	2.09	1.97	4.37	2.21
PI.B40.D30. AG12 (part1)	8.72	5.40	0.44	1.62	19.89	12.31
PI.B40.D30. AG12 (part2)	14.90	5.28	0.40	2.82	37.07	13.15
PI.B40.D100. AG12 (part1)	11.11	5.33	0.47	2.08	23.69	11.37
PI.B40.D100. AG12 (part2)	11.72	4.28	0.72	2.74	16.39	5.98
PI.B30.D30. AG 12 (part1)	13.51	4.65	0.38	2.90	35.67	12.28
PI.B30.D30. AG 12 (part2)	11.05	3.92	0.46	2.82	24.27	8.61
PI.B30.D30. AG 20 (part1)	10.07	3.85	0.30	2.62	33.36	12.75
PI.B30.D30. AG 20 (part2)	12.64	4.76	0.35	2.66	36.06	13.58
PEBAX 1657 coated PI.B20.D30. AG12 (part1)	6.43	2.73	0.26	2.35	24.76	10.52
PEBAX 1657 coated PI.B20.D30. AG12 (part2)	6.58	2.71	0.22	2.42	30.15	12.44
PEBAX 1657 coated PI.B20.D100. AG12 (part1)	5.31	2.07	0.18	2.57	28.82	11.23
PEBAX 1657 coated PI.B20.D100. AG12 (part2)	5.32	2.19	0.18	2.43	29.85	12.30
PEBAX 1657 coated PI.B40.D30. AG12 (part1)	1.15	2.43	0.29	0.48	4.02	8.46
PEBAX 1657 coated PI.B40.D30. AG12 (part2)	6.80	2.73	0.20	2.50	33.76	13.53
PEBAX 1657 coated PI.B40.D100. AG12 (part1)	9.79	3.82	0.27	2.56	36.28	14.17
PEBAX 1657 coated PI.B40.D100. AG12 (part2)	6.97	3.82	0.21	1.83	33.07	18.10



## **APPENDIX F**

### **EFFECTS OF THE DOPE SOLUTION FLOW RATE ON THE HOLLOW FIBER MEMBRANE MORPHOLOGY**

The effects of the dope solution flow rate on the membrane morphology were shown in Figure F.1 and Figure F.2.



a)

Bore diameter: 376  $\mu\text{m}$

Membrane diameter: 718  $\mu\text{m}$

Thickness of dense layer: 6  $\mu\text{m}$

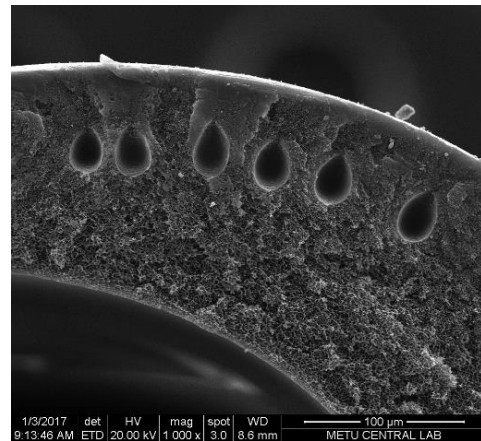
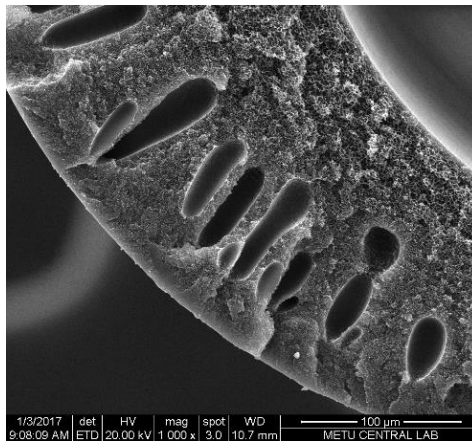
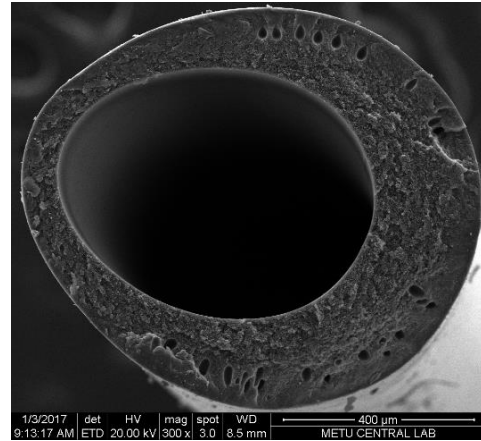
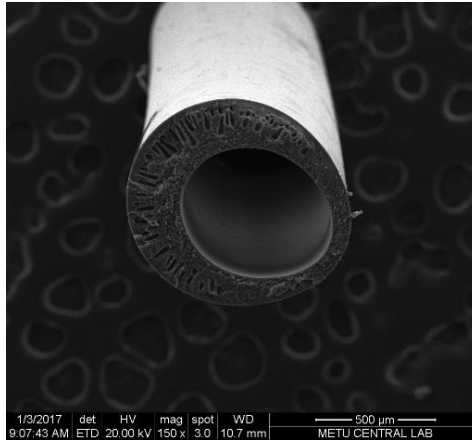
b)

Bore diameter: 370  $\mu\text{m}$

Membrane diameter: 710  $\mu\text{m}$

Thickness of dense layer: 4  $\mu\text{m}$

Figure F.1. The SEM images of hollow fiber membranes produced by using 35°C convective heating zone with the mass ratio of 30 PI: 0 THF: 70 DMF a) PI.B20.D30.AG 12 b) PI.B20.D100.AG 12



a)

Bore diameter: 600 μm  
 Membrane diameter: 920 μm  
 Thickness of dense layer: 6 μm

b)

Bore diameter: 610 μm  
 Membrane diameter: 750 μm  
 Thickness of dense layer: 12 μm

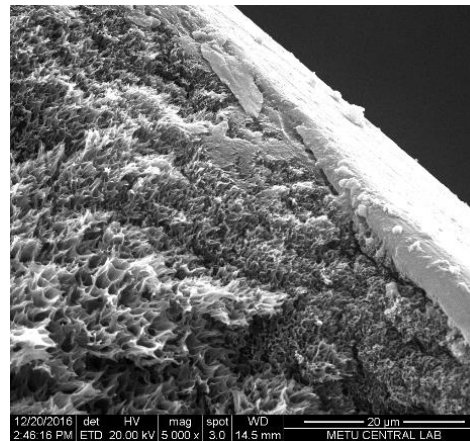
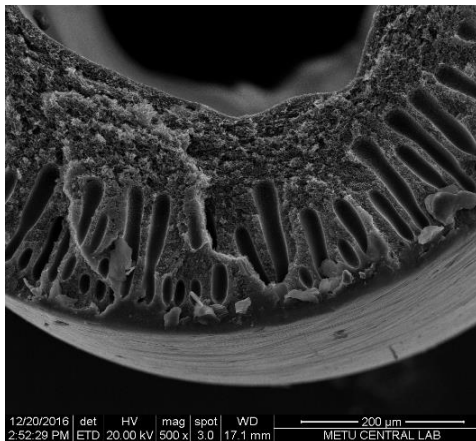
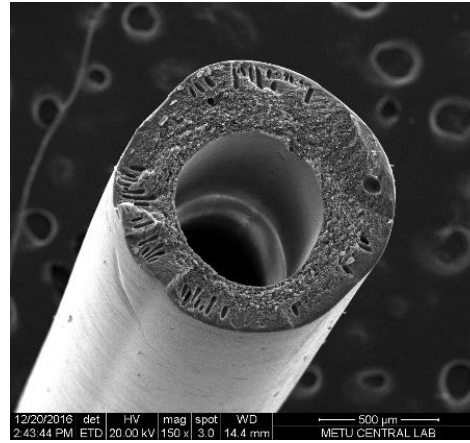
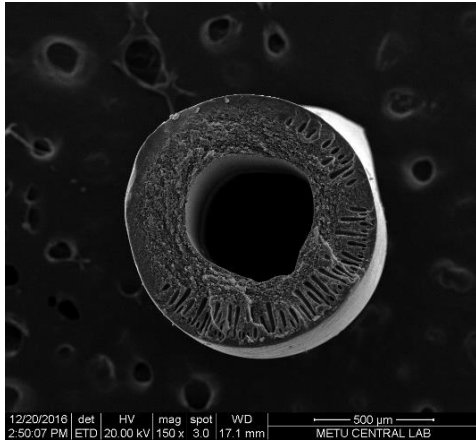
Figure F.2. The SEM images of hollow fiber membranes produced by using 35°C convective heating zone with the mass ratio of 30 PI: 0 THF: 70 DMF a) PI.B40.D30.AG 12 b) PI.B40.D100.AG 12



## **APPENDIX G**

### **EFFECTS OF THE BORE SOLUTION FLOW RATE ON THE HOLLOW FIBER MEMBRANE MORPHOLOGY**

The effects of the bore solution flow rate on the membrane morphology were shown in between Figure G.1 and Figure G.7.



**a)**

Bore diameter: 557 μm

Membrane diameter: 1067 μm

Thickness of dense layer: 14 μm

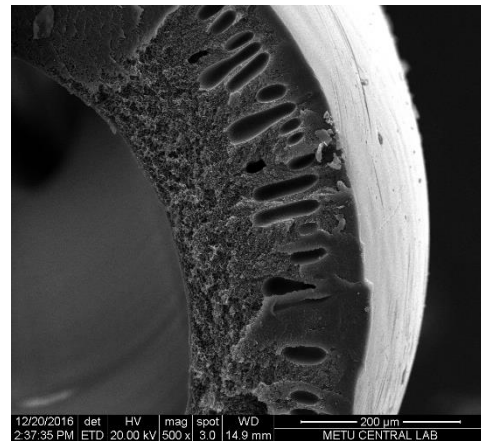
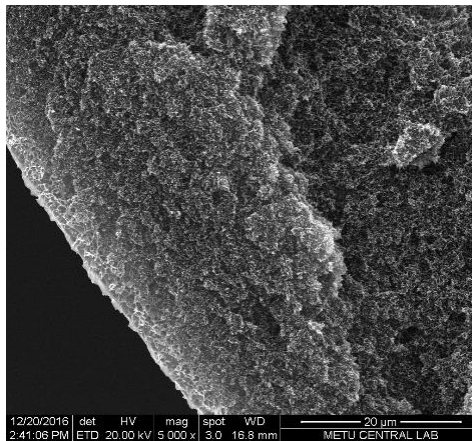
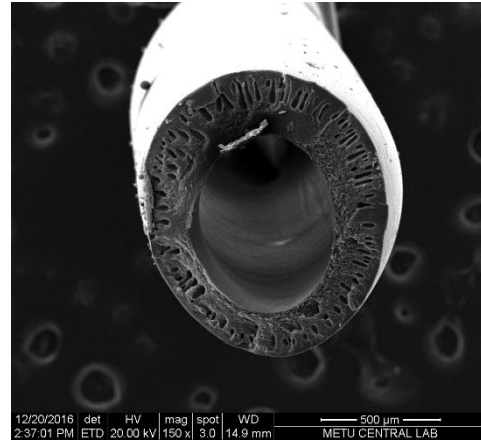
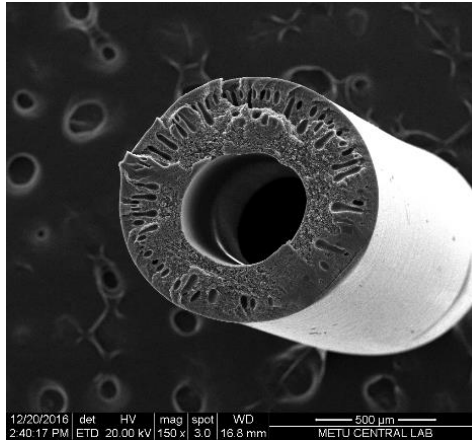
**b)**

Bore diameter: 642 μm

Membrane diameter: 1114 μm

Thickness of dense layer: 4 μm

Figure G.1. The SEM images of hollow fiber membranes produced by using 15°C convective heating zone with the mass ratio of 30 PI: 0 THF: 70 DMF a) PI.B20.D30.AG 6 b) PI.B30.D30.AG 6



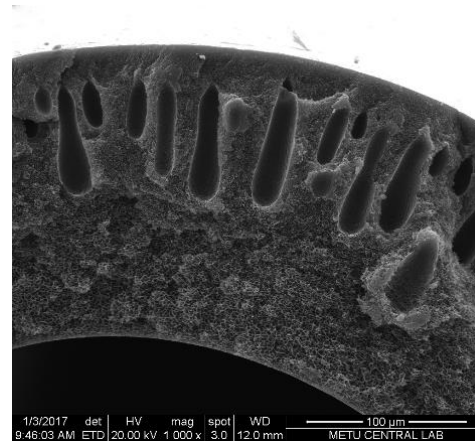
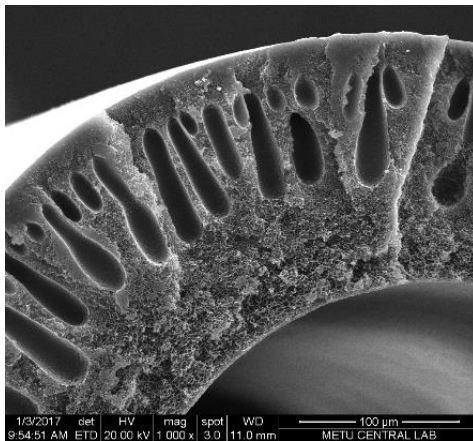
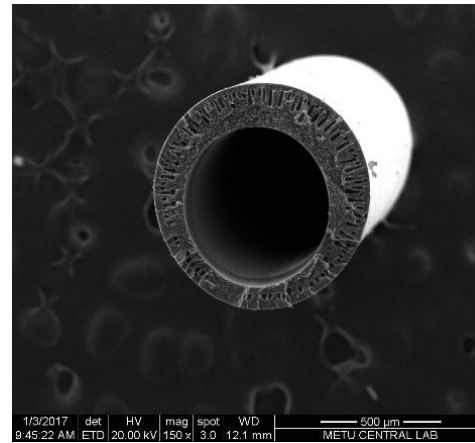
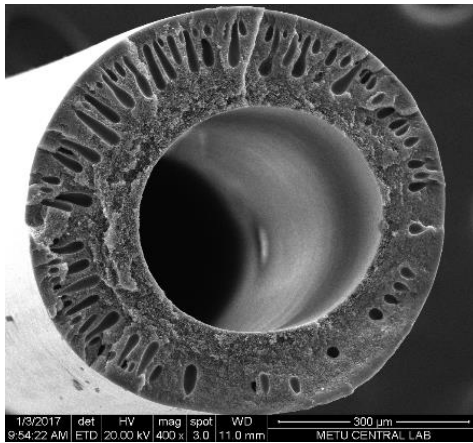
**a)**

Bore diameter: 504 μm  
 Membrane diameter: 1044 μm  
 Thickness of dense layer: 2 μm

**b)**

Bore diameter: 685 μm  
 Membrane diameter: 1107 μm  
 Thickness of dense layer: 19 μm

Figure G.2. The SEM images of hollow fiber membranes produced by using 15°C convective heating zone with the mass ratio of 30 PI: 0 THF: 70 DMF a) PI.B20.D30.AG 12 b) PI.B40.D30.AG 12



**a)**

Bore diameter: 377  $\mu\text{m}$

Membrane diameter: 651  $\mu\text{m}$

Thickness of dense layer: 7  $\mu\text{m}$

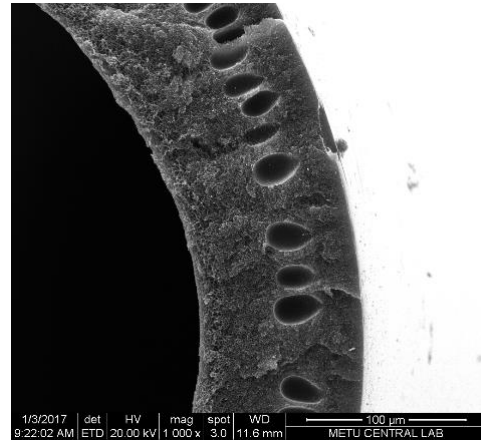
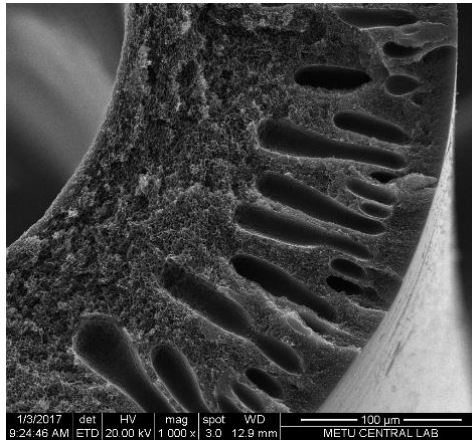
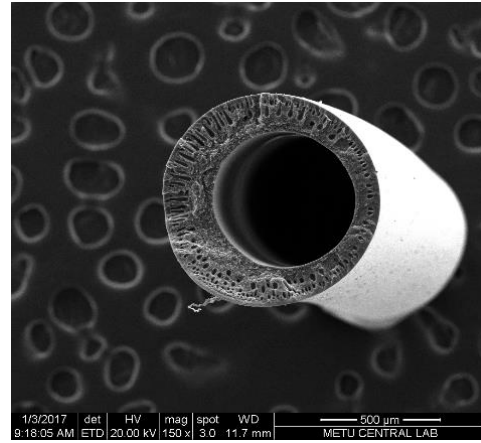
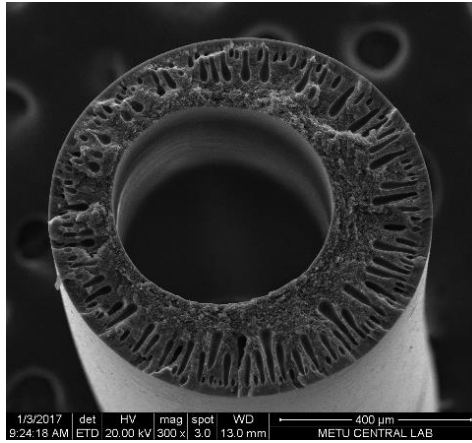
**b)**

Bore diameter: 633  $\mu\text{m}$

Membrane diameter: 776  $\mu\text{m}$

Thickness of dense layer: 3  $\mu\text{m}$

Figure G.3. The SEM images of hollow fiber membranes produced by using 35°C convective heating zone with the mass ratio of 30 PI: 7 THF: 63 DMF a) PI.B20.D30.AG 6 b) PI.B40.D30.AG 6



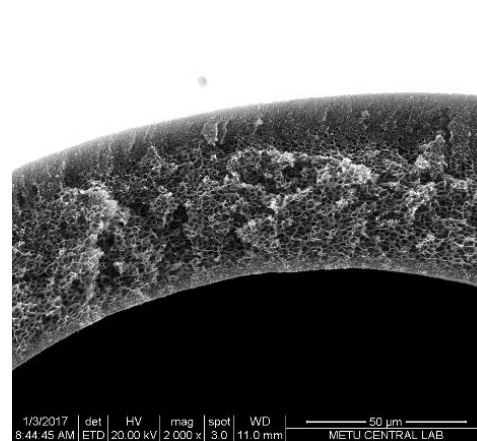
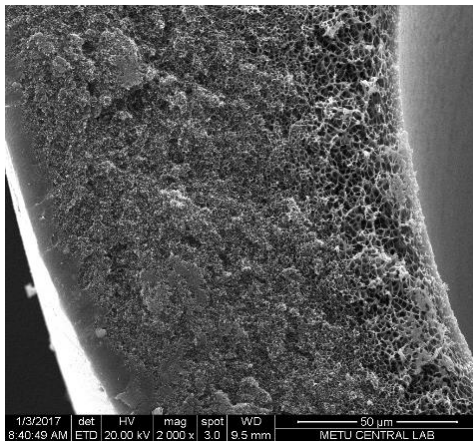
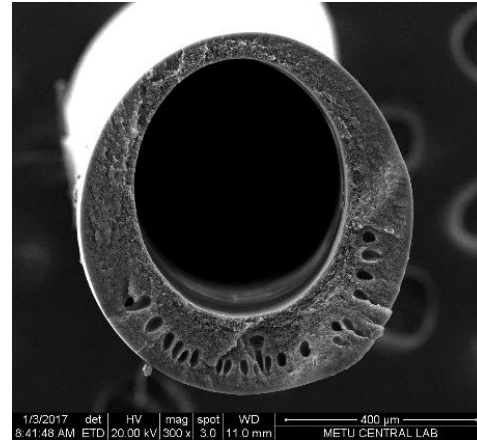
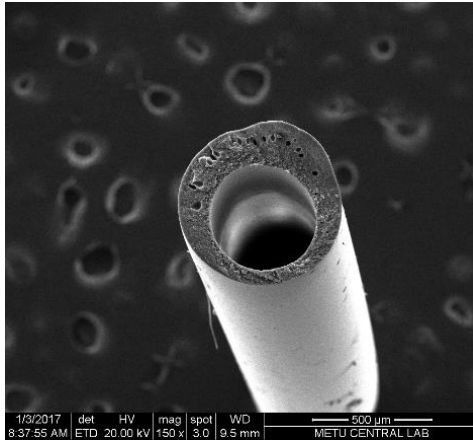
**a)**

Bore diameter: 454 μm  
 Membrane diameter: 793 μm  
 Thickness of dense layer: 4 μm

**b)**

Bore diameter: 586 μm  
 Membrane diameter: 901 μm  
 Thickness of dense layer: 1 μm

Figure G.4. The SEM images of hollow fiber membranes produced by using 35°C convective heating zone with the mass ratio of 30 PI: 7 THF: 63 DMF a) PI.B20.D100.AG 10 b) PI.B40.D100.AG 10



**a)**

Bore diameter: 450  $\mu\text{m}$

Membrane diameter: 678  $\mu\text{m}$

Thickness of dense layer: 7  $\mu\text{m}$

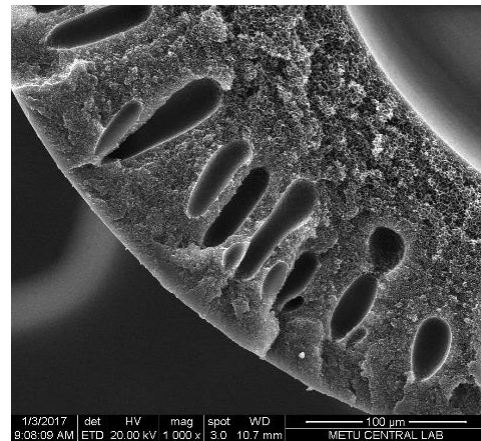
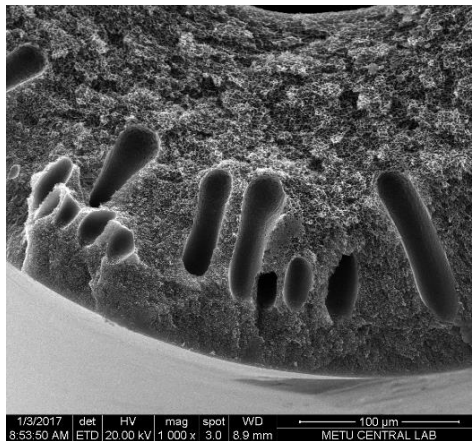
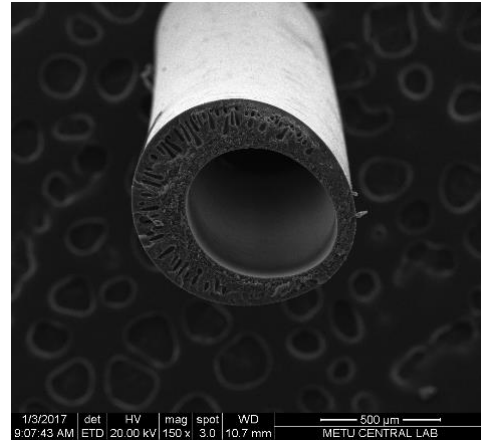
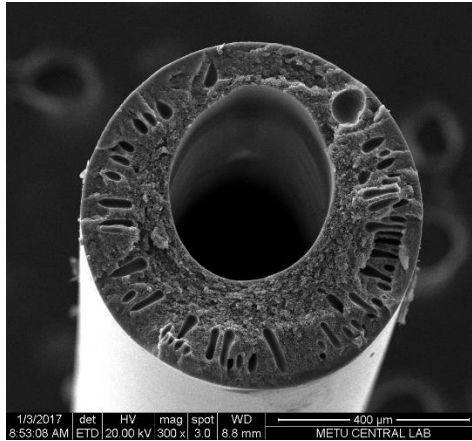
**b)**

Bore diameter: 499  $\mu\text{m}$

Membrane diameter: 728  $\mu\text{m}$

Thickness of dense layer: 5  $\mu\text{m}$

Figure G.5. The SEM images of hollow fiber membranes produced by using 35°C convective heating zone with the mass ratio of 30 PI: 0 THF: 70 DMF a) PI.B30.D30.AG 20 b) PI.B40.D30.AG 20



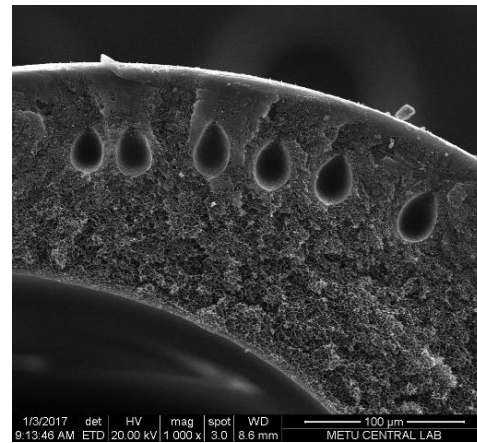
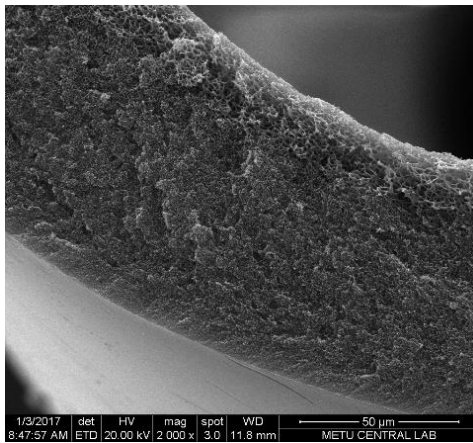
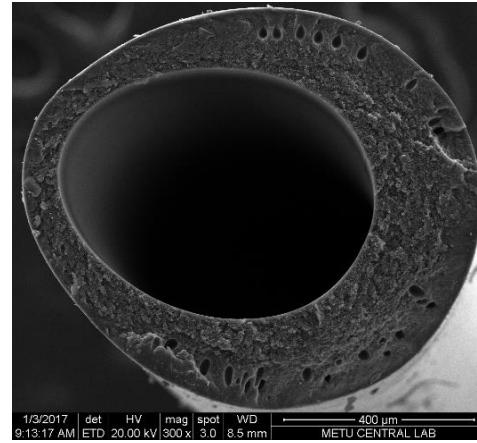
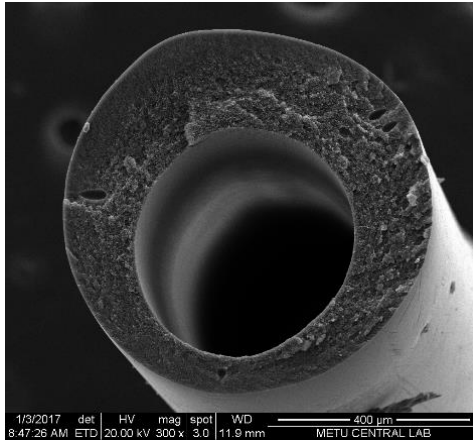
**a)**

Bore diameter: 376 μm  
 Membrane diameter: 718 μm  
 Thickness of dense layer: 6 μm

**b)**

Bore diameter: 600 μm  
 Membrane diameter: 920 μm  
 Thickness of dense layer: 6 μm

Figure G.6. The SEM images of hollow fiber membranes produced by using 35°C convective heating zone with the mass ratio of 30 PI: 0 THF: 70 DMF a) PI.B20.D30.AG 12 b) PI.B40.D30.AG 12



**a)**

Bore diameter: 463 μm

Membrane diameter: 770 μm

Thickness of dense layer: 6 μm

**b)**

Bore diameter: 610 μm

Membrane diameter: 750 μm

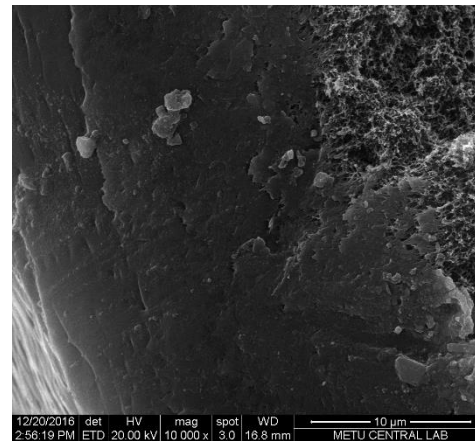
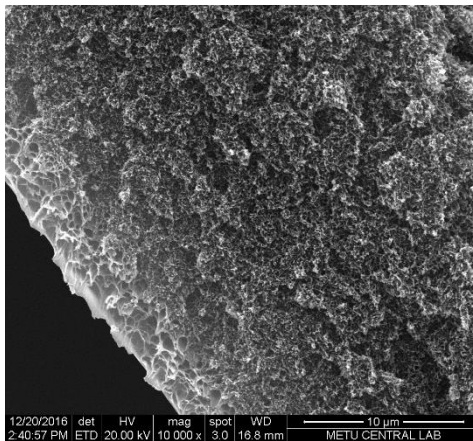
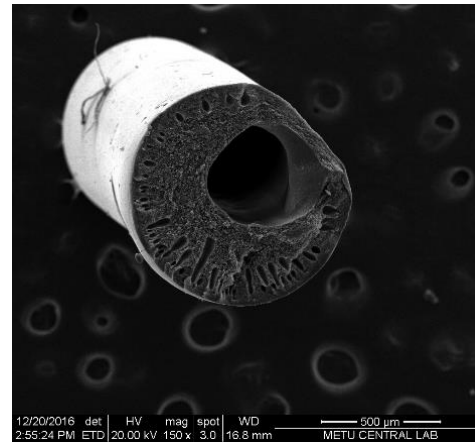
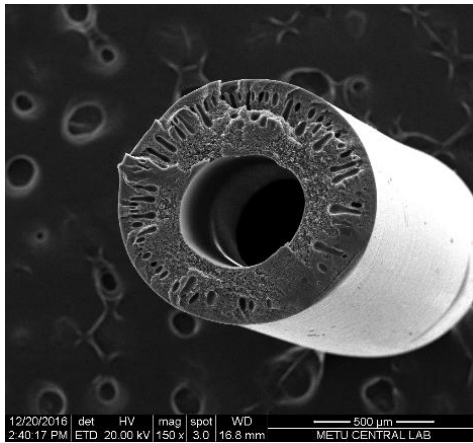
Thickness of dense layer: 12 μm

Figure G.7. The SEM images of hollow fiber membranes produced by using 35°C convective heating zone with the mass ratio of 30 PI: 0 THF: 70 DMF a) PI.B30.D100.AG 12 b) PI.B40.D100.AG 12

## **APPENDIX H**

### **EFFECTS OF THE THF ADDITION ON THE HOLLOW FIBER MEMBRANE MORPHOLOGY**

The effects of the addition of more volatile solvent to dope solution on the membrane morphology were shown in Figure H.1 and Figure H.2



**a)**

Bore diameter: 504 µm

Membrane diameter: 1044 µm

Thickness of dense layer: 2 µm

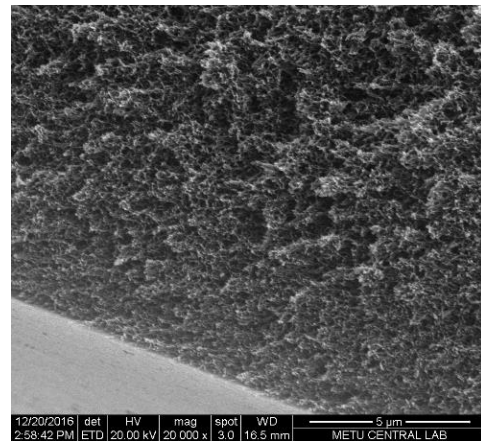
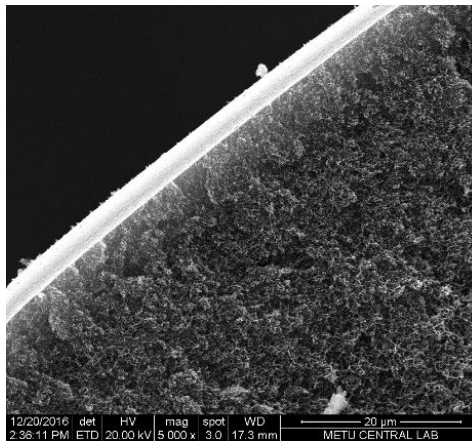
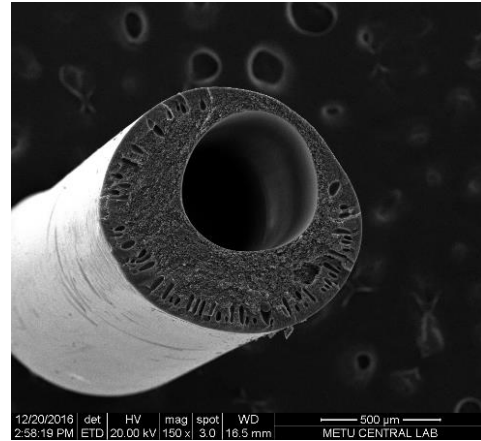
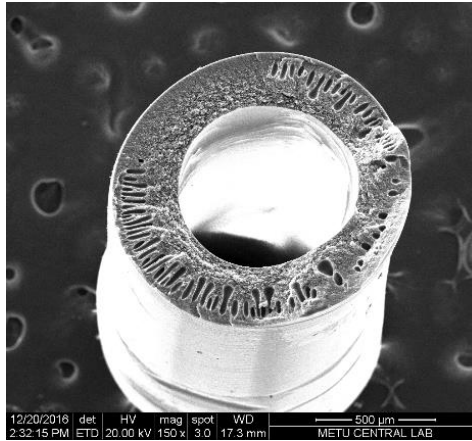
**b)**

Bore diameter: 459 µm

Membrane diameter: 917 µm

Thickness of dense layer: 21 µm

Figure H.1. The SEM images of hollow fiber membranes with a membrane code PI.B20.D30.AG 12 produced by using 15°C convective heating zone a) (PI: THF: DMF) (w/w) 30:0:70 b) (PI: THF: DMF) (w/w) 30:7:63



**a)**

Bore diameter: 703  $\mu\text{m}$   
 Membrane diameter: 1182  $\mu\text{m}$   
 Thickness of dense layer: 3  $\mu\text{m}$

**b)**

Bore diameter: 585  $\mu\text{m}$   
 Membrane diameter: 1029  $\mu\text{m}$   
 Thickness of dense layer: 1  $\mu\text{m}$

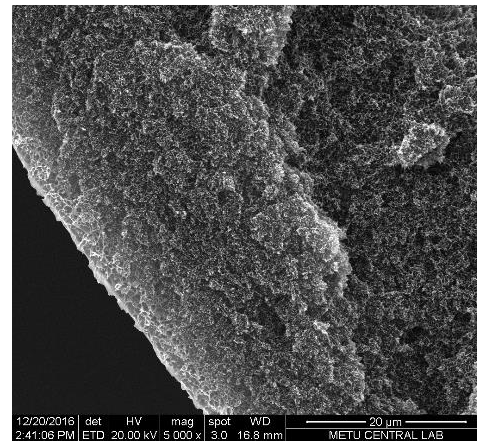
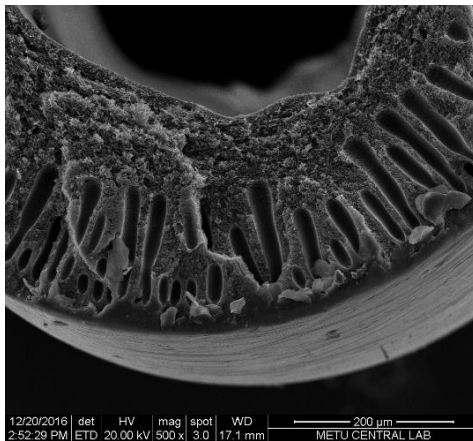
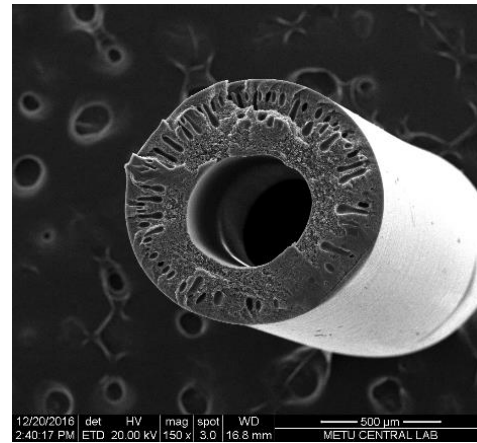
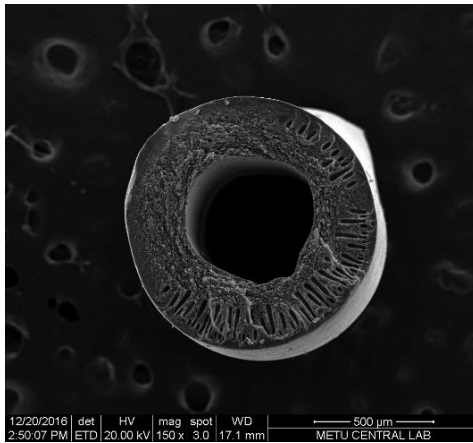
Figure H.2. The SEM images of hollow fiber membranes with a membrane code PI.B30.D30.AG 12 produced by using 15°C convective heating zone a) (PI: THF: DMF) (w/w) 30:0:70 b) (PI: THF: DMF) (w/w) 30:7:63



## **APPENDIX I**

### **EFFECTS OF THE AIR GAP HEIGHT ON THE HOLLOW FIBER MEMBRANE MORPHOLOGY**

The effects of the air gap height on the membrane morphology were shown in between Figure I.1 and Figure I.5.



**a)**

Bore diameter: 557  $\mu\text{m}$

Membrane diameter: 1067  $\mu\text{m}$

Thickness of dense layer: 14  $\mu\text{m}$

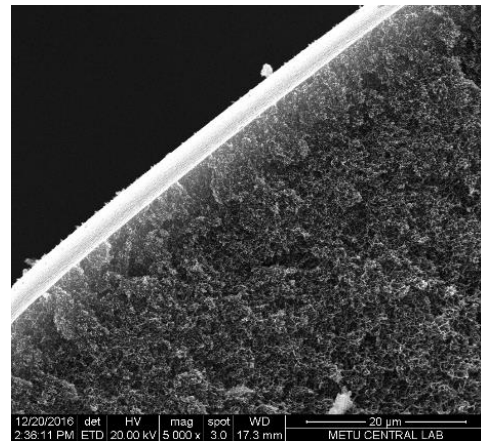
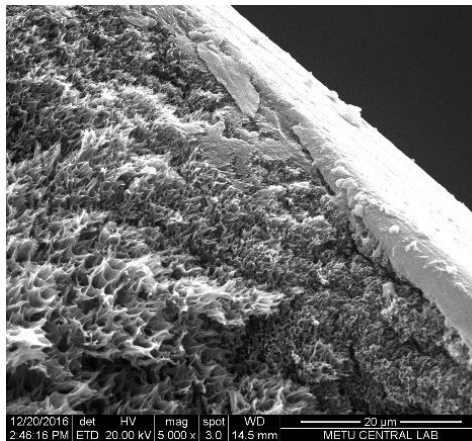
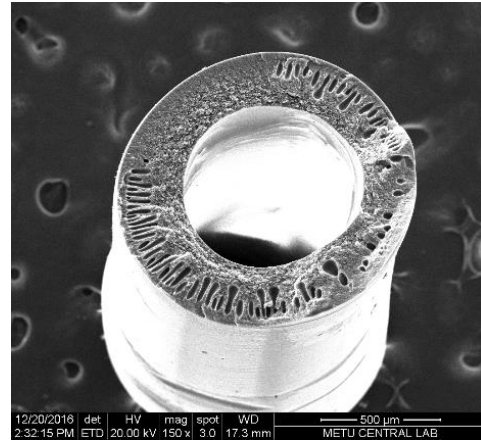
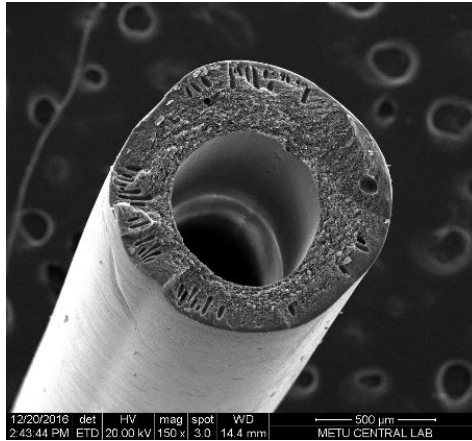
**b)**

Bore diameter: 504  $\mu\text{m}$

Membrane diameter: 1044  $\mu\text{m}$

Thickness of dense layer: 2  $\mu\text{m}$

Figure I.1. The SEM images of hollow fiber membranes produced by using 15°C convective heating zone with the mass ratio of 30 PI: 0 THF: 70 DMF a) PI.B20.D30.AG 6 b) PI.B20.D30.AG 12



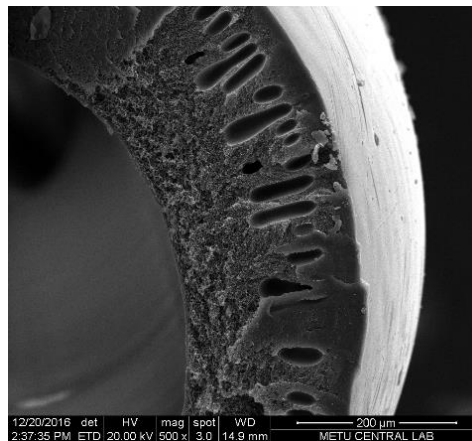
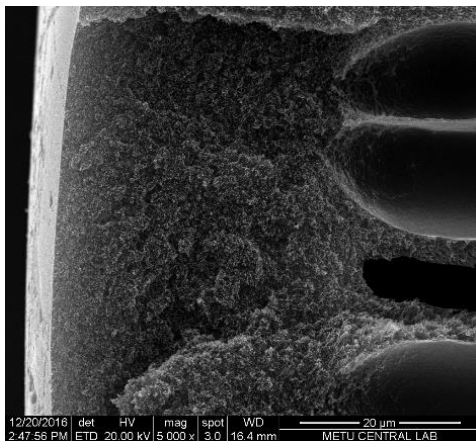
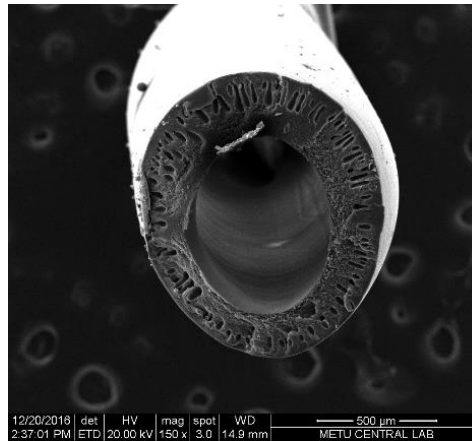
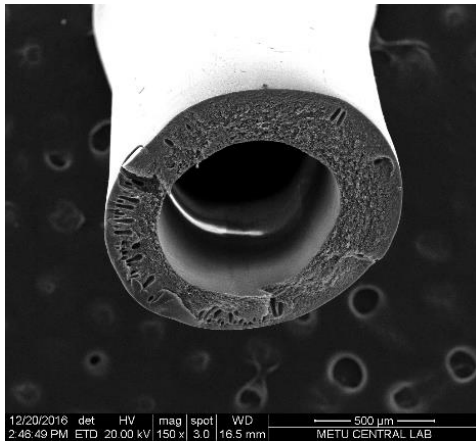
**a)**

Bore diameter: 642 μm  
 Membrane diameter: 1114 μm  
 Thickness of dense layer: 4 μm

**b)**

Bore diameter: 703 μm  
 Membrane diameter: 1182 μm  
 Thickness of dense layer: 3 μm

Figure I.2. The SEM images of hollow fiber membranes produced by using 15°C convective heating zone with the mass ratio of 30 PI: 0 THF: 70 DMF a) PI.B30.D30.AG 6 b) PI.B30.D30.AG 12



**a)**

Bore diameter: 713  $\mu\text{m}$

Membrane diameter: 1162  $\mu\text{m}$

Thickness of dense layer: 1  $\mu\text{m}$

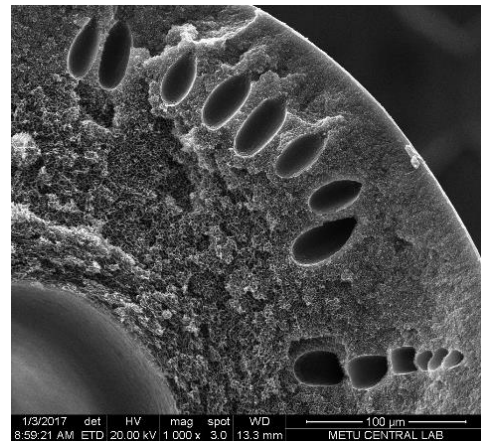
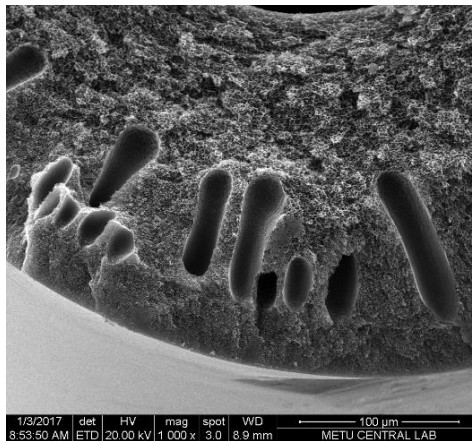
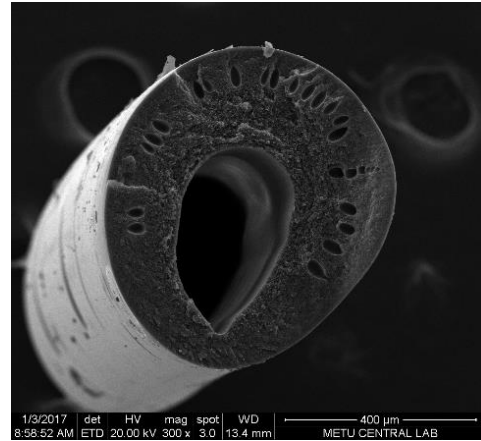
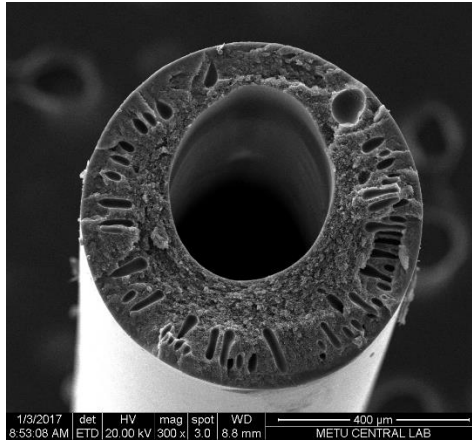
**b)**

Bore diameter: 685  $\mu\text{m}$

Membrane diameter: 1107  $\mu\text{m}$

Thickness of dense layer: 19  $\mu\text{m}$

Figure I.3. The SEM images of hollow fiber membranes produced by using 15°C convective heating zone with the mass ratio of 30 PI: 0 THF: 70 DMF a) PLB40.D30.AG 6 b) PLB40.D30.AG 12



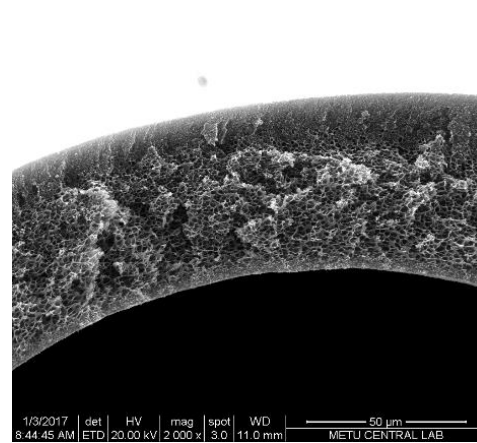
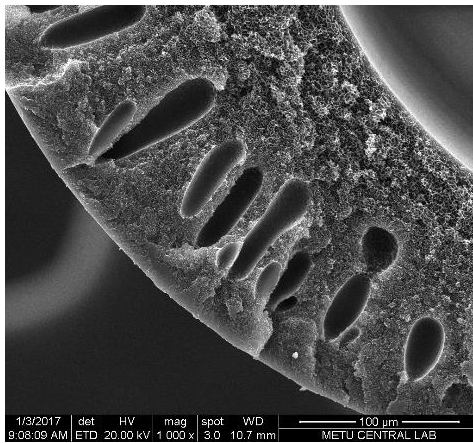
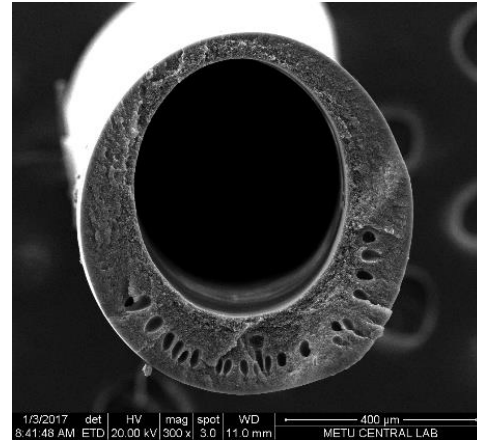
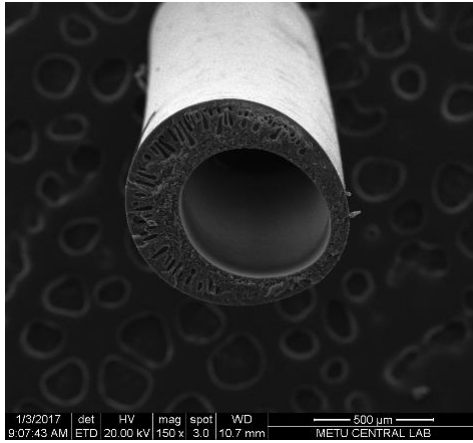
**a)**

Bore diameter: 376  $\mu\text{m}$   
 Membrane diameter: 718  $\mu\text{m}$   
 Thickness of dense layer: 6  $\mu\text{m}$

**b)**

Bore diameter: 298  $\mu\text{m}$   
 Membrane diameter: 608  $\mu\text{m}$   
 Thickness of dense layer: 4  $\mu\text{m}$

Figure I.4. The SEM images of hollow fiber membranes produced by using 35°C convective heating zone with the mass ratio of 30 PI: 0 THF: 70 DMF a) PI.B20.D30.AG 12 b) PI.B20.D30.AG 20



**a)**

Bore diameter: 600 μm

Membrane diameter: 920 μm

Thickness of dense layer: 6 μm

**b)**

Bore diameter: 499 μm

Membrane diameter: 728 μm

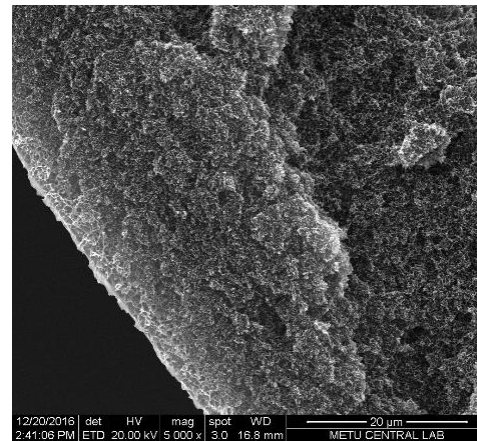
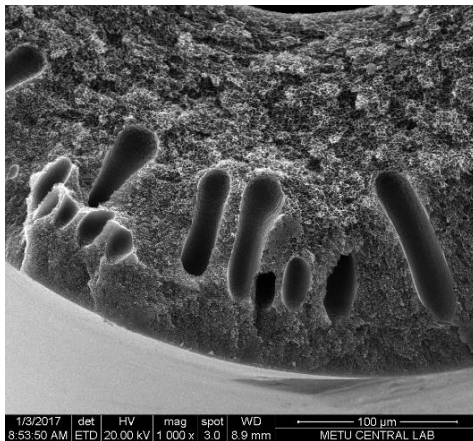
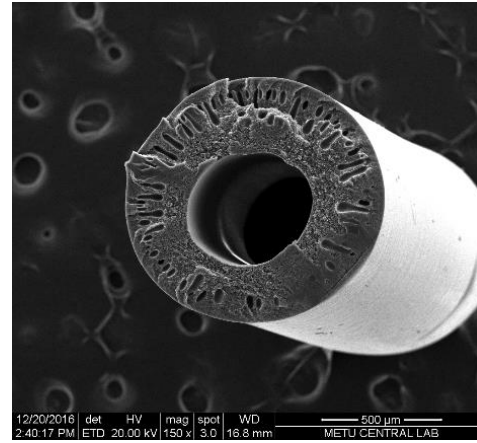
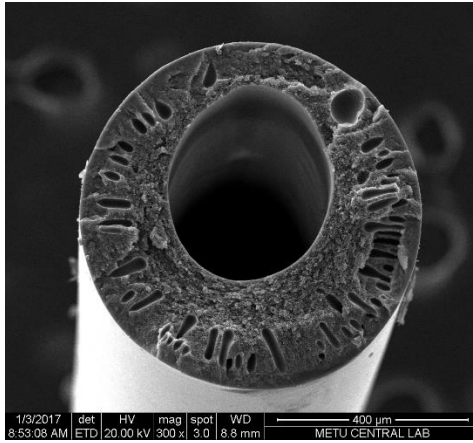
Thickness of dense layer: 5 μm

Figure I.5. The SEM images of hollow fiber membranes produced by using 35°C convective heating zone with the mass ratio of 30 PI: 0 THF: 70 DMF a) PI.B40.D30.AG 12 b) PI.B40.D30.AG 20

## **APPENDIX J**

### **EFFECTS OF THE TEMPERATURE ON THE HOLLOW FIBER MEMBRANE MORPHOLOGY**

The effects of the temperature on the membrane morphology were shown in Figure J.1 and Figure J.2.



**a)**

Bore diameter: 376  $\mu\text{m}$

Membrane diameter: 718  $\mu\text{m}$

Thickness of dense layer: 6  $\mu\text{m}$

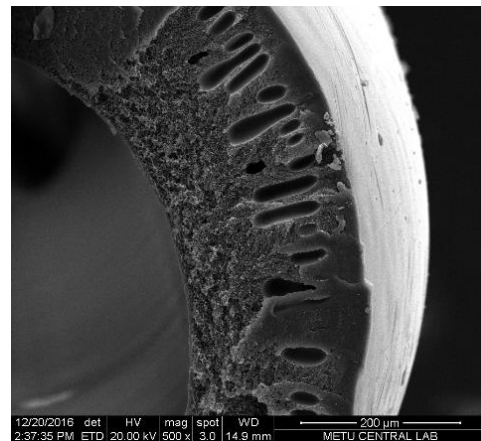
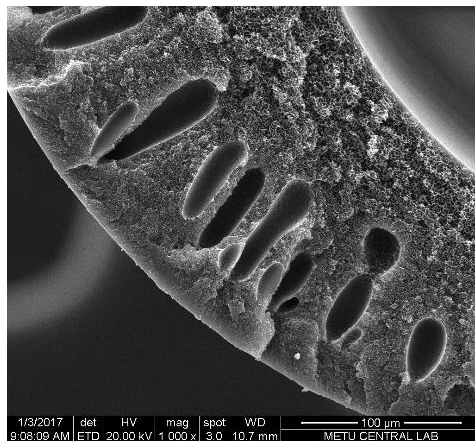
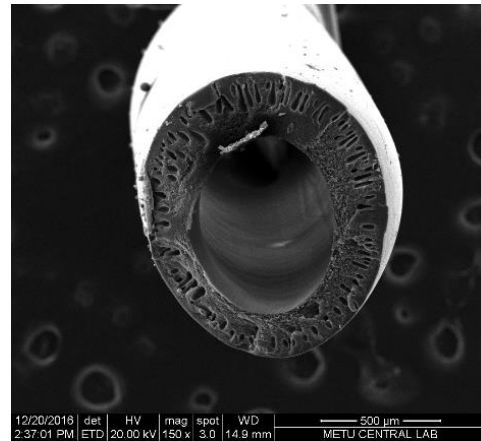
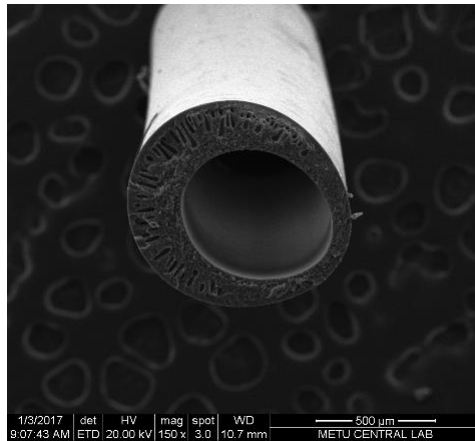
**b)**

Bore diameter: 504  $\mu\text{m}$

Membrane diameter: 1044  $\mu\text{m}$

Thickness of dense layer: 2  $\mu\text{m}$

Figure J.1. The SEM images of PI.B20.D30.AG12 hollow fiber membranes produced with the mass ratio of 30 PI: 0 THF: 70 DMF a) 35°C b) 15°C



**b)**

Bore diameter: 600 μm

Membrane diameter: 920 μm

Thickness of dense layer: 6 μm

**b)**

Bore diameter: 685 μm

Membrane diameter: 1107 μm

Thickness of dense layer: 19 μm

Figure J.2. The SEM images of PI.B40.D30.AG12 hollow fiber membranes produced with the mass ratio of 30 PI: 0 THF: 70 DMF a) 35°C b) 15°C